



Department of Bioengineering, Polytechnic of Milan, Milan, Italy

# **Exposure Assessment of Electromagnetic Fields on children, newborns and fetuses due to RFID devices**

**Serena Fiocchi**

Advisor: Prof. Paolo Ravazzani

Co-Advisor: Dr. Marta Parazzini

Tutor: Prof. Anna Maria Bianchi

PhD in Bioengineering – XXV Cycle



## Table of Contents

	<b>Page</b>
<b>Glossary</b>	<b>6</b>
<b>Abstract</b>	<b>10</b>
<b>Summary</b>	<b>12</b>
<b>Introduction</b>	<b>19</b>
<b>Chapter 1: Computational exposure assessment of EMF generated by an HF RFID system for mother-newborn identity reconfirmation</b>	
1. Introduction	27
2. Materials and methods	28
2.1 Model of newborn and mother	28
2.2 Model of the RFID system and RFID technical parameters	30
2.3 Simulations	31
2.4 Compliance with exposure guidelines	31
2.5 Sensitivity to the variation of dielectric properties in newborn	32
3. Results	33
4. Discussion	38
<b>Chapter 2: RFID system for newborn identity reconfirmation: exposure assessment of a realistic newborn model and effects of the variation of the dielectric properties with age</b>	
1. Introduction	42
2. Materials and methods	43
2.1 Newborn Model	43
2.2 Tissue Dielectric Properties	44

2.3 Model of the RFID system and RFID technical parameters	47
2.4 Simulations	48
3. Results	48
3.1 Baby model with ADP dielectric properties	48
3.2 Effect of change of the dielectric properties with age	50
4. Discussion	51

**Chapter 3: SAR assessment in human anatomical body models exposed to handheld UHF RFID reader antenna**

1. Introduction	55
2. Materials and methods	56
2.1 RFID Antenna Model	56
2.2 Antenna Model Validation	57
2.3 Anatomical Models	58
2.4 Dielectric Properties	59
2.5 Exposure Scenarios	59
2.6 Child models and antenna position variability	61
2.7 Computational approach	61
3. Results	61
3.1 Adult and child exposure	61
3.2 Variation of Dielectric Properties	63
3.3 Pregnant and Non-Pregnant Woman Exposure	64
3.4 Human and Source position variability	66
4. Discussion	66

**Chapter 4: Estimate of the Human Fetus Temperature Increase due to UHF RFID exposure**

1. Introduction	71
2. Material and Methods	72

	2.1 Anatomical Models and Exposure scenarios	72
	2.2 Thermal Model	73
	2.3 Thermal Parameters	74
3.	Results	74
4.	Discussion	81
	<b>Conclusions</b>	<b>84</b>
	<b>Bibliography</b>	<b>89</b>
	<b>List of Papers published during the PhD course</b>	<b>100</b>

---

## Glossary

BHE	Bio Heat Equation. Partial Differential equation describing the temperature distribution inside the body.
$c$	Specific heat (J/kg·°C)
CW	Continuous Wave
Dielectric Properties	Electric properties of dielectric materials that can be polarized by an applied electric field at a defined frequency $f$ . It is described by a complex number: $\hat{\epsilon}_r = \epsilon_r' - j\epsilon_r'' = \epsilon_r - j\frac{\sigma}{2\pi f\epsilon_0}$ where $\epsilon_r$ (dimensionless number. It is $\epsilon_r = 1$ in vacuum) is the relative permittivity of the material, $\sigma$ (S/m) is the electric conductivity, and $\epsilon_0 = 8.854187817 \cdot 10^{-12}$ F/m
Dosimetry	The discipline devoted to quantify the three-dimensional distribution of an agent in tissues and organs of individuals exposed to that agent (in this thesis EMF).
E	Vector Electric Field (V/m)
e.g.	Exempli gratia, it means “for example”
EMF	Electro Magnetic Field is a physical vector field due to the combination of electric field and a magnetic field produced by electrically charged objects. It affects the behavior of charged objects in the vicinity of the field. The electromagnetic field extends indefinitely throughout space and describes the electromagnetic interaction.
ERP	Effective Radiated Power (W or dBW) of a transmission system (antenna)
Exposure Matrix	Three-dimensional distribution of EMF and of the other quantities that allow to estimate the dose of EMF inside tissues and organs
FDTD	Finite-difference time-domain method. It is a numerical analysis technique used for modeling computational electrodynamics (finding approximate solutions to the associated system of differential equations).
FIT	Finite Integration Technique method. It is a numerical technique based on a spatial discretization scheme to numerically solve electromagnetic field problems in time and frequency domain.

---

$H$	Convective heat transfer rate ( $\text{W}/\text{m}^2\cdot^\circ\text{C}$ )
H	Vector Magnetic field (A/m)
HF	High Frequency. Range of RF between 3 – 30 MHz (wavelength 10 – 100 m)
HPA	Health Protection Agency (UK)
HRA	Health Risk Assessment. It is the process aimed to estimate the nature and probability of adverse health effects in humans who may be exposed to potential environmental stressors.
$H_{\text{th}}$	Average threshold level for the magnetic field in the space necessary to activate the RFID tag. It is one of the technical specifications of HF RFID systems.
IARC	International Agency for Research on Cancer
ICNIRP	International Commission on Non-Ionizing Radiation Protection
IEEE	Institute of Electrical and Electronics Engineers
i.e.	Id est. It means “that is”
LF	Low Frequency Range of RF between 30 – 300 kHz (wavelength 1 – 10 km)
MW	Microwaves. Range of RF between 300 MHz – 300 GHz (wavelength 1mm - 10 cm)
$K$	Thermal conductivity ( $\text{W}/\text{m}\cdot^\circ\text{C}$ )
$Q$	Metabolic heat generation rate ( $\text{W}/\text{kg}$ )
Reader (RFID)	One of the components of a RFID system, it is a two-way radio transmitter-receiver. able to transmit and decode a signal to/from the tag via EMF. Depending on the frequency of communication it consists in a coil or an antenna. It can be, depending on the application, movable or fixed.
RF	Radio Frequency. Range of frequencies of EM wave oscillating between 3 kHz and 300 GHz (wavelength 1 mm – 1000 km)
RFID	Radio Frequency Identification technology.
RR	Read Range distance. Maximum distance at which the reader is capable to activate the tag.

---

SAR	Specific Absorption Rate (W/kg). It is the metric used at the RF to account the EM power absorbed by a body per mass unit.
wbSAR	Measure of SAR averaged over the whole-body
psSAR <sub>10g</sub>	Maximum of all measurements of SAR averaged over small cubes of 10g of the same tissue
SAR <sub>ht</sub>	Maximum of psSAR <sub>10g</sub> found over the head and trunk
SAR <sub>l</sub>	Maximum of psSAR <sub>10g</sub> found over the limbs
SCENIHR	Scientific Committee on Emerging and Newly Identified Health Risks
T	Temperature (°C)
Tag (or Transponder)	Label that contains electronically stored information that univocally identifies the person/object to which is attached.
T <sub>incr</sub>	Temperature increase (°C)
TSL	Tissue Simulating Liquid. Used in experimental testing application with phantoms to simulate the average dielectric properties of a body
ToU	Time of Use of the reader near the tag. It's the time the reader needs to read the tag.
UHF	Ultra High Frequency. Range of RF between 300 MHz – 3 GHz (wavelength 10 cm – 1 m)
Voxel	Voxel (volumetric pixel or Volumetric Picture Element) is a volume element, representing a value on a regular grid in three dimensional space
WHO	World Health Organization
$\epsilon$	Permittivity (F/m). It's a measure of the resistance that is encountered by a dielectric medium, when forming an electric field.
$\rho$	Density (kg/m <sup>3</sup> )
$\sigma$	Electrical conductivity (S·m <sup>-1</sup> ). It measures a material's ability to conduct an electric current.
$\omega$	Volumetric blood perfusion rate (m <sup>3</sup> /kg·s)

---

## Abstract

Gli ultimi anni hanno visto un massiccio incremento di sorgenti di campi elettromagnetici (CEM) nelle più svariate applicazioni, tanto da indurre numerosi organismi internazionali a richiedere alla comunità scientifica sforzi volti a valutare il rischio per la salute legato a tale esposizione. E' noto come una corretta valutazione del rischio non possa prescindere da un'accurata valutazione dell'esposizione del soggetto, intesa come misura della dose dell'agente in esame (in questo caso i CEM) assorbita dal soggetto.

Fra le tipologie di popolazione che più destano interesse e preoccupazione, ci sono sicuramente i bambini.

Questo è, in primo luogo, dovuto alla relativa ristrettezza di studi scientifici che li riguardano, dato che tutta la ricerca scientifica si è concentrata per decenni sugli adulti e solo negli ultimissimi decenni sui giovani ed i bambini. Di maggiore rilievo scientifico sono invece le considerazioni relative all'esposizione sia di individui in rapido sviluppo che di individui che, proprio a causa dell'esposizione precoce, potenzialmente verranno esposti per più anni.

Peraltro, negli ultimi 4-5 anni si sono andati diffondendo nella vita quotidiana tecnologie emergenti, basate su campi elettromagnetici a varie frequenze. Fra di esse, di gran lunga fra le più diffuse è la tecnologia RFID (Radio Frequency IDentification), utilizzata in un numero enorme e sempre più crescente di applicazioni, allo scopo di permettere una rapida e sicura tracciatura di merci, prodotti, persone, ecc.... La loro diffusione è tale da coinvolgere l'intera popolazione, quindi includendo anche i neonati e i bambini. Nonostante questo, gli studi volti alla valutazione del rischio sulla salute legato all'esposizione ai CEM generati da questi dispositivi risultano ancora limitati.

Il lavoro descritto in questa tesi è quindi indirizzato in particolare alla:

- 1) Valutazione dell'esposizione ai campi elettromagnetici mediante tecniche di elettromagnetismo computazionale
- 2) In feti (donne gravide), neonati e bambini

dovuta ad esposizione a lettori RFID a 13.56 MHz e a 880 MHz.

I risultati indicano che, al fine di evitare la sovraesposizione del neonato, si deve porre particolare attenzione alle specifiche tecniche e al tempo di utilizzo dei dispositivi a 13.56 MHz. Per quanto riguarda la seconda classe di dispositivi invece, i livelli maggiori sono stati trovati considerando l'esposizione delle donne incinte, che tuttavia non comportano un significativo aumento di temperatura sul feto.

## **Abstract**

In the last few years, the incredible diffusion of sources of electromagnetic fields (EMF) used in ubiquitous applications, has induced the main International organizations for health protection to encourage efforts on the potential health effects of EMF exposure. Every process of health risk assessment includes, among the others steps, the exposure assessment, aimed to quantify the levels of the potential harmful agent (in this case EMF) to which the people are exposed.

Among the class of population exposed, children, neonates and fetuses have been for a long recognized as possibly more susceptible to EMF, either because of the precocity of their exposure, and because the time of the exposure coincided with the development and maturation of their system. Despite that, their exposure to EMF has been little investigated till now, most of studies addressing only the exposure assessment of adults.

Moreover, in the last 4-5 years, the new emerging technologies revolution, has led to the diffusion of new sources of EMF in a countless number of general public applications. Among them, Radio Frequency IDentification (RFID), born for purpose of automatic identification of people or objects, is becoming particularly pervasive. Its diffusion is likely to involve the entire population, thus also including children, neonates and fetuses. Also to that regard, studies aimed to assess the health risk related to RFID exposure are almost completely lacking.

To this purpose, this thesis wants to address:

- 1) the exposure assessment of EMF using computational techniques;
- 2) in fetuses (pregnant women), neonates and children

due to HF RFID systems operating at 13.56 MHz and UHF RFID operating around 880 MHz.

The results show that attention should be paid to the choice of the optimal reader–tag HF RFID technical specifications and that exposure time should be reduced to avoid in particular newborn overexposure. As to the UHF RFID, exposure levels close to the existing exposure guidelines on pregnant women were found. Moreover, the related temperature increases on fetuses result to be far from the threshold of biological effects even considering the worst case exposure conditions.

## Summary

The surging growth of exposure to Electromagnetic Fields (EMF) represent one of the main factors of people concern about negative biological effects generated by environmental stressors. Reasons of that concern are not totally irrational, since the great efforts, aimed to estimate those effects, carried on in the last few years have produced contradictory results, thus convincing some experts that the threat is real and thus leading the International Agency for Research on Cancer (IARC) to classify EMF as possibly carcinogenic to humans (Group 2B).

In view of the increasing rate of exposure due to the development of new technologies which make use of EMF, the “Health Risk Assessment” (HRA), defined as the process aimed to estimate the nature and probability of adverse health effects in humans who may be exposed to potential environmental stressors, addressing precisely EMF, become unavoidable. That process, among the others steps, include the specific assessment of the levels of EMF to whom people are exposed, also known as “exposure assessment”, which is the goal of this dissertation.

The high rate of increase of EMF exposure is inherently speed up by the nonstop proliferation of wireless technologies, which make use of EMF at frequencies still unexplored.

That is the case of RadioFrequency IDentification (RFID) technology, a generic term for technologies that make use of EMF to automatically identify people or objects. It is substantially based on the communication of information towards EMF between a label, named “RFID tag” or “RFID transponder”, which unmistakably identifies the person/object to which is attached, and an interrogator, named “RFID reader”, able to transmit to the tag, to receive from the tag and to decode the EMF signal. On the basis of the operating frequency of the reader, which is the frequency of EMF used for the physical coupling, three classes of RFID exist: Low-Frequency or LF (around 125 KHz), the High-Frequency or HF (13.56 MHz) and the Ultra-High-Frequency or UHF (860-960 MHz).

RFID applications can be find everywhere: asset tracking, manufacturing, supply chain management, payment systems, security and access control, transport systems, electronic passports and ID cards, animal identifications, medical applications, sporting events, and any other application that can take advantages by an automatic identification of people and objects.

However, if the RFID great diffusion is surely justified by the advantages that it offers in terms of automatism, reliability, safety, versatility, speed of reading and tracking, relatively low costs, etc.. the lack of accurate exposure assessment studies remains unmotivated and should be urgently addressed.

This is even more true considering the lack of selectivity of the RFID exposure, which can involve subjects who are considered more vulnerable to EMF exposure, and the lack of studies which address the peculiarity of their exposure.

To this purpose, children, newborn and fetuses have been for a long recognized as possibly more susceptible to EMF, either because of the precocity of their exposure, and because the time of the exposure coincided with the development and maturation of their system.

Therefore, the EMF assessment here discussed is mainly addressed to their exposure. That substantially means to identify, by solving Maxwell equations, the three-dimensional distribution, also known as “3D exposure matrix”, of EMF and of the other quantities that allow to estimate the dose of EMF inside tissues and organs.

The importance of this topic has led the International Commission on Non-Ionizing Radiation Protection (ICNIRP), in cooperation with the Environmental Health Division of the World Health Organization (WHO), to provide, within the process of exposure assessment, guidelines for limiting EMF exposure that will provide protection against known adverse health effects. An adverse health effect is defined as the one which causes detectable impairment of the health of the exposed subject or of his or her offspring. A biological effect, on the other hand, may or may not result in an adverse health effect [WHO <http://www.who.int/peh-emf/about/WhatisEMF/en/index1.html>]. A long process of review of different experts opinions, together with an exhaustive summary of the results of laboratory and epidemiological studies, have driven the draft of these guidelines, which resulted in 1998 a comprehensive publication [ICNIRP, 1998] that covered frequency range up to 300 GHz. The limits provided, are intended to give an adequate level of protection from exposure to time-varying EMF for both public and occupational exposure, and they will be considered for comparison in every EMF exposure assessment process, including the ones discussed in this dissertation. In particular, at the frequencies of RFID devices, i.e. radiofrequencies (RF), dosimetric studies and exposure guidelines usually refer to the Specific Absorption Rate (SAR) as the metric used to account the rate at which energy is absorbed by the body when exposed to RF EMF and to the temperature increase to directly quantify the heating produced by that absorption. In particular localized SAR and whole body SAR levels are here discussed and compared to the ICNIRP limits, chosen to avoid the risks for health that result from localized rises in tissue temperature and from the physiologic stress due to excessive whole-body heat loads, respectively.

The great advances in technology of the last years, have made particularly valuable and reliable to perform that assessment through computational (numerical) techniques on computers-based models.

Those techniques present the great advantage to determine EMF inside the tissue non invasively, to investigate a wide range of exposure scenarios and a wide range of frequency, stimuli, objects, to perform an easy sensitivity analysis of model parameters, and allow a flexible design phase and post processing.

Computational exposure assessment includes in particular: the source modeling and validation, the definition and discretization of the source and of the exposure scenarios.

In this thesis numerical methods, which provide a discretized resolution of Maxwell equations, as implemented by commercial platform CST (CST EM STUDIO by CST GmbH, Darmstadt, Germany) and SEMCAD (Schmid & Partner Engineering AG, Zurich, Switzerland), are used.

The dosimetric models of the human body used in this work consist of whole-body voxel models. The first very simple prototypes of these models were born several decades ago for ionizing radiation dosimetry studies. Recently, progress in medical imaging technology (in particular CT and MRI) has enabled the development of very accurate whole-body voxel models for a wide variety of humans, from newborns to children to adolescents to adults, male and female of different races, height and weight, as well as pregnant women. In particular, the models used in this work are based on high resolution MRI scans, from which a large number (more than 80) of tissues and organs have been segmented and reconstructed as three-dimensional CAD objects.

After the definition of human voxel models, which includes also the critic choice of the dielectric properties parameters of the tissues, the last step in the computational modeling consists in the modeling of the source of EMF, here represented by the RFID reader, and the related exposure scenarios, which depend by the type of RFID application.

Up to now, HF and UHF systems are the most diffused in applications which can expose general public for more than few seconds, and for that reason they are investigated in this thesis.

In particular in the first chapter of this dissertation (Chapter 1), the exposure to EMF generated by an High Frequency HF RFID system for a specific application of patient identification in hospital is assessed. Among the others RFID technology for identity check, the specific one for newborn-mother identity reconfirmation was simulated. Since it is expected to be particularly useful to avoid risk of miss-match of newborn and respective mother, it's becoming relatively diffused even in some Italian hospitals. Moreover, the subject involved can be particularly sensitive to EMF exposure, as outlined above. That RFID application consists substantially in a bracelet, usually placed to the wrist, with the passive RFID tag attached, which is provided to both mother and newborn; and the reader provided to the hospital personnel (nurse or doctor), able towards the communication by EMF to read the information in the tag. The computation is performed on realistic anatomical 2 mm resolution voxel

---

models of the mother and of newborn, this latter obtained scaling, on the basis of realistic anatomical literature data, a voxel model of a six years old child. The reader is modeled as a circular coil next to the mother and the neonate wrist, in the three different positions expected to be the worst cases achievable. The current in the coil, is calculated on the basis of the technical specification provided for devices which faces the same purpose of identification. These specifications, which include the Read-Range (RR) distance, that is the maximum distance at which the reader is still capable to activate the tag, the average threshold level for the magnetic field ( $H_{th}$ ) necessary to activate the tag, and the corresponding current calculated from them, are varied to allow to enlarge the results to a large range of devices (i.e.  $5\text{ cm} < RR < 10\text{ cm}$  and  $90 < H_{th} < 130\text{ dB}\mu\text{A/m}$ ).

The electromagnetic computations was performed using a the Low Frequency Solver within CST EM STUDIO. In all simulations the magnetic field (H) and the electric field (E) levels are estimated together with SAR levels on sub-body regions. The compliance of the SAR generated by RFID systems exposure with the ICNIRP guidelines [ICNIRP, 1998] was investigated as a function of the time of use of the system close to the body and of the change of maximum permitted  $H_{th}$  and RR in typical ranges of commercial devices.

The results show that attention should be paid in the identification of the optimal reader-tag technical specifications to be used in this type of application in particular for what concern newborn exposure, being the compliance with ICNIRP guidelines strongly affected by the choice of the  $H_{th}$  and the time of use of the device close to the body, while RR variability resulted almost irrelevant for the compliance both for mother and newborn exposure, for all reader positions. More precisely, the need to reduce as much as possible the exposure time (even less than 20 seconds for  $H_{th} > 120\text{ dB}\mu\text{A/m}$ ) suggests the importance of specific training of the involved personnel to the practical use of the RFID device.

Chapter 2 starts from these last results going one step further, by considering the possible factor of uncertainty introduced by the newborn modeling to which they are mostly affected. Those comprehend the scaling of the 6-years old child to model newborn and the use of adult dielectric parameters to newborn tissues, disregarding their possible variation with age due to the changes in body tissues composition. To that purpose, the same experiment performed in Chapter 1 was repeated, considering the same range of the RFID system technical specifications and the same exposure scenarios, on a realistic newborn model and the results were compared with the previous one. The new exposure matrix shows that the system complies with the ICNIRP guidelines almost ever, being the area of no compliance restricted to the couple of time of use and  $H_{th}$  longer than 2 minutes and higher than  $125\text{ dB}\mu\text{A/m}$  and such suggesting one time more that the great difference in the two models,

---

particularly in terms of geometry, number and type of dielectric tissues included, forms and position, is decisive in an accurate exposure assessment and that the use of the previous scaled model is more conservative than the realistic newborn one. In regard to the second open issues, four models for the assignment of dielectric properties to newborn tissues and the corresponding four exposure matrix calculated by the computation, were compared. The first model, named “Adult Dielectric Properties” - ADP model, is the classical approach used in dosimetric studies, based on data measured on adult animals. The second and the third model (named “Wang Dielectric Properties” - WDP and “Dimbylow Dielectric Properties” - DDP) are taken from parametric models developed by two different research groups and here readapted to the newborn model and the RFID operating frequency. The fourth model (i.e. “Literature Dielectric Properties” – LDP) is proposed by the author of this work, by reviewing the scattered data available from literature for all tissues of the model and by integrating them in a model which is expected the most accurate possible. The comparison of the exposure matrices in terms of electric field show, in general terms, an average difference of no more than 0.5 dB for WDP, DDP and LDP when compared to ADP. In particular not well defined trend was identified. Same considerations held also for the compliance in terms of SAR is considered, being the very slight (< 15%) maximum distances between all curves in the plane “ $H_{th}$ -maximum time of use of the reader” . This result, however, continues to support the consideration that there is no clear evidence of which is the best choice in terms of dielectric properties for newborn model, even if a trend towards a slight underestimation of the exposure using adult properties was found.

In Chapter 3 the focus is shifted to the other class of RFID system here investigated, that is the UHF RFIDs. As discussed before, these systems work around 880 MHz and are able to read objects at longer distances (up to 10 m) than HF systems with a faster data rate. Therefore, they are particularly suitable to be used in the great range of applications that require longer read ranges and hence their exposure can involve people that occasionally and accidentally pass close to the system. The reader, since those systems generally desire omnidirectional tag reading, was modeled as circularly polarized patch antennas. Exposure levels were quantified in different scenarios and subjects. In particular accidental head exposure was identified to represent the worst case exposure scenario for children (5-, 6-, 8-, 14- years old) and adult for comparison; abdomen exposure as the worst case for pregnant woman (both 7- and 9-months pregnant) and non-pregnant for comparison. The results of the computation are presented in terms of whole body SAR (wbSAR) and peak spatial SAR (psSAR<sub>10g</sub>) averaged over 10 g to allow the comparison with the basic restrictions of the exposure guidelines and normalized to 1 W radiated power and 100% of duty cycle to allow an easy rescaling of the results depending on the type of antenna and the standards of the country. Maximum levels of wbSAR largely

below the suggested ICNIRP limits were found (from -12 to -22 dB depending on the model), but, as expected, they present an increasing trend with age. Similar conclusions hold also for local exposure of children and adult (maximum peak SAR levels  $< -2$  dB far from the limits) but on the contrary, more concern can be raised with respect to abdomen exposure where the maximum psSAR<sub>10g</sub> levels for the 7- and 9- months pregnant female result higher than the exposure guidelines [ICNIRP, 1998] (+2.2 dB and +2.1 dB, respectively). These last findings, even if in the most countries of Europe the scaling factor discussed above is of 0.05, could induce an overexposure of the fetus who has a limited capability to dissipate the heat produced by power absorption. In particular, considering the existing link between SAR and the raise in temperature in the body organs, the temperature raise assessment in the previous worst case scenarios in terms of peak SAR values found in the 7- and 9-months old fetuses, is discussed in the last chapter. That estimate was performed by using the classical approach based on the finite different solution of the BioHeatEquation BHE as implemented in the Thermal solver within simulation platform SEMCAD X. However, the temperature exposure assessment performed in those critic exposure scenarios, results in negligible average temperature increase in the fetal body core (i.e. 0.004 °C at the steady-state) for both exposure scenarios.

Maximum temperature increase at the steady-state ( about 0.2 °C and 0.6 °C over 7- and 9- months fetuses, respectively) was found on the superficial tissues. However, the great spread of the temperature raise distributions together with the consideration that RFID exposure is unlikely to last the 2-3 hours needed to reach the steady-state, assures that those values represent a great conservative estimate of maximum temperature increase and, therefore, UHF RFID are very far to be a potential harmful source for fetus.

To sum up, this dissertation aims to give a quite exhaustive assessment of EMF generated by the exposure to devices, such as RFIDs, pervasively penetrating into our life, considering potentially harmful exposure scenarios that can be really met in practice. In this process, which represent an unavoidable step in the whole process of health risk assessment, several issues related to the complex modeling of children exposure assessment will be faced up and a quantitative estimate of exposure matrix and temperature raise will be presented. Despite the limitlessness of possible RFID exposure scenarios investigated, that dissertation wants start to fill the many gaps in knowledge related to children exposure to RFID devices and, maybe, keeping people aware to the potential health risk due to the practical use of this technology.

---

## Introduction

Electromagnetic fields (EMF) represent one of the most pervasive and fastest growing environmental stressors, about which anxiety and concern are spreading. Exposure to electric and magnetic fields from 0 to 300 GHz has been increasing tremendously as people take advantage of the many new technologies, such as telecommunications. These levels will continue to increase, even because this seems to be an irreversible process.

In this scenario the need to know the possible health effects of EMF, the levels below which EMF exposure provokes no human health risks, the existence of some people more likely susceptible and more exposed to such an environmental agent because of factors such as age, genetics, pre-existing health conditions, ethnic practices, gender etc. is unavoidable. The answers to these open issues are addressed by applying to EMF and health issues the so-called “Health Risk Assessment” (HRA) process, which includes, among the others steps, the quantification of the levels of an environmental stressor, in this case EMF, to whom people are exposed, also known as “exposure assessment”.

In the previous decades, the incredible diffusion of cellular telephony, has driven all the efforts into assessing the EMF generated by mobile phone on general public exposure.

To this purpose the Commission already launched two research projects on the potential health effects of microwaves (300 MHz – 300 GHz) under the 7<sup>th</sup> Framework Program for research (FP7; 2007-2013). The first one was MOBIKIDS<sup>a</sup> a case-control epidemiological study aiming at determining whether there is a link between mobile phone use and brain cancer in children and adolescents, whereas the second one is SEAWIND<sup>b</sup> a project aiming at developing instrumentation and procedures for the accurate assessment of exposure to microwaves. In parallel, the recent findings about the possible connection between leukemia and exposure to low frequency (i.e. 50 Hz) magnetic field exposure, has inspired the last FP7 project (i.e. ARIMMORA<sup>c</sup>).

---

<sup>a</sup> MOBI-KIDS – “Study Risk of brain cancer from exposure to radiofrequency fields in childhood and adolescence” (01/03/2009-28/02/2014; Grant Agreement n. 226873) - <http://www.mbkds.net/>

<sup>b</sup> SEAWIND – “Sound exposure and risk assessment of wireless network devices” (01/12/2009-30/11/2012; Grant Agreement n. 244149) – <http://seawind-fp7.eu/>

<sup>c</sup> ARIMMORA – “Advanced Research on Interaction Mechanisms of electromagnetic exposures with Organisms for Risk Assessment” (01/10/2011-30/09/2014; Grant Agreement n. 282891) – <http://arimmora-fp7.eu/>

However, these projects are addressing only a narrow band of the RF spectrum, whereas the so-called wireless revolution technology, driven by the surging growth of new technologies, is heavily affecting the completely unexplored band of the intermediate frequencies .

The increasing use of various sources operating in this band is considerably changing the level and the type of everyday public exposure both in time and space, leading to unknown highly heterogeneous exposure patterns which have to be investigated.

Among these technologies, one of the most known and diffused, but also less investigated, is the Radio Frequency Identification (RFID). RFID is a generic term for technologies that use radio waves to automatically identify people or objects. The development of RFID technology started more than 60 years ago [Stockman, 1948], through a series of studies [Harrington, 1964; Koelle et al., 1975]. Now it has become the most reliable, safe, and quick method of identification through the storage of serial numbers and others information that identify person or object, on a microchip that is attached to an antenna (the chip and the antenna together are called “RFID transponder” or “RFID tag”). When a reader is asking for identifying information, the antenna enables the chip to transmit back them to the reader antenna, which decode them [Finkenzeller,1999].

RFID devices are used in a huge number of applications (see Figure 1): asset tracking, manufacturing, supply chain management, payment systems, security and access control, transport systems, electronic passports and ID cards, animal identifications, medical applications, sporting events, and any other application that can take advantages by an automatic identification of people and objects.

Depending on the operating frequency, three main classes of RFID exist: Low-Frequency or LF (around 125 KHz), the High-Frequency or HF (13.56 MHz) and the Ultra-High-Frequency or UHF (860-960 MHz). The choice of the most appropriate one is usually made on the basis of the maximum distance at which that tag can be still read by the reader (read range distance). Generally LF RFIDs provide a shorter read range distance (< 0.5m) and, obviously, a lower read speed than the RFID of the other classes, but has the strongest ability to read tags in objects with high water or metal content. Typical low-frequency RFID applications includes access control, animal tracking, vehicle immobilizers, healthcare applications, product authentication and various point-of-sale applications. High Frequency HF RFID systems has a typical read range of 1 meter and a good ability to read tags on objects with high water or metal content. These systems are used in smart cards and smart shelves, to track library books, healthcare patients, product authentication and airline baggage. Ultra High Frequency RFID devices have a Read Range is up to 10 m, the greatest one with respect to the other RFID classes, with a fast data transfer rate (till 1000 kbit/s versus 10 and 100 for LF and UHF,

respectively). One drawback of UHF systems is a limited ability to read tags on objects with or surrounded by high water or metal content. This is typically the RFID solution recommended for distribution and logistics applications.

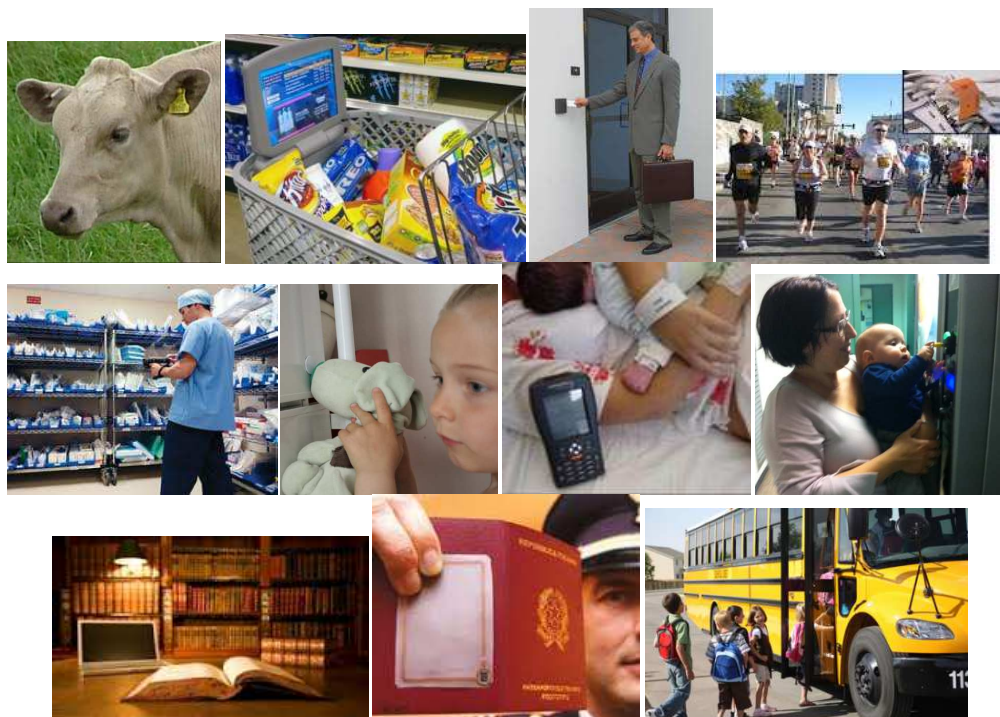


**Figure1 Example of applications of RFID technology**

As an example of the global diffusion of RFID system, the latest RFID market research provided by IDTechEx, which is one the most important companies which offers independent research and advice about emerging technologies, finds that at the end of 2012 the value of the entire RFID market will be \$7.67 billion, up from \$6.51 billion in 2011 and it's expected to reach \$30 billion in 2022 (more detailed forecasts are available in the recently updated ["RFID Forecasts, Players and Opportunities 2012-2022" at [www.IDTechEX.com/forecast](http://www.IDTechEX.com/forecast), last accessed on December 5<sup>th</sup>, 2012]).

The great diffusion of such a pervasive technology is not counterbalanced by a parallel exposure assessment aimed to define the potential health effects caused by the public exposure to these devices. Based on a weight of three evidences (epidemiological, animal and in vitro studies) for exposure to radiofrequencies (3 kHz – 300 GHz), the main health protection organizations (e.g., World Health Organization WHO, Health Protection Agency HPA) and scientific commissions (e.g., the European Commission DG SANCO Scientific Committee on Emerging and Newly Identified Health Risks SCENIHR) have concluded that exposure at levels below those proposed ICNIRP guidelines

[ICNIRP, 1998] is unlikely to lead to adverse health effects. However, so far the possible influence on these health assessment related to new exposure scenarios generated by the diffusion of RDIF devices were practically not yet investigated.

That applies even more to children. They are considered possibly more sensitive than adult to EMF for two main reasons. On the one hand because of the precocity of their exposure, which causes that they are exposed much greater part of their lifespan than adults. On the other hand, because that exposure coincides with the development and maturation of critical organs, such as the central nervous system and the hematopoietic and immune system, the reproductive system.

It is well known that the developmental processes are vulnerable to disruption by agents that may not be toxic to mature systems [Grandjean and Landrigan, 2006] and hence the possible influence of EMF exposure on the children development cannot be discharged.

As previously stated, an accurate and reliable exposure assessment (often referred as “dosimetry”, which is the science of quantifying the three-dimensional distribution of an agent inside tissues and organs) is an important key requirement of scientific studies on EMF biological effects.

Computational studies on children exposure started very recently (i.e. [Findaly et al. 2009; Bakker et al. 2010; Wang et al. 2006; Conil et al. 2008; Kühn et al. 2009]). In 2010, WHO dedicated the entire research agenda to children exposure, identifying the improvement of the exposure assessment in children as one of the highest priority issues to be addressed. Exposure assessment can be performed both by experimental and computational techniques. However, in the recent past the availability on one side of the realistic whole body computational models and, on the other one, of low-cost high-performance computing systems, generated an increase of interest in results achieved by computational techniques. In that perspective, and speaking of children, despite large differences in the size, shape, and tissue distribution, for more than two decades, due to the lack of accurate anatomical dosimetric models for children, the studies on adult models have been considered enlargeable to children. With the progress of computers, morphing techniques, such as uniform [see e.g., Gandhi et al. 1996] and non-uniform down scaling have been developed (see e.g., Dimbylow, 2002; Hirata et al. 2007; Conil et al. 2008]). However, these approaches still miss the issues related to the different rates of growth of the various tissues, which led to local inaccuracies of SAR [Wiert et al. 2011]. In the last 2-3 years many realistic high-resolution whole-body computational models of children, infants and fetuses have been developed and made available (see i.e. “Virtual Population” by IT’IS foundation [Christ et al. 2010], “HPA phantoms” by [Dimbylow 1997, 2005, Dimbylow and Bolch, 2007], “NICT Japanese models” [Nagaoka et al. 2004], “Korean models” [Lee et al. 2009a]. Moreover recently, due to the ubiquity of RF sources, the need of new models, in particular of

pregnant women and newborn, has been pointed out to assess their exposure. The numerous efforts carried on to this purpose have made available those models (see i.e. [Cech et al., 2007; Dimbylow, 2006; Xu et al., 2007; Nagaoka et al. 2007, 2008, Christ et al. 2012, Dimbylow et al., 2010]), allowing to increase, even in children, the reliability of the exposure assessment studies.

Computational electromagnetics applied to the EMF exposure assessment in biological systems needs the identification as accurate as possible of the dielectric properties of all the modeled biological tissues. Although many studies were published on this subject in the last 15 years [Gabriel et al. 1996; Peyman et al. 2001, 2010, 2011], this still remain an open issue, considering the difficulties in performing this type of studies and the consequent high level of uncertainty still present in the available data. Moreover, the mass of this information is relative to adult data only, and their applicability as they are to children is still questionable. This is also considering that the dielectric properties of tissues are highly frequency and temperature dependent and exhibit systematic changes due to the tissue water content [Peyman, 2011], the latter strongly age-dependent. Scattered measures of some animals young tissues have been made (see i.e. [Thurai et al., 1984, 1985; Lu et al., 1996; Gabriel, 2005; Olawale et al., 2005; Schmid and Überbacher, 2005; Peyman et al. 2001, 2005, 2007]) and some models to account the dependence on tissue water content have been proposed (see i.e. [Wang et al. 2006; Dimbylow et al., 2010]) up to a recent study by [Peyman et al. 2009], who provide a systematic review of most of young body tissues dielectric properties to use in dosimetric studies on children.

This dissertation aims to provide responses to some of these open issues about the computational EMF exposure assessment related to exposure to high frequency and UHF classes of RFID devices. An EMF exposure matrix, which includes the levels of magnetic field  $H$  (A/m), electric field  $E$  (V/m), and specific absorption rate SAR (in W/kg which is the metric used to account the rate at which power is absorbed by the body when exposed to radio frequencies), will be estimated case by case. In particular this thesis will address the exposure matrix estimated in neonate exposed to high frequency HF RFID systems and of fetuses (and related pregnant women) of different gestational ages exposed to UHF RFID. In this latter case, the increase of temperature of fetal tissues due to the exposure (well-known health effects of high level power radiofrequencies) will be also addressed.

This will contribute in providing answers to specific open questions, such as what are the exposure levels of neonates and fetuses to these devices, what is the influence of dielectric properties variation with age on the exposure assessment, what is the actual temperature increase due to the exposure to such electromagnetic fields due to RFID.

This route will run across four chapters, built on four papers already published or submitted by the author of this thesis to international peer reviewed journals. All those works have been In Chapter 1 (built on: “Fiocchi S, Parazzini M, Paglialonga A, Ravazzani P. 2011. Computational exposure assessment of electromagnetic fields generated by an RFID system for mother-newborn identity reconfirmation. *Bioelectromagnetics*. 32(5): 408–416”) a close examination of EMF levels generated by a specific RFID medical application for mother-newborn identity reconfirmation will be discussed. The levels of electric field, magnetic field and SAR estimated will be compared to EMF exposure guidelines [ICNIRP, 1998] as a function of the change in reader-tag specifications (magnetic field threshold and maximum distance of the reader to awake the tag) and time of use of the reader close to the body. These limits, drafted after a long process of review of different experts opinions, together with an exhaustive summary of the results of laboratory and epidemiological studies, are intended to provide an adequate level of protection to time-varying EMF for both public and occupational exposure against known adverse health effects, here intended as the one which causes detectable impairment of the health of the exposed subject or of his or her offspring. A biological effect, on the other hand, may or may not result in an adverse health effect [WHO <http://www.who.int/peh-emf/about/WhatisEMF/en/index1.html> ].

Since individual anatomy and exposure conditions are highly diverse, while the threshold dose is unique for different groups of people, Chapter 2 (built on “Fiocchi S, Parazzini M, and Ravazzani P. 2011. RFID System For Newborn Identity Reconfirmation In Hospital: Exposure Assessment Of A Realistic Newborn Model And Effects Of The Change Of The Dielectric Properties With Age. *Progress in Biophysics and Molecular Biology*, 107(3): 443–448) propose an improvement of the previous one, taking into account in particular the issues related to the model of newborn exposure which can affect the results of the computation and therefore the comparison with the limits. In particular the previous results obtained on a scaled model of a child will be compared to the ones calculated on a realistic newborn model (“Baby”). As second aim, the effects of the change of the tissue dielectric properties with age on the “exposure matrix” is addressed, by proposing different models of dielectric properties assignment.

The Chapter 3 (built on: “Fiocchi S, Markakis I, Ravazzani P, Samaras T. 2012. SAR assessment in human anatomical body models exposed to handheld UHF RFID reader antenna” under final phase of revision to *Bioelectromagnetics*), shifts the focus on the UHF RFID system, by addressing a computational exposure assessment of the electromagnetic radiation generated by a realistic UHF RFID reader, and by quantifying the exposure levels in different exposure scenarios and subjects (two adults, four children, and two anatomical models of 7- and 9-months pregnant women).

In light of the rather high levels of SAR estimated in case of pregnant women exposure, the 4<sup>th</sup> Chapter (built on: “Fiocchi S, Markakis I, Parazzini M, Samaras T, Ravazzani P. Estimate of the human fetus temperature increase due to UHF RFID exposure” in final phase of preparation for submission) will provide an estimation of the temperature increase in the fetal tissues, which could results from the physiological stress due to power heat loads. In particular the increase in temperature will be assessed in the worst case exposure scenario in terms of SAR met in the previous work, by applying the classical approach based on the resolution of the Bio Heat equation.

The work discussed in this dissertation has been done at the Department of Bioengineering of the Polytechnic of Milan and at the Institute of Biomedical Engineering ISIB of the National Research Council CNR, under the supervision of Prof. Paolo Ravazzani. Moreover, the works discussed in Chapter 3 and Chapter 4, have been performed in collaboration with the “Department of Physics” of the “Aristotle University of Thessaloniki” and with the company “THESS-Thessaloniki Software Solution S.A.”, under the supervision of Prof. Theodoros Samaras.

---

# Computational exposure assessment of EMF generated by an HF RFID system for mother-newborn identity reconfirmation

*(This chapter is based on “Fiocchi S, Parazzini M, Paglialonga A, Ravazzani P. 2011. Computational exposure assessment of electromagnetic fields generated by an RFID system for mother-newborn identity reconfirmation. Bioelectromagnetics. 32(5): 408–416”)*

## 1. Introduction

Among the countless application based on RFID technology, recently some innovative health applications for patient identification (ID) have been introduced in healthcare. They consists in setting new standards in the ID process by replacing the conventional ID barcode wristband with one that is RFID-enabled. This solution allows to increase safety and security levels, together with the speed of tracking and recording process. The RFID system envisaged for this application usually operates in the Low Frequency LF band (120-135 kHz) or in the High Frequency HF band (13.56 MHz). The RFID tag is usually embedded in an anklet or wristband and, with the patient or parent consent, the tag ID number is linked to the database of the hospital, allowing a rapid check of identity and often other information. Among this type of applications, one specific is the use of RFID systems for newborn-mother reconfirmation, used in particular, to address the problem of a mix-up of newborns or false association with their mothers.

This unfortunate scenario can be caused by many mistakes, most of them falling in the human error category: misreading infant or mother bracelet information, bracelet falling off ankle or wrist, bed mix-ups and mix-ups of babies with similar or identical names, misreading of sequential names or ID numbers, etc. RFID technology is supposed to be particularly suitable to prevent these scenarios, and therefore several projects based on this idea are currently running worldwide [see e.g. Dalton et al., 2005; Thuemmler et al., 2007; Ngai et al., 2009]. Briefly they are planned as follows: at birth, an RFID programmer generates two identical tags based on the mother unique hospital identification number; one tag is inserted into the mother’s wrist bracelet, the other is inserted into the infant’s wrist (ankle) bracelet. For the mother-baby mix-up prevention system, the RFID reader verifies all mother-

baby transactions and, at discharge, verifies the right match between mother and baby in a final check before the discharge can proceed.

Despite its growing diffusion and the sensitivity of the two subjects involved, this application has not been yet object of research on the possible health effects of exposure to the EMF generated, neither for patients, nor for staff and, more generally, into the healthcare environment, being the available studies limited to some reports on possible electromagnetic interferences [see e.g., Christe et al., 2008; Van der Togt et al., 2008]. Besides, many different body regions are potentially involved by the EMF emitted considering varying device configurations, both in terms of reader-tag relative position, geometry and electrical parameters.

The work discussed in this chapter addresses the estimate by computational techniques of the EMF distribution in body regions of newborn and mother generated by passive RFID at 13.56 MHz, simulating reader-tag technical specifications in ranges similar to what applied in commercial devices.

## 2. Materials and Methods

### 2.1. Model of newborn and mother

Two realistic models of newborn and mother were taken from the Virtual Family (available for research purposes through the IT'IS Foundation [Christ et al., 2010a]) . They are based on high resolution magnetic resonance (MR) images of healthy volunteers, segmented in a voxel-based format at a resolution of 2 mm, thus allowing to distinguish more than 80 tissues. The two models are shown in Figure 1.1, together with three reader positions used in this study. The mother is a 26-year-old female adult model (“Ella”, Body Height 1.60 m, Body Weight 58 kg) . As to the newborn, the model was obtained scaling the 6-year-old male child (“Thelonious”, Body Height 1.17 m, Body Weight 19.5 kg). The scaling was performed by considering the average ratio between the average size of the upper limbs (i.e. those ones on which the bracelets are supposed to be positioned in this study) of newborn and that one of a 6 years-old child (sizes derived from [Singh and Gupta, 1994; International Commission on Radiological Protection ICRP, 2002;]). The corresponding ratio is of 0.58. To estimate the error introduced by the scaling method, two morphological factors, the Body Mass Index (BMI) and the Body Surface Area (BSA) and two derived parameters (“BSA/ weight” and “weight<sup>1/3</sup>”) were calculated.

The comparison between the indexes computed from anatomical data of the newborn average data [ICRP, 2002], and from the sizes of the scaled model used in this study, are as follows:

$$[\text{BMI}]_{\text{reference}}=13.4 \text{ kg/m}^2; [\text{BMI}]_{\text{model}}=11.1 \text{ kg/m}^2 \text{ (difference of +17.7\%)}$$

$$[\text{BSA}]_{\text{reference}}=0.00751 \text{ m}^2; [\text{BSA}]_{\text{model}}= 0.00861 \text{ m}^2 \text{ (-14.6\%)}$$

$[\text{BSA}/\text{weight}]_{\text{reference}}=0.00215 \text{ m}^2/\text{kg}$ ;  $[\text{BSA}/\text{weight}]_{\text{model}}=0.00226 \text{ m}^2/\text{kg}$  (-5.4%)

$[\text{weight}^{-1/3}]_{\text{reference}}=0.659 \text{ kg}^{-1/3}$ ;  $[\text{weight}^{-1/3}]_{\text{model}}=0.641 \text{ kg}^{-1/3}$  (+2.7%)

where *reference* refers to anatomical data, whereas *model* refers to the child scaled model used here.

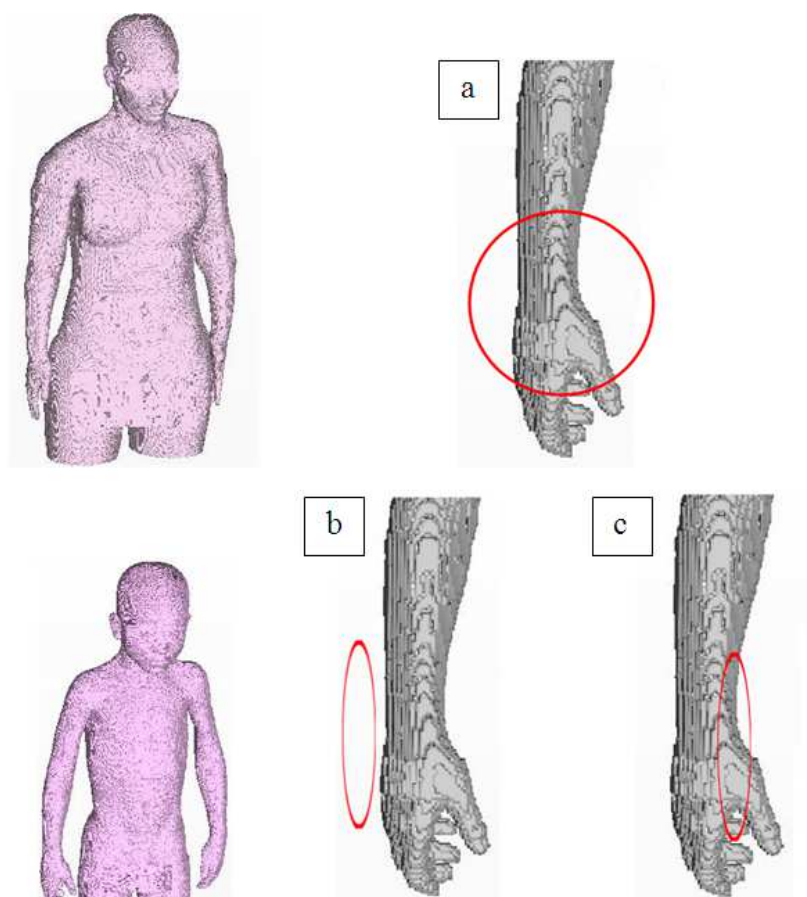


**Figure 1.1** Voxel models of the mother and the newborn male (on the left). The newborn model is not a scale drawing, being the height of the newborn model 0.42 times that one of the mother.

The RFID tag-reader placements considered in this study are shown on the right: a) **Position\_1**: reader in the coronal plane, in front of the body; b) **Position\_2**: reader in the sagittal plane, next to the wrist; c) **Position\_3**: reader in the sagittal plane, in front of the body. In this figure and in all the figures of this thesis, faces and genitals of the models have been disguised in a non-recongnizable manner according to the agreement for the use of Virtual Family.

The two morphological factors, BMI and BMA, show quite significant differences passing from *reference* to *model* data. This is due to the choice of the scaling criteria, aimed to fit the upper limb dimension (i.e., the body region closest to the RFID reader). However, when the differences are estimated on the derived data (“BSA/weight” and “weight<sup>-1/3</sup>”), the results show lower differences than for the morphological factors. To this purpose, some recent publications have shown a relationship

between the derived parameters and the Whole Body SAR (wbSAR) [Dimbylow and Bolch, 2007; Hirata et al., 2007; Kühn et al., 2009]. These studies found a good agreement of wbSAR in the down-scaled models. Therefore, from the EMF point of view, the applied scale could be considered acceptable. This is also in accordance with the results from different studies [Conil et al., 2008; Christ et al., 2010b], which found that, under specific conditions and at frequencies far from the whole-body resonance frequency, the scaling from adult to child doesn't affect the solution.

The tissues dielectric properties were taken from the data set available [Gabriel et al., 1996a; Gabriel, 1996b] and set according to the frequency of the specific simulation under investigation (in this case, 13.56 MHz). Possible variations of these values in newborn were not taken into account here, according also to Wang and Gabriel [Gabriel, 2005; Wang et al., 2006] that have shown small variations of dielectric properties with age, but hereinafter in this section.

## 2.2. Model of the RFID system and RFID technical parameters

Typically, the technical specifications of RFID readers and tags used in patient identification applications, show high variability because these devices are supposed to be general purpose. In general, these systems are based on passive inductive coupling RFID, mostly working at 13.56 MHz. Both reader and tag are air coils. The reader specifications provide, typically, the Read-Range (RR) distance, that is the maximum distance at which the reader is still capable to activate the tag and an average threshold level for the magnetic field ( $H_{th}$ ) necessary to activate the tag.

In order to identify RR average values for this type of applications, a reader from DATALOGIC s.r.l. (DATALOGIC J-Series) was considered to start the analysis here presented, as it is used in clinical applications for newborn-mother reconfirmation in Italian hospitals **[Errore. Riferimento a collegamento ipertestuale non valido.]**. The RR starting value was set to an RR distance of 10 cm. The classes of decoded tag were then identified accordingly to the technical specifications of the reader itself. The check of the related tag technical specifications allowed to calculate an  $H_{th}$  of 104 dB $\mu$ A/m (see, e.g., the class of tags Texas Tag-It ISO 15693 at <http://www.ti.com>).

For the sake of generality, the analysis was then enlarged from the values identified above (RR = 10 cm,  $H_{th}$  = 104 dB $\mu$ A/m), ranging RR from 5 to 15 cm and  $H_{th}$  from 90 to 130 dB $\mu$ A/m.

The reader coil was modeled in all simulations as a circular air coil of radius 3.5 cm, roughly estimated from the dimensions of the case of the DATALOGIC J-Series readers used for identity reconfirmation. For the sake of simplicity, the coil was modeled by only one turn.

As to the tag, its dimension is highly variable as well, so it was considered just as a passive element interposed between the reader and the body, and it consisted in a circular ring of copper with external and internal radius of 0.15 cm and 0.13 cm, respectively.

Reader and tag were placed near the models, in three different positions as shown in previous Figure 1.1, named as follows:

1. Reader in the coronal plane, positioned in front of the body (Figure 1.1a)
2. Reader in the sagittal plane, positioned next to the wrist (Figure 1.1b)
3. Reader in the sagittal plane, positioned in front of the body (Figure 1.1c)

In the first two cases, the tag is positioned on the axis of the reader at a distance of 1 cm from the reader, whereas, in the last case, the tag is positioned on the reader coil plane, at a distance of 1 cm from the coil edge, close to the wrist to account for the worst case exposure scenario. The minimum distance between the reader and the body was of 1.2 cm.

### 2.3. Simulations

The electromagnetic computations were performed using a commercial software package [CST EM STUDIO by CST GmbH, Darmstadt, Germany], which provides a solution to the time-dependent Maxwell's equations under magneto-quasi-static approximation . using a frequency-domain variant of the finite integration technique (FIT), based on the code originally described by Weiland [Weiland, 1977]. The whole computation domain was discretized using an automatic non-uniform hexahedral meshing algorithm, made available by the computational software itself. As a consequence the mesh cell resolution ranged from 0.32 to 2.4 cm, depending on the total volume on which the EMF computation was performed and on the relative position and dimension between the biological models and the RFID system.

In all simulations the magnetic field (H) and the electric field (E) levels were estimated and they will be shown as root-mean-square values of amplitude (*rms*). The point-SAR levels were estimated by exporting Electric field data in Matlab format [The MathWorks 2007b, Natick, Massachusetts, USA], by means of the well known expression binding it with the electric field E through the values of conductivity and density of each involved tissue. The whole body volume was partitioned into sub-body regions and the SAR was obtained by averaging point SAR values over these sub-volumes.

### 2.4. Compliance with exposure guidelines

The compliance of the EMF generated by RFID systems for newborn-mother identity reconfirmation, with the International Commission on Non-Ionizing Radiation Protection ICNIRP

guidelines [ICNIRP, 1998] was investigated calculating the maximum permitted  $H_{th}$  and RR as a function of the time of use of the reader close to the body. The basic restrictions for SAR were taken into account in terms of both whole body average SAR (wbSAR) and localized SAR (head and trunk,  $SAR_{ht}$  and limbs,  $SAR_l$ ), averaged over 6 minutes. Due to the SAR definition used here (i.e. peak instead of mass average), the peak localized point-SAR was calculated in place of the same measures averaged over 10 g of tissue ( $SAR_{10g}$ ). However, since the peak values of point-SAR are by-definition higher than the  $SAR_{10g}$ , the obtained results represent a conservative approach in terms of compliance to the guidelines. In the following, for the sake of clarity, the terms “compliance” should be always interpreted as “compliance” by the conservative approach described above.

### 2.5. Sensitivity to the variation of dielectric properties in newborn

In order to take into account possible changes in properties with age in this study the newborn dielectric properties were varied. In the last decade, several studies [Peyman et al., 2001; Gabriel, 2005; Wang et al., 2006; Peyman et al., 2009; Dimbylow et al., 2010; Peyman and Gabriel, 2010], addressed this issue, finding a strong correlation between the dielectric properties values and the age of the corresponding tissues. This is associated with the decrease of water content with time of the tissue itself.

Applying an approach recently proposed in literature [Dimbylow et al., 2010], an estimate of the variation of the newborn dielectric properties respect to the adult ones was derived from the ratios between the dielectric properties of newborn rat and adult rat (data from [Peyman, 2001]) calculated at 250 MHz. These ratios were then used to multiply the Gabriel adult’s properties values at 13.56 MHz to compute the corresponding newborn’s dielectric properties.

Dimbylow and colleagues [Dimbylow et al., 2010] approach is as follows: newborn tissues are classified in four classes, that is bone, skin and soft tissues, where soft tissues include the remaining tissues of the body except those ones whose properties would not change with age (e.g. air, blood, CSF, gallbladder bile and vitreous humor, i.e. the fourth class). In this study these four classes of tissues were applied to “Thelonious” model. From a quantitative point of view, the conductivity ratios were set to 3.9, 2.2 and 1.5 for bone, skin and soft tissues, respectively, while the permittivity ratios were set to 2.2, 1.9 and 1.25, setting the ratio of both conductivity and permittivity for the remaining tissues (fourth class) to 1 [Dimbylow et al., 2010].

### 3. Results

Figure 1.2 shows an example of the results obtained in the three tag-reader positions for newborn and mother. Magnetic (1<sup>st</sup> row) and electric (2<sup>nd</sup> row) fields magnitude have been shown on the surface of the two body models, for  $H_{th} = 104 \text{ dB}\mu\text{A/m}$  and  $RR=10 \text{ cm}$ . The distributions were limited to the reference values for human exposure defined by the ICNIRP guidelines [ICNIRP, 1998] at 13.56 MHz: that is to 0.073 A/m for the magnetic field and to 28 V/m for the electric field. As expected, magnetic field distribution is not affected by the presence of biological tissues, since their magnetic properties are the same of the vacuum (i.e. magnetic permeability  $\mu=\mu_0$  since  $\mu_r=1$  and magnetic susceptibility  $\chi=0$ ).

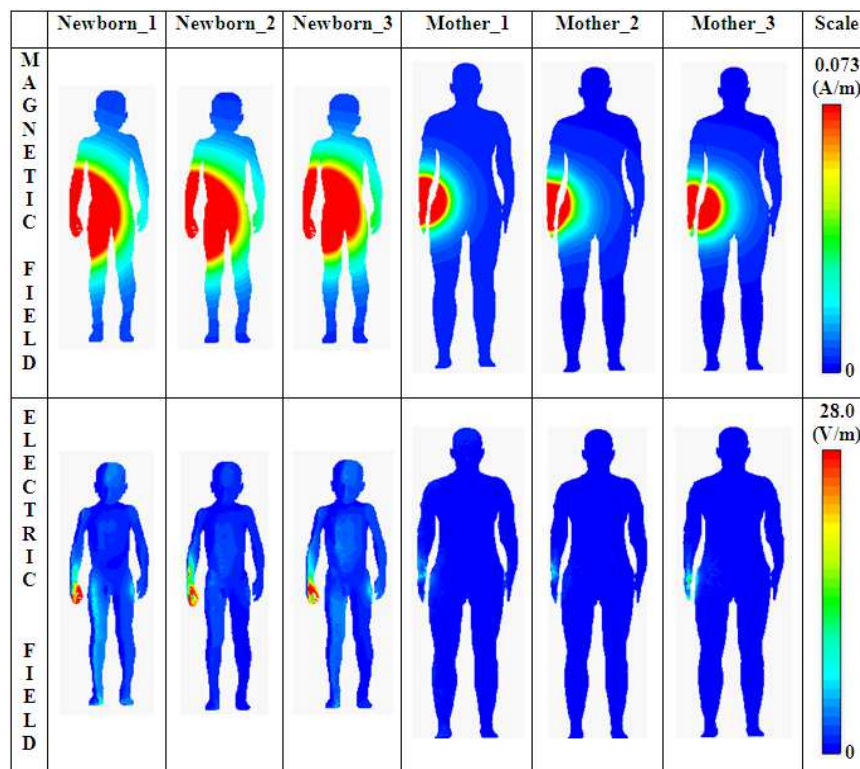


**Figure 1.2** Distribution of the magnetic field  $H$  (1<sup>st</sup> row) and the electric field  $E$  (2<sup>nd</sup> row) amplitude on the surface of the two body models in the three different coil positions. The distributions are limited to the value specified by the relative scale corresponding to the ICNIRP reference values for E- and H-field at 13.56 MHz. The newborn and mother models are shown in different scales to enhance the readability of the figure.

To better investigate the differences of the fields in different regions of the body, Figure 1.3, Figure 1.4 and Figure 1.5 show the amplitude mean values of  $H$ ,  $E$  and point-SAR, respectively, obtained for

$H_{th} = 104 \text{ dB}\mu\text{A/m}$  and RR of 10 cm, averaged over the various body regions, for the three considered reader positions, considering both mother and newborn exposure.

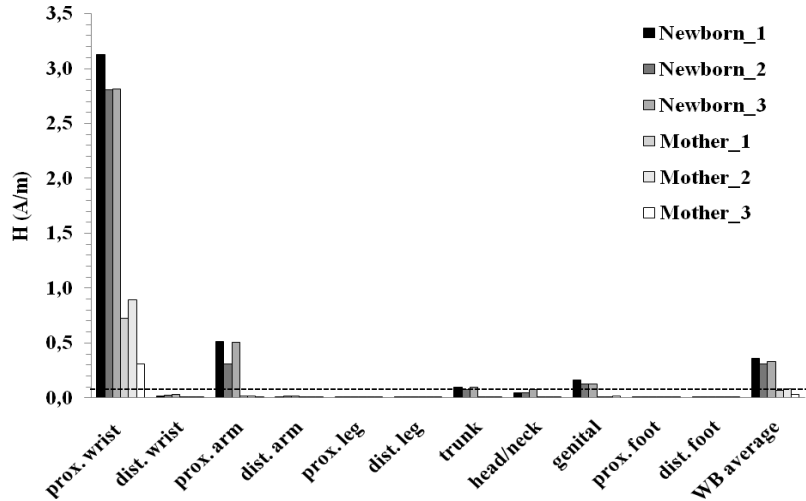


Figure 1.3. Amplitude mean values of the magnetic field H, averaged over different body regions, for the 3 configurations of mother and newborn. “prox.” and “dist.” indicate proximal and distal body districts, respectively, in regard to the position of the reader. The term “wrist” in the “prox. wrist” and “dist. wrist” should be read as “hand plus wrist”. The dashed line indicates the to the ICNIRP reference value for H-field at 13.56 MHz.

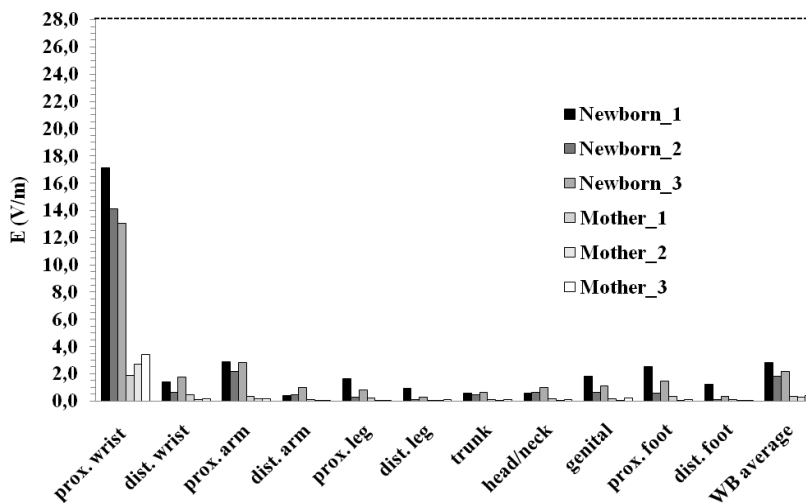
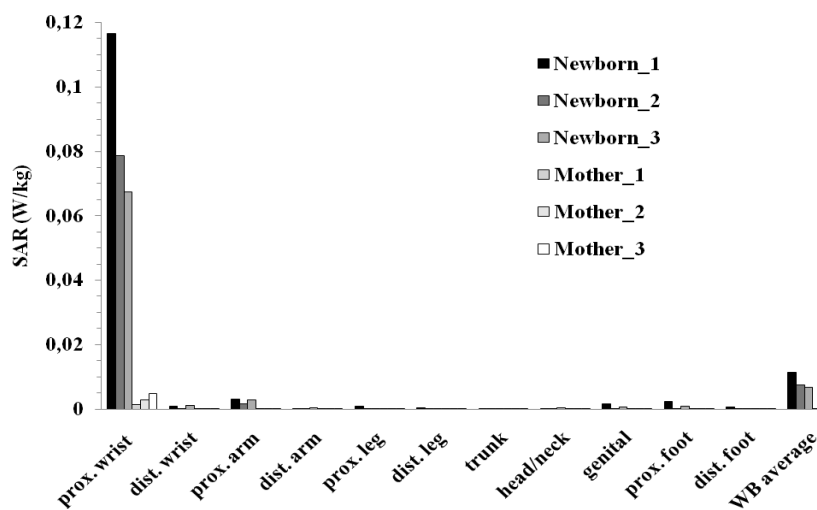


Figure 1.4. Amplitude mean values of the electric field E, averaged over different body regions, for the 3 configurations of mother and newborn. prox.” and “dist.” indicate proximal and distal body districts, respectively, in regard to the position of the reader. The term “wrist” in the “prox. wrist” and “dist. wrist” should be read as “hand plus wrist”. The dashed line indicates the ICNIRP limit.

These figures clearly show that for both mother and newborn the regions of the body closer to the reader are exposed to substantially higher level of EMF compared to the distal ones (mean reduction of about 57% for H values, 64% for E values and 74% for SAR values) and that E, H and SAR exposure levels in the newborn are always higher than the corresponding values for the mother (mean increase of about 6.6, 6.4 and 41.4 times respectively). Moreover, Figure 1.3 shows that in the newborn model the region of the body exposed to the higher level of H are not only the proximal wrist and arm but also the trunk, the genital organs and the head/neck regions, whereas in the mother model the highest levels of H exposure is restricted to the proximal wrist and arm.



**Figure 1.5. Mean values of point-SAR, averaged over different body regions, for the 3 configurations of mother and newborn. Legend: “prox.” and “dist.” indicate proximal or distal body districts, with respect to the position of the reader. The term “wrist” in the “prox. wrist” and “dist. wrist” should be read as “hand plus wrist”.**

Figure 1.6 shows the results of the study of the compliance with the ICNIRP guidelines. The curves represent the levels of  $H_{th}$  below which the exposure complies with EMF guidelines for a given Time of Use (ToU). The three panels show the maximum permitted  $H_{th}$  versus the ToU for the three SAR restrictions (wbSAR, point-SAR<sub>ht</sub> and point-SAR<sub>p</sub>, from top to bottom, respectively).

In each panel the three reader positions for each model are considered. Basically, the area below the curves corresponds to pairs of ToU and  $H_{th}$  values in compliance with ICNIRP guidelines. Being the typical range of the ToU in clinical practice from few s to 20 s, the vertical dashed lines on the panels divide them into two regions corresponding to:

- 1) a Critical Region, in which the ToU is lower than 20 s;

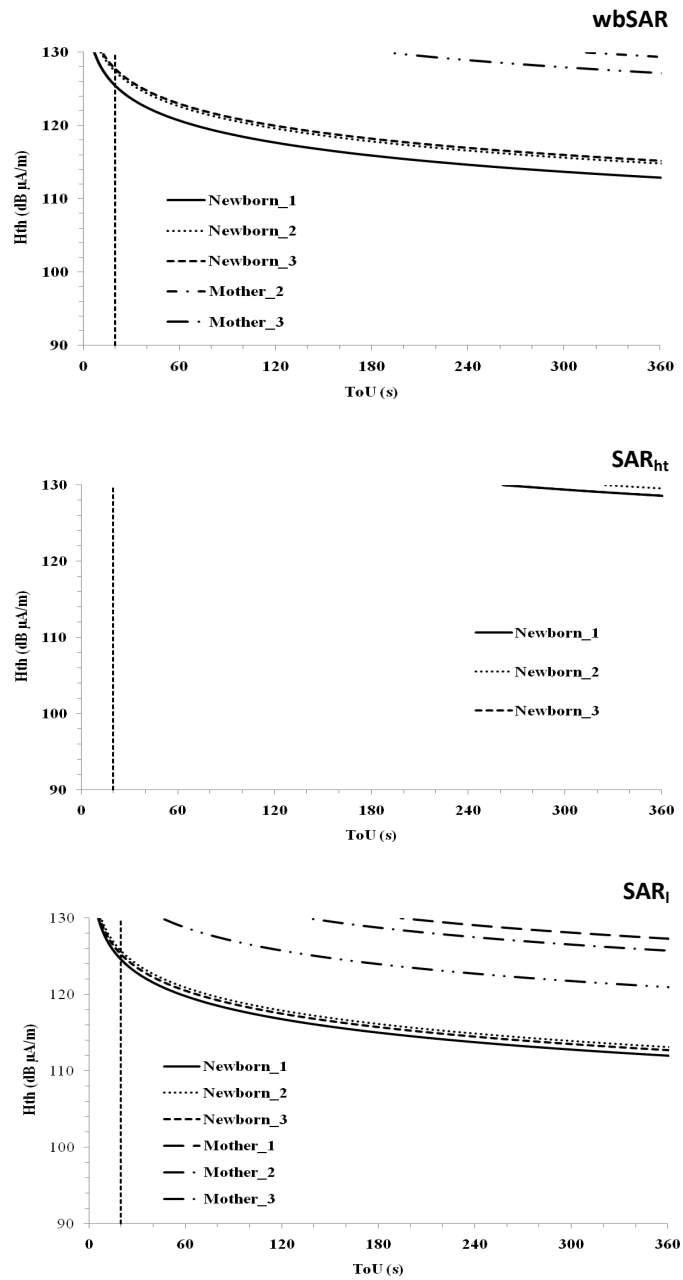


Figure 1.6. Maximum permitted  $H_{th}$  as a function of ToU of the reader close to the body for mother and newborn exposure in all tested reader positions, taken into account the basic restrictions for SAR. The vertical dashed line represents the boundary between the Critical and the Non-Clinical Practice region. A reader position not represented in the graphs means that the compliance is always achieved. The values on the vertical axis are in  $\text{dB } \mu\text{A/m}$ , where 100, 110, 120, and 130  $\text{dB } \mu\text{A/m}$  correspond to 0.100, 0.316, 1.00 and 3.16  $\text{A/m}$ , respectively.

- 2) Non-Clinical Practice Region, in which the ToU is between 20 s and 6 minutes, less probably occurring in practice.  $H_{th}$  values corresponding to ToU above 360 s are not shown because they are by definition in compliance.

In the Critical Region non compliance was found only for the three reader positions related to newborn exposure, limited to wbSAR (Figure 1.6, top panel) and  $SAR_l$  (Figure 1.6, bottom panel). In these cases, the worst case in which the newborn exposure was found not in compliance was for ToU higher than about 6 s and  $H_{th}$  of 130 dB  $\mu A/m$  ( $SAR_l$ , Newborn\_1 position). Furthermore, for ToU up to 20 s the compliance was always achieved for  $H_{th}$  less than 125 dB  $\mu A/m$ .

In the Non-Clinical Practice Region, for any ToU with  $H_{th}$  lower than 113 dB  $\mu A/m$  compliance is assured. On the contrary, mother exposure shows not compliance for wbSAR and  $SAR_l$  only in the Non-Clinical Practice Region. At  $H_{th}$  of 130 dB  $\mu A/m$  non compliance was found for ToU higher than about 45, 135 and 194 s for Mother\_3, Mother\_2 and Mother\_1 positions, respectively ( $SAR_l$ , Figure 1.6 bottom panel). Compliance of mother was achieved at any ToU for  $H_{th}$  lower than 121 dB  $\mu A/m$ . As to  $SAR_{ht}$ , only newborn exposure raises some issues of compliance (Newborn\_2 and Newborn\_3) but at  $H_{th}$  and ToU levels higher than the ones calculated for the other SAR estimates, which means that those levels are higher than pairs  $H_{th}$  and ToU already not in compliance for wbSAR and  $SAR_l$ .

The compliance is obviously affected also by the other technical parameter of an RFID system, that is the RR. Mother exposure complies with the guidelines for any ToU and RR (data not shown here). Roughly the same consideration holds also for newborn exposure, considering that compliance was found for any ToU lower than 240 s and for any RR lower than 14 cm.

The influence of possible variation with age of the dielectric properties of tissues in the newborn model was studied considering only “Newborn\_1” position, the one which has been found to be the worst case scenario in terms of compliance with ICNIRP guidelines. Table 1.1 shows the effect of the change in dielectric properties on the whole body average SAR (wbSAR) and on the localized SAR (head and trunk,  $SAR_{ht}$  and limbs,  $SAR_l$ ). The effect is provided in terms of ratio between these quantities estimated by means of the Dimbylow approach [Dimbylow et al., 2010] with respect to the ones calculated by means of the adult dielectric properties (“Newborn\_1” position). Data in the table clearly show that varying the dielectric properties results in negligible changes in the  $SAR_{ht}$  (about 5% lower) and more noticeable changes in the wbSAR and  $SAR_l$  (an increase of about 23% and 19%, respectively).

#### 4. Discussion

The ubiquity of RFID technology, including health applications, does not correspond to a parallel increase of studies on its possible impact on health in terms of EMF exposure. To date, no studies addressed this issue, neither on possible adverse health effects nor on exposure assessment, that is one of the most crucial steps in any risk assessment processes related to potentially hazardous agents. In this work, the exposure assessment to EMF generated by an increasingly diffuse RFID health applications, such as that one of systems for identity reconfirmation of mother and newborn by use of tagged wristbands, is addressed.

Results show that the mean values of E, H and SAR averaged over different body regions are higher in the body's region closer to the reader than in the distal one, with a trend of higher values in the newborn model compared to the mother for all reader positions (see Figures 1.3-1.5). Moreover, for newborn exposure, the field distribution across body's region shows that the part of the body exposed to the highest value is not only restricted to the proximal limb, but tends to extend up to the trunk, genital organs and head/neck region, including therefore more sensitive organs. This results particularly clear looking at the H field distribution (see Figure 3). As a consequence to position, when possible, the RFID tag on the ankle in place of the wrist, as sometime is done in clinic for newborns, could be advisable. So doing, the reader would result at major distance from the more sensitive organs, exposing those body regions to lower levels of fields and thus reducing the whole body averaged power absorption. The influence of the different reader positions varies as a function of the body region or of the model taken into account (i.e. newborn vs. mother). For example on average, the highest values were found for newborn exposure and reader in the coronal plane positioned in front of the body (Newborn\_1), . On the other side, the reader in the sagittal plane, positioned next to the wrist (Newborn\_2) is the more advisable to reduce the exposure levels.

The study of the compliance of EMF levels generated by RFID systems with the basic restrictions of the ICNIRP guidelines [ICNIRP, 1998] was investigated. as a function of the variability of some reader technical specifications, such as the magnetic field level  $H_{th}$  needed to awake the tag and the read-range distance RR, and the Time of Use (ToU) of the device close to the body.

In the Critical Region, that is the region corresponding to ToU lower than 20 s, the compliance was found related to  $H_{th}$  variability, only for newborn exposure (even for ToU of few seconds).

In the Non-Clinical Practice Region (i.e., for ToU ranging from 20 s up to 360 s), both the compliance of newborn and mother exposure were found a function of  $H_{th}$  ( $H_{th}$  higher than 113 dB  $\mu$ A/m for newborn and  $H_{th}$  higher than 121 dB  $\mu$ A/m for mother exposure). Conversely, the RR variability

resulted almost irrelevant for the compliance both for mother and newborn exposure, for all reader positions.

As to the sensitivity to the variation of dielectric properties with age, major variations were found in the  $wbSAR$  and  $SAR_i$ , while almost negligible variation were found in the  $SAR_{ht}$  (see Table 1.1).

**Table 1.1. SAR values calculated modeling “Thelonious” model by the Dimbylow approach (2<sup>nd</sup> column from the left) and by the adult’s dielectric properties (3<sup>rd</sup> column from the left). The last column from the left shows the ratios between these two quantities estimated.**

	Dimbylow	Adult	Ratios (Dimbylow/Adult)
$wbSAR$ (W/kg) *	0.0141	0.0115	1.23
$Point-SAR_{ht}$ (W/kg) *	0.00114	0.00121	0.95
$Point-SAR_i$ (W/kg) *	0.350	0.294	1.19

\* The units indicated refer only to “Dimbylow” and “Adult” columns.

That difference could be explained considering the different rate of variations of the tissues conductivity in the various regions together with the corresponding negligible changes in the electric field. For example the increase in conductivity of the limbs tissues is higher than that one for head and trunk tissues. However, one should take into account that these results were obtained considering only a roughly estimation of the dielectric properties in newborn. Hence, the concluding remark of previous authors [Gabriel, 2005], who stated that elaboration of the question of the exposure of children versus adults must await more appropriate dielectric data, is still valid.

Same considerations hold also for the newborn exposure assessment, which could be affected by the use of a scaled model of a child. On the one hand, as suggested by Bakker and colleagues [Bakker et al., 2010], the down-scaling shows good agreement for whole body SAR as was done in this work. On the other hand, additional studies should be performed using a non-uniform down scaling thus taking into account the variation of the development timing of different body tissues or, even better, using a real newborn model when it will be available.

To complete that analysis, the human variability in fat thickness due to pregnancy could, in perspective, affects the results and should be considered. To that purpose in the mother model the ratio between fat and muscle mass was increased and the effect of this change was evaluated in terms of

SAR variation. Both whole-body SAR and localized SAR ( $SAR_l$  and  $SAR_{ht}$ ) resulted mildly affected by the increased fat/muscle ratio: in particular  $wbSAR$ ,  $SAR_l$  and  $SAR_{ht}$  showed a decrease of 12.3%, 11.3% and 6.1%, respectively. These results are consistent with previous studies [Dimbylow, 2007; Nagaoka et al., 2007] and suggest that the values obtained using the mother model. and suggest that the values obtained using the mother model (Ella) are a conservative predictor of SAR in a pregnant woman.

---

# **RFID system for newborn identity reconfirmation: exposure assessment of a realistic newborn model and effects of the variation of the dielectric properties with age**

*(This chapter is based on “Fiocchi S, Parazzini M, and Ravazzani P. 2011. RFID system for Newborn identity reconfirmation in hospital: exposure Assessment of a realistic newborn model and effects of the change of the dielectric properties with Age. Progress in Biophysics and Molecular Biology, 107(3):443–448”)*

## **1. Introduction**

In the previous chapter the great advantages in terms of reliability, safety, speed and automatism that RFID application can offer has been discussed together with an accurate exposure assessment by a computational approach of EMF generated on mother and newborn by a specific RFID system for identity reconfirmation. Results of that study (detailed in [Fiocchi et al., 2011]) showed a trend of higher exposure in newborn compared to the mother and indicated that the time of use of the reader close to the body plays a crucial role in the assessment of the compliance with current EMF exposure guidelines.

In particular has been found that the use of readers typical for such RFID application, even for less than 10 s, could produce an overexposure of the newborn in terms of SAR levels compared to the International Commission on Non-Ionizing Radiation Protection [ICNIRP 1998] limits. However, that study presented two critical issues to be addressed. First of all, the newborn model used was derived by scaling uniformly a six-year old child, method that could introduce uncertainties in the results of dosimetry as reported by several authors [Gandhi et al., 1996, 2002; Schönborn et al., 1998; Wang and Fujiwara, 2003; Wiart et al., 2005]. Secondly, the use as dielectric properties of the data available for human adults [Gabriel et al., 1996 and Gabriel, 1996], disregarding their possible variation with age, should introduce additional uncertainties.

The detailed knowledge of the dielectric properties of the biological tissues is essential for the understanding of the interaction of the EMF with the body. For that reason, the variability of the dielectric properties with age due to the changes in body tissues composition has been object of different studies both in the past [e.g. Thurai et al., 1984, 1985], particularly on brain tissue for

newborn, young and adult species of mice and rabbits, and also more recently [e.g. Gabriel, 2005; Lu et al., 1996; Olawale et al., 2005; Peyman et al., 2001, 2007; Peyman and Gabriel, 2010; Schmid and Uberbacher, 2005]. In general, these studies showed an increased conductivity and permittivity of the young tissues with respect to the old ones. However, these results were mainly found investigating the microwave frequency range (higher than 300 MHz up to hundreds GHz), addressing the exposure to communication systems, whereas little is known about the influence at lower frequencies.

The study presents hereafter aims to address a complete exposure assessment of the EMF generated by a realistic RFID system at 13.56 MHz on a realistic newborn model, starting from both these two open issues. On one hand, the exposure was estimated on a realistic voxel model of a newborn (only recently made commercially available). On the other hand, in the same newborn model, the influence of the variation of the dielectric properties with age is investigated.

## 2. Materials and Methods

The EMF induced in a newborn model generated by a typical RFID system for newborn-mother identity reconfirmation were estimated by computational techniques implemented by a commercial code (CST EM STUDIO by CST GmbH, Darmstadt, Germany).

### 2.1 Newborn Model

Figure 2.1 shows the newborn realistic voxel model, in the following called “Baby”, together with the model of the RFID source for newborn-mother reconfirmation, used in the simulations.

The Baby model belongs to the so called CST Voxel Family (CST GmbH, Darmstadt, Germany), a group of seven human models of different gender, age, stature and weight. Baby is an 8-week female (size 57 cm and weight 4.2 kg) based on high resolution magnetic resonance (MR) images segmented in a voxel based format at a resolution of  $0.85 \times 0.85 \times 4$  mm. The segmentation, made partially automatically by GSF (GSF National Research Centre for Environment and Health, Neuherberg, Germany) allows to distinguish 30 tissues types, listed in Table 2.1 together with the correspondence between them and those ones considered by the dielectric properties database of the National Research Council, Institute for Applied Physics “Nello Carrara” [IFAC CNR] (see the two columns on the left of Table 2.1). The voxel model has originally been made for ionizing radiation dosimetry purposes. It is a hybrid model, in which testes have been inserted into the originally female model to be able to cover both sexes without the need of two separate models.

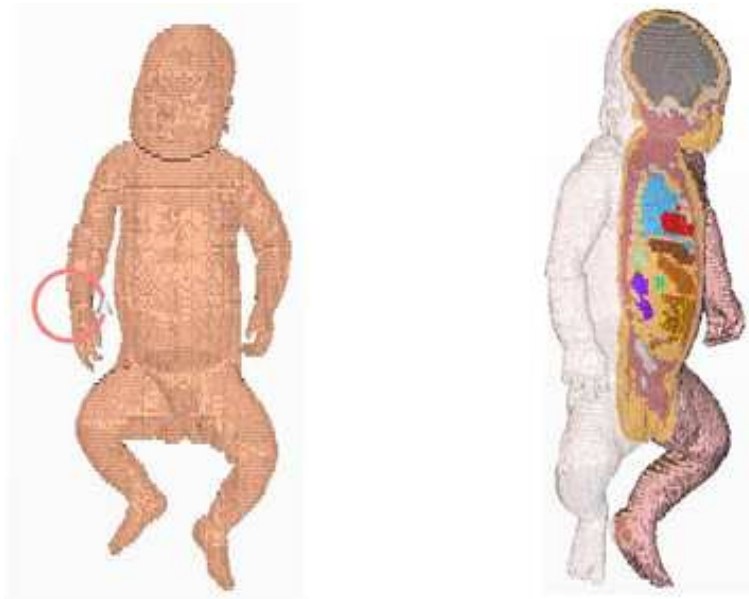


**Figure 2.1.** Left: Realistic newborn voxel model and RFID source. The coil used in the simulations, modeling the reader, is visible over the right wrist. Right: Longitudinal section of the Baby model that also allows to distinguish some tissues.

## 2.2 Tissue dielectric properties

As discussed above, four models of dielectric parameters were applied to “Baby” tissues

- 1) *Adult Dielectric Properties (ADP) model.* It is based on the data measured by [Gabriel et al. 1996] and made available on the web by a calculator provided by the National Research Council, Institute for Applied Physics “Nello Carrara” [IFAC CNR] according to the frequency of the specific simulation under investigation (in this case, 13.56 MHz).
- 2) *Wang Dielectric Properties (WDP) model.* Wang and colleagues [Wang et al., 2006] derived an empirical formula for the complex relative permittivity of various tissues as a function of age in a range of frequencies from 900 to 1800 MHz. This formula allows to calculate the dielectric properties as a function of the total body water content which varies with age. This mechanism, based on the polarization of tissue water, is typical of the dispersion range  $\gamma$  (i.e. in the GHz region). However, due to the lack of data at low frequency, this approach has been extended to the tail end of the  $\beta$  dispersion (i.e. in the kHz region), based on the assumption that changes in the water content at lower frequencies are similar to those at microwave frequencies. In this study, the extension of the Wang approach at the frequency of 13.56 MHz was performed using as relative permittivity of water a value obtained applying the approach

proposed by Kaatze [Kaatze, 1989], and calculated at the frequency and at the temperature (37 °C) of interest.

- 3) *Dimbylow Dielectric Properties (DDP) model.* Dimbylow and colleagues [Dimbylow et al., 2010] estimated the newborn dielectric properties calculating the ratios between the dielectric properties of newborn rat and adult rat (using the data measured in the study of Peyman and colleagues [Peyman et al., 2001]) and by using these ratios as multipliers of the adult dielectric properties in a frequency range from 20 MHz to 6 GHz. They proposed a classification of the newborn tissues in four groups: bone, skin, soft tissues and a set of tissues whose properties would not change with age (e.g. air, blood, CSF, gallbladder bile and vitreous humor, i.e. the fourth group). As to class of the soft tissues, it includes all the remaining tissues of the body whose properties change with age. The conductivity ratios were set to 3.9, 2.2 and 1.5 for bone, skin and soft tissues, respectively, while the permittivity ratios were set to 2.2, 1.9 and 1.25, setting the ratio of both conductivity and permittivity for the remaining tissues (fourth group) to 1. Here the same approach was used with the same ratios at 13.56 MHz to compute the corresponding newborn dielectric properties, applied to the adult properties values (ADP approach).
- 4) *Literature Dielectric Properties (LDP) model.* In this model, additional tissues with respect to the DDP approach were included. For all considered tissues, the ratios between the dielectric properties of adult and newborn were estimated on the basis of data available in literature [Gabriel, 2005; Lu et al., 1996; Peyman et al., 2001, 2005, 2007, 2009; Thurai et al., 1984, 1985; Schmid and Uberbacher, 2005]. That ratio was set to 1 for the tissues of the model for which information are available only on adult dielectric properties. In case of more than one ratio identified in literature at different frequencies for the same tissue, the one at the frequency closest to 13.56 MHz was selected.

The full list of the tissues and the related ratios used in this study for the various approaches are shown in Table 2.1, where also the correspondence between the tissues of the “Baby” model and the IFAC CNR database are reported.

Particular attentions should be given to the dielectric properties of the bone, whose dielectric properties are particularly different in adult and children, due to the physiological changes between them and to its variegate composition.

As a common approach to all models, the dielectric properties of the bone structure were estimated as a weighted average of the properties of its components, based on the relative percentage of the

composition as published by International Commission on Radiological Protection ICRP in 2002 [ICRP, 2002].

**Table 2.1. Column 1 and 2 from the left: Correspondence between the tissues of the Baby model and the IFAC CNR database of dielectric properties tissues. Column 3, 4 and 5: Conductivity ratios used in the different models. As to the bone structure (Bone\*) see the text for details. The permittivity ratios are not reported due to the magneto quasi-static approximation.**

<i>Baby Tissue</i>	<i>Correspondence IFAC CNR</i>	<i>WDP Conductivity Ratios</i>	<i>DDP Conductivity Ratios</i>	<i>LDP Conductivity Ratios</i>
Adrenals	Glands	0.85	1.50	1.00
Bone average	Bone*	2.61	3.90	3.91
Brain	Grey/White matter (avg)	0.74	1.50	1.23
Breast glandular tissue	Glands	0.85	1.50	1.00
Colon contents	Colon	0.73	1.50	1.00
Colon wall	Colon	0.73	1.50	1.00
Eye bulb	Eye sclera	1.02	1.00	0.96
Eye lens	Lens	0.82	1.50	1.42
Fat	Fat	1.50	1.50	3.60
Gall bladder	Gall bladder	0.92	1.50	1.00
Gall bladder contents	Gall bladder bile	0.87	1.00	1.00
Heart	Heart	0.70	1.50	0.58
Kidney average	Kidney	0.68	1.50	0.51
Liver	Liver	0.78	1.50	0.82
Lung	Lung inflated	0.93	1.50	2.00
Muscle	Muscle	0.83	1.50	1.01
Oesophagus	Oesophagus	0.76	1.50	1.00
Ovaries	Ovaries	0.69	1.50	1.00
Pancreas	Pancreas	0.85	1.50	1.00
Skin	Skin dry	0.63	2.20	1.22
Small intestine contents	Small intestine	0.64	1.50	1.00
Small intestine wall	Small intestine	0.64	1.50	1.00
Spleen	Spleen	0.65	1.50	0.85
Stomach contents	Stomach	0.77	1.50	1.00
Stomach wall	Stomach	0.77	1.50	1.00
Testes	Testis	0.65	1.50	1.00
Thymus	Thymus	0.85	1.50	1.00
Thyroid	Thyroid	0.84	1.50	1.00
Urinary bladder conts.	Bladder	1.16	1.50	1.00
Urinary bladder wall	Bladder	1.16	1.50	1.00
Uterus cervix	Uterus	0.69	1.50	1.00

This is because the bone structure experiences considerable changes in composition with age [Peyman et al., 2001]. The full list of the bone structure components and the related percentages used in the weighted averaging approach are shown in Table 2.2.

**Table 2.2. Bone structure components for adult and newborn. The relative percentage for adult and newborn bone composition was derived from [ICRP, 2002].**

<i>Component of bone tissue</i>	<i>% in the bone tissue</i>	
	<i>Adult</i>	<i>Newborn</i>
Bone cortical	52.9	46.1
Bone marrow	34.8	13.6
Cartilage	10.5	35.1
Miscellaneous (average blood-periosteum)	1.8	5.2

### 2.3 Model of the RFID system and RFID technical parameters

The source of the RFID system (i.e. the reader) was modeled as a coil in which the current flows at a frequency of 13.56 MHz, whose technical specifications were derived by commercial devices as described in the above mentioned study [Fiocchi et al, 2011]. The Read-Range (RR) distance, that is the maximum distance at which the reader is still capable to activate the tag and the magnetic field threshold level ( $H_{th}$ ) necessary to activate the tag were considered as technical specifications of the RFID system. They were set to an average value of  $RR = 10$  cm,  $H_{th} = 104$  dB  $\mu A/m$  and used to calculate and to model the source (one turn circular air coil of radius 3.5 cm, current of 0.31 A for the reader, a coil with external and internal radius of 0.15 and 0.13 cm respectively for the tag). For the sake of generality, the analysis was then enlarged from the values given above ( $RR = 10$  cm,  $H_{th} = 104$  dB  $\mu A/m$ ), ranging from 5 to 15 cm for RR and 90 to 130 dB  $\mu A/m$  for  $H_{th}$ . The tag was placed coaxially between the reader and the Baby model (distance tag-Baby of 1 cm), in the frontal plane.

The positioning of the reader (and hence of the tag) was set according to the worst exposure scenario identified in the previous publication [Fiocchi et al., 2011], i.e. reader positioned in front of the body in the frontal-plane near to the wrist, as shown in Figure 2.1. The minimum distance between the reader and the body was set to 1.2 cm.

### 2.4 Simulations

The commercial software package used for electromagnetic computation (CST EM STUDIO by CST GmbH, Darmstadt, Germany) provides a solution to the time-dependent Maxwell's equations using a frequency-domain variant of the Finite Integration Technique (FIT) under magneto quasi-static approximation. The whole computation domain was discretized using an automatic hexahedral meshing algorithm. The applied meshes were of 7.890.372 cells, with a minimum and maximum mesh resolution of 0.85 mm and 4 mm (corresponding to the minimum and maximum voxel size in the three different dimensions). The mesh was non-uniform in the Baby model, while it was uniform in the background. The magnetic field ( $\mathbf{H}$ ) and the electric field ( $\mathbf{E}$ ) were calculated as the root-mean-square (*rms*) values of their magnitudes.

The SAR *Basic Restrictions* were taken into account in terms of both whole-body average SAR (wbSAR) and localized SAR (head and trunk,  $\text{SAR}_{\text{ht}}$  and limbs,  $\text{SAR}_{\text{l}}$ ), averaged over 6 min. Due the SAR definition (i.e., peak instead of mass average) adopted here, the peak localized point SAR was calculated in place of the same measures averaged over 10 g of tissue (SAR<sub>10g</sub>). However, since the peak values of point SAR are, by definition, higher than the SAR<sub>10g</sub>, the obtained results represent a conservative approach in terms of compliance with the guidelines. For clarity, in the following the term “compliance” should be interpreted as compliance using the conservative approach described above. The point-SAR levels were estimated by exporting data of the electric field in Matlab format (The MathWorks 2007b, Natick, Massachusetts, USA), and computing using the well-known expression binding it with  $\mathbf{E}$  through the values of conductivity and density of each involved tissue. The whole body volume was divided into body regions (proximal and distal limbs, head/trunk). The point SAR levels over limbs ( $\text{SAR}_{\text{l}}$ ) and over the head and trunk ( $\text{SAR}_{\text{ht}}$ ) were computed, considering the maximum point SAR values among the levels over the tissue in the sub-volumes considered. The whole body SAR (wbSAR) was obtained averaging the point SAR levels.

## 3. Results

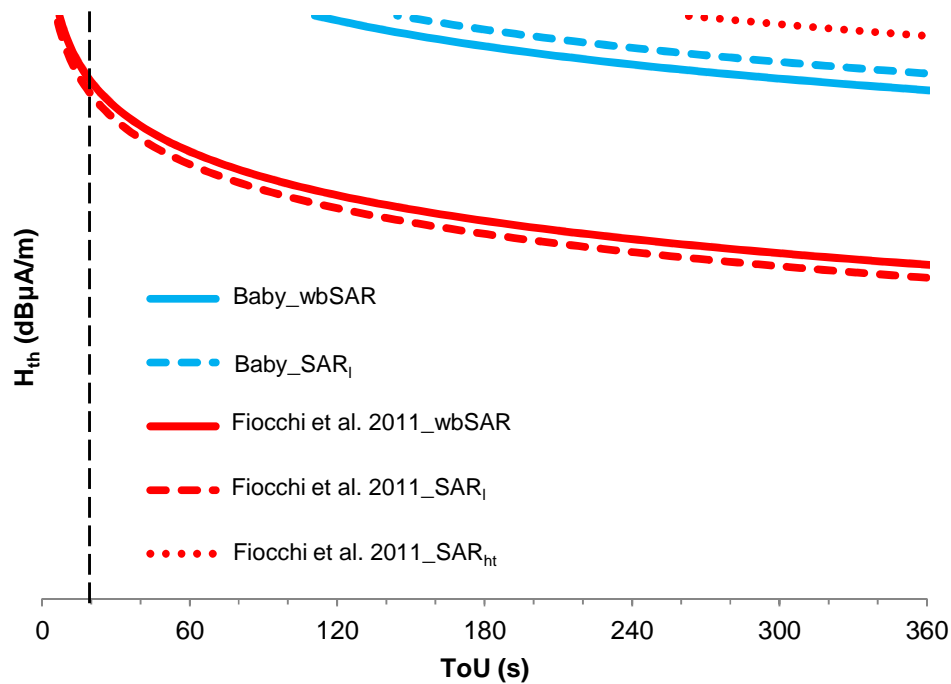
### 3.1 Baby model with ADP dielectric properties

Figure 2.2 shows the analysis of the compliance with the ICNIRP guidelines [ICNIRP, 1998] when the exposure of the Baby model is considered. The curves represent the levels of  $H_{\text{th}}$  below which the exposure complies with EMF guidelines for a given Time of Use (ToU). The blue lines show the maximum permitted  $H_{\text{th}}$  versus the ToU for the SAR basic restrictions computed for the Baby model. The area below each curve corresponds to pairs of ToU and  $H_{\text{th}}$  values in compliance with ICNIRP guidelines. As discussed in Fiocchi et al., 2011, the typical range of the ToU in clinical practice is

from a few seconds to 20 s, and the vertical dashed line divides them into two regions corresponding to: (1) a critical practice region, in which the ToU is lower than 20 s; and (2) a non-clinical practice region, in which the ToU is between 20 s and 6 min, probably less occurring in practice.  $H_{th}$  values corresponding to ToU above 6 minutes are not shown because they are, by definition, in compliance.

In the same figure the results obtained in the identical condition with the scaled child model [Fiocchi et al., 2011] are shown.

The curves relative to the Baby model (blue curves in Figure 2.2) are totally inside the non-clinical practice region, running from a minimum ToU of about 110 s (for the wbSAR curve) with an  $H_{th}$  of 130 dB  $\mu\text{A}/\text{m}$ .  $\text{SAR}_{nt}$  is not shown because results in compliance for any ToU and  $H_{th}$  values considered here. Therefore, this means that, at least for the range of  $H_{th}$  considered here, the system is always in compliance inside the critical practice region for all SAR restrictions.



**Figure 2.2.** Maximum  $H_{th}$  as a function of the time of use ToU of the reader close to the body for Baby exposure in the tested reader position, taking into account the SAR Basic Restrictions. The vertical dashed line represents the boundary between the critical and the non-clinical practice region (see text for details). The values on the vertical axis are in dB  $\mu\text{A}/\text{m}$ , where 100, 110, 120, and 130 dB  $\mu\text{A}/\text{m}$  correspond to 0.1, 0.316, 1.00, and 3.16 A/m, respectively. The blue curves are relative to the Baby model, while  $\text{SAR}_{nt}$  curve is not shown because results in compliance for any ToU and  $H_{th}$  considered in this study. The results on the scaled newborn model obtained in the same condition and published in [Fiocchi et al., 2011] are shown for comparison (red curves).

Noticeable differences can be found among these results and those ones obtained with the scaled child (red curves), being the red curves fully included in both regions (critical and non-clinical practice regions), at least for  $wbSAR$  and  $SAR_1$ . As an example, the point  $wbSAR$  and the  $SAR_1$ , estimated with the scaled child resulted of about 12 dB and of about 14 dB, respectively, greater than in the Baby model, on equal average technical specifications ( $H_{th}=104 \text{ dB}\mu\text{A/m}$  and  $RR=10 \text{ cm}$ ).

### 3.2. Effect of change of the dielectric properties with age

Figure 2.3 shows the 99<sup>th</sup> percentile of the magnitude of the electric field, computed in different tissues (bone, brain, fat, hearth, liver, lung, muscle, ovaries, skin and testes), for all four dielectric properties models considered in this study, due to the exposure of the Baby model to the RFID system. As one can expect, the maximum values were found for skin disregarding the model considered (values from 4.6 to 5.6 V/m). As to the differences between the approaches, considering the ADP model as reference, the average variation was of about 0.61 dB. The maximum increase is shown by the WDP model in the brain (4.17 dB) whereas the maximum decrease of E is in the ovaries (-9.85 dB) using the LDP model. Excluding skin, brain and ovaries, the average variation decrease to 0.30 dB, with a maximum increase of 0.95 dB in the bone and a maximum decrease of 3.86 dB in the heart tissue, both obtained using LDP model. In general terms, the LDP model was found the one with the maximum average change across tissues (-1.72 dB), whereas the WDP model showed the minimum average change (-0.01 dB). Similar computation was performed for magnetic field, but as expected, no significant differences were obtained among the four approaches.

Figure 2.4 shows the curves of compliance with ICNIRP guidelines [ICNIRP, 1998] for  $wbSAR$  (Figure 2.4a) and  $SAR_1$  (Figure 2.4b).  $SAR_{ht}$  is not shown because in compliance for any combination of  $H_{th}$  and ToU. The details of the structure of the figure are the same argued for the Figure 2.2 above.

As discussed for ADP model (corresponding to the blue curves of Figure 2.3 above), also for all the other models, the curves are well inside into the non-clinical region (the curves start from a minimum ToU of 60-80 s). However, the DDP model shows a curve of compliance closer to the critical region (i.e., with ToU lower than 20 s) with respect to ADP and the other models, at least for  $wbSAR$ . For  $SAR_1$  the curve related to WDP model is the closest one to the critical region.

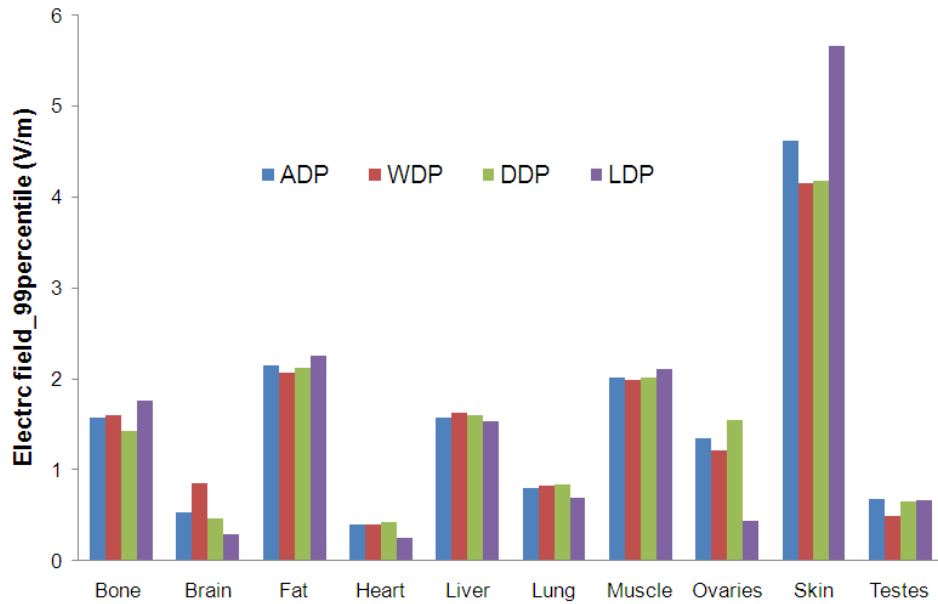


Figure 2.3. 99<sup>th</sup> percentile of the magnitude of the electric field E in different body regions for the four considered dielectric property models.

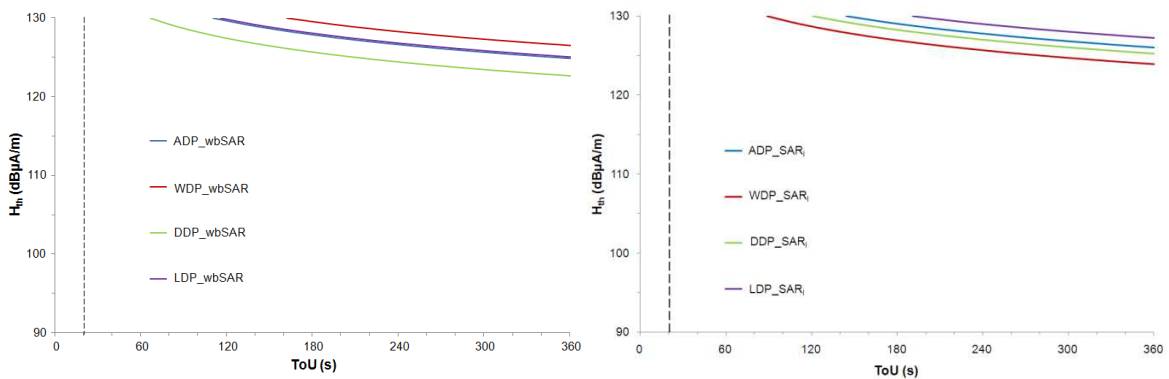


Figure 2.4: Maximum  $H_{th}$  as a function of time of use of the reader close to the body for Baby exposure in the tested reader position, taking into account the basic restrictions for SAR (4a wbSAR; 4b SAR<sub>l</sub>). Details as in previous Figure 2.3. Each curve is relative to one of the four Baby model tested (as described by the label in the panel).

#### 4. Discussion

As previously discussed there are very few studies on EMF exposure assessment of newborn and this lack of knowledge is particularly critical considering the spread of a new technology, such as the RFID. Starting from two critical issues of modeling highlighted in a previous study on assessment of EMF generated by an RFID system for mother-newborn identity confirmation in hospital [Fiocchi et

al., 2011], this work investigated the exposure matrices (including induced magnetic field, electric field and SAR levels) computed on a realistic newborn model (Baby) applying adult dielectric properties. After that, using approaches and data available in literature, the effect of the variations of the tissues dielectric properties with age was addressed versus the adult properties.

Considering the average technical specifications currently in use, the exposure matrix in Baby shows the systems comply with the ICNIRP guidelines [ICNIRP, 1998]. Only for Time of Use longer than about 2 minutes and for  $H_{th}$  values (i.e., power level of the reader) higher than 125 dB $\mu$ A/m, the computation shows no compliance, at least for wbSAR and SAR<sub>r</sub>. This is different from what was obtained using a scaled child [Fiocchi et al., 2011], for which the compliance is not fulfilled even for Time of Use of just a few seconds. Moreover, using Baby, the SAR compliance curves (see Figure 2.2 above) are completely in the non-clinical practice region, differently from the SAR compliance curves for the scaled child, partially in the critical region.

These results, and the consideration that the area below each curve is largely wider for the Baby curves than for the scaled child ones, suggest that the computation obtained in the previous study is more conservative than for a realistic newborn model. The large discrepancy in the SAR values is probably due to the great difference in the two models, particularly in terms of geometry, number and type of dielectric tissues included, forms and position.

As to the effect of the variation with age of the dielectric properties for this application (at 13.56 MHz), three different approaches were implemented for the Baby model, and compared with a model based on the adult dielectric properties. The comparison of the exposure matrices in terms of electric field shows, in general terms, an average difference of no more than 0.5 dB (see Figure 2.3 above). In particular not well defined trend can be identified, that is no model shows similar differences (in terms of value and sign) across tissues. When the compliance in terms of SAR is considered, all curves were still found in the non-clinical region, distant from the critical one. However, some more specific differences can be identified. For wbSAR, the model based on the DDP approach [Dimbylow et al., 2010] is not in compliance after a ToU of about 1 minute (i.e., half the value for the adult model ADP). For SAR<sub>r</sub>, both DDP and WDP [Wang et al., 2006] models do not fulfill the compliance at ToU shorter than ADP (about 1 minute for WDP and 2 minutes for DDP). On the contrary, the model built on literature data (LDP) is the only one showing compliance for ToU longer than ADP, for both wbSAR and SAR<sub>r</sub>.

Results of this study could lead to the conclusion that the effects of the changes in dielectric properties at 13.56 MHz on SAR levels cannot be negligible. However, these changes are lower than one could expect, considering the variation of the dielectric properties among the models, i.e., on the

average: -20% for WDP tissues, +45% for DDP tissues and +1% for LDP tissues (see Table 2.1, above).

In summary, the choice of the dielectric properties model does not change the final conclusion about compliance, but could influence the maximum permitted time of use of a given RFID system for newborn identification in hospital. Moreover, these results could suggest a trend towards a slight underestimation of the exposure using adult properties.

This result, however, continues to support the consideration that there is no clear evidence of which is the best choice in terms of dielectric properties for newborn model. This reinforces the need of further investigations based on measures on newborn dielectric properties in the low frequency range.

---

---

## Exposure assessment of a UHF RFID reader in adult, child, pregnant woman and fetus anatomical models

*(This chapter is based on “Fiocchi S, Markakis I, Ravazzani P, Samaras T. 2013. SAR exposure from UHF RFID reader in adult, child, pregnant woman and fetus anatomical models” Bioelectromagnetics, in press”)*

*The author wishes also to thank Dr. Sven Kühn who provided the measurement data for the validation of the antenna*

### 1. Introduction

Among the various RFID system categories, recently the Ultra High Frequency (UHF) RFID systems started to find large use in a great deal of applications, most of them in the class of the general public. UHF RFID generally operates at about 900 MHz, but the frequency allocation is variable with country: in Europe it is in the frequency band 866–869 MHz, in North and South America in the frequency range 902–928 MHz, and in Japan and Asian countries in the band 950–956 MHz [Rao et al., 2005].

In a passive Ultra High Frequency (UHF) RFID system, the reader transmits a modulated RF signal to the tag, consisting of an antenna and an Integrated Circuit (IC) chip powered only by the received RF energy. It responds via the modulation of its backscattering aperture (or radar cross section) linked to its input impedance. Thus, the reflection of electromagnetic waves is used for the transmission of data from the reader to the tag and vice-versa [Finkenzeller, 1999]. Generally, because omnidirectional tag reading is wished in most solutions, the UHF RFID reader antenna are circularly polarized. To this purpose, and even for their manufacturing simplicity, patch antennas, as the one proposed in this study, are preferred for the UHF RFID reader.

Depending on the application, they can either be portable and handled by an operator or placed at fixed positions. In particular, the former, is mainly used in occupational or industrial environments, so affecting only occasionally and accidentally the general public exposure. On the contrary, the latter can be found in several general public applications and, as a consequence, the customers and the professionally not-exposed personnel, can be in the read range of these devices (i.e., in some stores near the dressing room entrance and connected to informational video to allow the costumers to read

specific information about that product, as a timing-systems in marathons/sprint, as well as in cycling and golf races, in the libraries to provide and enhance self-service operations, and to increase the speed and the security of inventory functions, etc.).

Despite the penetration of this technology in such a wide number of applications, the literature on the exposure assessment and dosimetry of those systems is still scarce. To the best of author knowledge only [Kainz et al. [2003]; Martínez-Búrdalo et al. [2010]; Fiocchi et al. [2011a,b)] assessed the EMF generated by RFID and electronic article surveillance (EAS) systems on various human models, but at completely different frequencies and applications. In the UHF range, the only studies conducted were the one by Fung et al. [2007], who performed the exposure assessment of a 900 MHz radiofrequency identification (RFID) baggage handling system at the Hong Kong International Airport, and another by Hong and Yun [2010], who evaluated the EMFs generated by a 900 MHz RFID circularly polarized patch antenna in an adult model.

The study described below aims at addressing the computational near-field exposure assessment of the EMF generated by an UHF RFID reader antenna. In particular the exposure levels together with the identification of the worst-case exposure situation and the corresponding compliance conditions for the RFID system has been identified in anatomical models of adult, children, pregnant women at different gestational age and respective fetuses.

## 2. Material and Methods

### 2.1 RFID Antenna Model

The RFID reader antenna was modeled from commercially available fixed and handheld UHF readers (Figure 3.1).

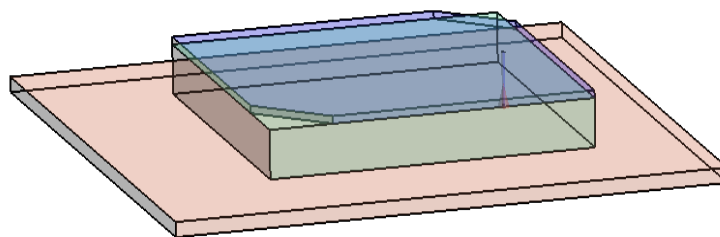


**Figure 3.1 Numerical model of the RFID reader antenna.**

In this work an antenna with the geometrical and physical characteristics as shown in Table 3.1 has been considered.

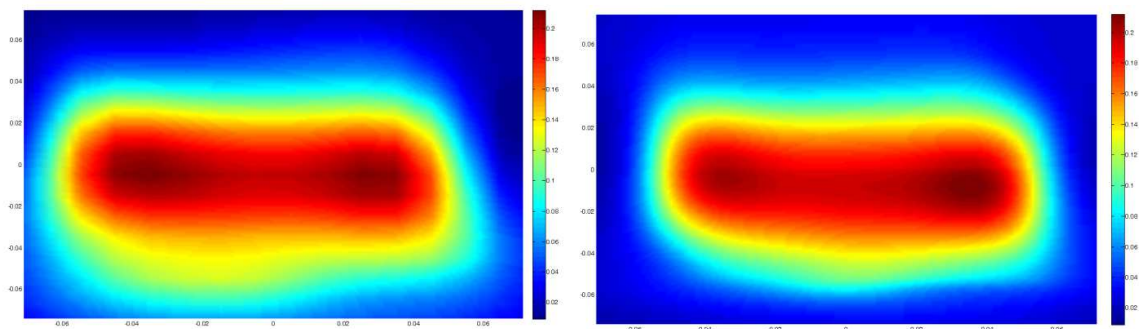
**Table 3.1. Characteristics of the RFID reader antenna.**

Component	Notes	Size [mm]	Material
ground plane		180×180×4	PEC
dielectric substrate		106×106×13	polystyrene ( $\sigma=0.00047\text{S/m}$ , $\varepsilon=2.54$ )
patch		106×106×2	PEC
radome	External dimension	220×210×120	kydex ( $\sigma=0.00252\text{S/m}$ , $\varepsilon=2.46$ )
radome	Internal dimension	220×200×80	kydex ( $\sigma=0.00252\text{S/m}$ , $\varepsilon=2.46$ )

The antenna resonance frequency in free space was 870 MHz, i.e., close to the upper limits of the frequency range of UHF RFID applications in Europe.

### 2.2 Antenna Model Validation

The validation of the simulated antenna was performed with an elliptical phantom [IEC 62209-2 standard] filled with a TSL (tissue simulating liquid) using DASY52 for SAR measurements at SPEAG (Schmid & Partner Engineering AG, Zurich, Switzerland) under the supervision of Dr. Sven Kühn.



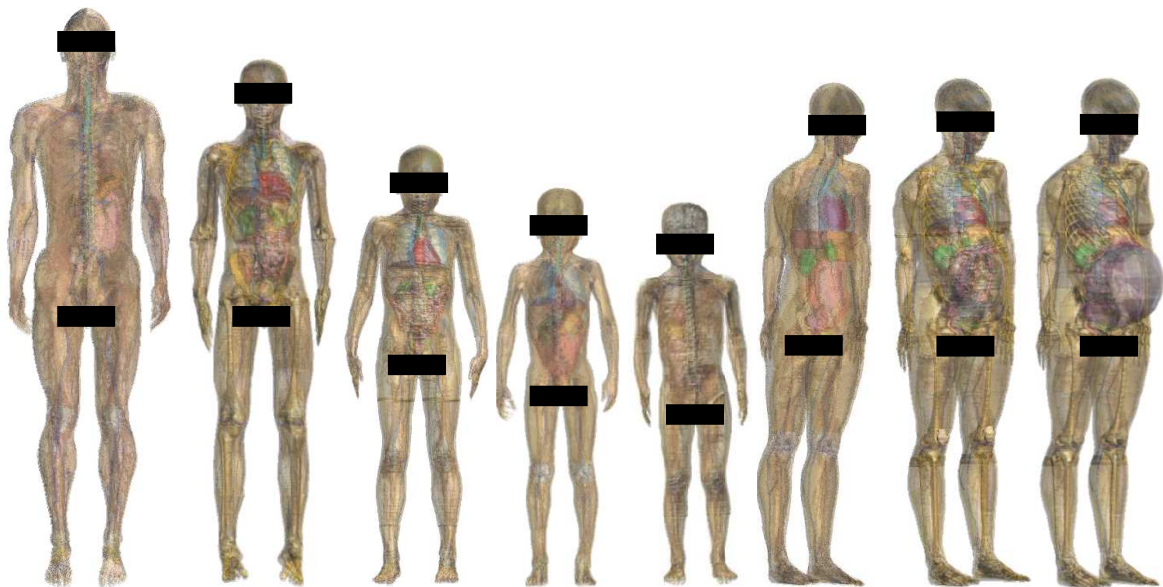
**Figure 3.2. Measured (left) and simulated (right) local SAR (W/kg) distribution in a plane parallel to the flat phantom and the antenna ground plane, at a depth of 5 mm inside the liquid. X- and Y- axes units are meters.**

Figure 3.2 shows the measured SAR (W/kg) distribution (left) and the simulated one (right). The maximum measured SAR local value was 2.12 W/kg for 1W input power, whereas the simulation provide a corresponding value of 2.39 W/kg, with a percentage difference of 12.73%.

The return loss of the antenna, measured with a vector network analyzer was below -20 dB in air and -5 dB when measured in front of the phantom, the latter indicating a good matching of the antenna with the body simulating phantom.

### 2.3 Anatomical models

Eight human voxel-based anatomical models developed from magnetic resonance images of volunteers were used in the computation. Six models are taken from the Virtual Family [Christ et al., 2010a], i.e., Duke (adult, male, 34-year-old), Thelonious (child, male, 6-year-old), Roberta (child, female, 5-years old), Eartha (child, female, 8-years old), Louis (child, male, 14 years old) and Ella (adult, female, 26-year-old). The two remaining models are two adult female models in two gestational ages of 7 and 9 months, respectively [Christ et al., 2012], derived from partial deformations of Ella's womb (Figure 3.3).



**Figure 3.3. Anatomical body models. From left to right: Duke (adult male), Louis (14-year-old male), Eartha (8-year-old female), Thelonious (6-year-old male), Roberta (5-year-old female) , Ella (adult female) from the Virtual Family, 7 months pregnant female and 9 months pregnant female. In this figure and in all the figures of this thesis, faces and genitals of the models have been disguised in a non-recongnizable manner according to the agreement for the use of Virtual Family.**

In all models up to 80 tissues can be distinguished. In the case of the pregnant woman models, the tissues considered include also up to 20 tissues in the fetus models. A minimum voxel resolution of 1 mm was kept for all the models.

#### 2.4 Dielectric Properties

The dielectric tissue properties for the four adult models (adult male, female, and adult tissues of the 7 and 9 months pregnant women) were assigned according to the parametric model described by Gabriel et al. [1996].

The tissues dielectric properties of the four children were calculated by the well-known Cole-Cole expression [Cole and Cole, 1941] at the patch-antenna operating frequency (870 MHz), using the values measured by Peyman and Gabriel [2010] on 10 kg pigs, corresponding to a child of 1 to 4 years of age (attributed to Roberta, Thelonious and Eartha, the available data being mostly close to their age) and on 50 kg pigs, corresponding to a child of 12-14 years of age (used for Louis). Since the available data cover only partially the tissues included in the anatomical models used in this study, the adult dielectric properties [Gabriel et al. 1996] were applied for the remaining tissues.

To investigate the effect of the change with age of the tissue dielectric properties, the exposure matrix was also estimated applying the adult dielectric properties [Gabriel et al., 1996] to all Thelonious tissues.

Data on the dielectric properties of fetal tissues are almost completely lacking and were reported for specific frequencies [Lu et al., 1996]. Recently Peyman et al. [2011] provided data of Cole-Cole parameters for human placenta, umbilical cord and amniotic fluid, which were applied in this study.

For that reason to all the fetal tissues, excluding the three ones mentioned above, were assigned properties applying the approach proposed by Dimbylow et al. [2007], in which the ratio between the dielectric properties of fetus (at different gestational ages) and adult tissues were estimated on the basis of the corresponding ratio of water content.

#### 2.5 Exposure Scenarios

The reader antenna was placed at three different angles (R1, R2 and R3) and at three different distances for each angle: 10, 20 and 50 cm from the end of the skin of the head (Duke and child models) or from the skin of the pregnant/non-pregnant woman wound, considering the reference systems, whose detail are reported in Figure 3.4. This positions was chosen to simulate some exposure scenarios that can be met in practice.

The simulated scenarios assume the head exposed from the side and the back (to reflect accidental exposure of a worker or a child), whereas the abdomen exposed from the side and the front, to account for the accidental exposure of the fetus.

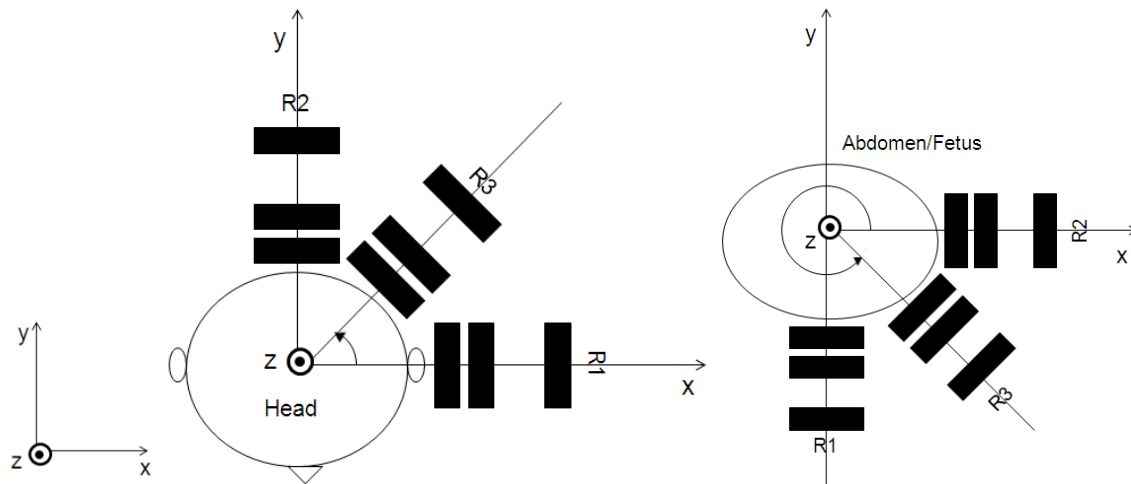


**Figure 3.4. Schematic representation of reader position with respect to the body models. The center of the coordinate system was found through the arithmetic mean of maximum and minimum  $x$ ,  $y$ , and  $z$  coordinates, and coincides with the center of the two anatomical structures (head for Duke and child models; and fetus or abdomen in the case of Ella). Left: for child models and Duke heads the antenna was placed in three positions R1 ( $0^\circ$ ), R2 ( $90^\circ$ ) and R3 ( $45^\circ$ ) with respect to the  $x$ - $y$  plane. Right: for Ella and pregnant woman fetuses the antenna was placed in three positions R1 ( $-90^\circ$ ), R2 ( $0^\circ$ ) and R3 ( $-45^\circ$ ) with respect to  $x$ - $y$  plane ( $z=0$ ). Distances between reader and reference system were calculated between skin and the center of the ground plane in both the exposure scenarios, at  $z=0$ .**

Recently, some authors [Findlay and Dimbylow, 2006; Findlay et al 2009; Lee and Choi, 2012] have stressed the importance of tackling the change in body posture, which can affect the radio frequency exposure pattern. They found noticeable SAR differences among standing arms down, standing arms-up and sitting postures of adult and children for plane-wave exposures around the corresponding body resonance frequency (about 80 MHz and 120 MHz), but negligible (under  $\pm 10\%$ ) differences at about 900 MHz. As to the fetus posture, in both pregnant woman models it was modeled with the head down, and this in agreement with data derived from pregnancy survey that reported about 98% and 62% of cases in such configurations at the end and between 25 and 27 weeks of pregnancy, respectively [Wiar et al., 2011]. Besides that, Akimoto and colleagues in their study addressing the pregnant women exposure to portable radios [Akimoto et al. 2010], identified that position as the worst case position for fetal exposure when the antenna is irradiating the fetal trunk.

### 2.6 Child models and antenna position variability

The effects of child variability with age was investigated reproducing the exposure scenario identified as the worst case by the simulations described above, to the other child models (i.e., Roberta, Eartha and Louis).

The change in the antenna position was investigated in the 9-months pregnant woman model identified as the worst case scenario in terms of fetus exposure, estimating the exposure matrix when the antenna was placed 10 cm over (R4) and under (R5) the center of the fetus and on the same plane as R1, R2 and R3 (see Figure 3.4), in a position opposite (i.e. behind the body) to R3, close to the skin (R3compl).

### 2.7 Computational approach

All the simulations were performed using the Finite-Difference Time-Domain (FDTD) technique, as implemented in the simulation platform SEMCAD X (Schmid & Partner Engineering AG, Zurich, Switzerland), which provides a hardware accelerated option for faster calculations of large electromagnetic problems. Non-uniform mesh with a maximum spatial step of 4 mm in free space was generated. The mesh step was restricted to 1 mm in the anatomical models, to account for numerical dispersion, and to 0.2 mm in the fetal skin to allow a good discretization of this thin layer of the body. The computational domain was terminated with perfectly matched layers (PML) absorbing boundary conditions. A distance of one wavelength between body or the reader and the boundaries of the computational domain was maintained.

The exposure assessment is presented in terms of whole body SAR (wbSAR) and maximum 10g-averaged (peak spatial) SAR over head/trunk ( $psSAR_{10g}$ ), normalized to 1W input power of the antenna.

## 3. Results

### 3.1 Adult and Child Exposure

Table 3.2 shows the wbSAR levels obtained for the adult male (Duke) and the 6-year-old boy (Thelonious), when exposed to the RFID reader in the three configurations and distances described above (see Figure 3.4). In both models the worst-case exposure scenario was found considering the reader in position R3, whereas the wbSAR values were found higher for Thelonious than for Duke (about 5 dB in the worst case position R3 with the antenna at a distance of 10 cm).

As to the variations of the wbSAR over distance, the SAR decreases as the source moves away from the body, as expected. However, the decrease seems to be model dependent, the rate of decrease being slightly faster (-2.0 dB vs -1.7 dB at 20 cm, and -5.3 dB vs -4.7 dB at 50 cm) for Thelonious than for Duke, averaging the rate of decrease of the three antenna positions.

**Table 3.2. wbSAR for the adult (Duke) and the 6-year-old child (Thelonious) for head exposure. Antenna positions R1, R2 and R3 (around the head) are shown in Figure 3.4. Results are normalized to 1 W CW input power of the reader antenna.**

Model		Duke wbSAR [mW/kg]			Thelonious wbSAR [mW/kg]		
Angle		R1	R2	R3	R1	R2	R3
Distance (cm)	10	5.4	4.9	5.5	16.4	13.1	17.4
	20	3.6	3.3	3.8	9.8	9.2	10.1
	50	1.8	1.7	1.9	4.4	4.5	4.7

Table 3.3 shows the maximum psSAR<sub>10g</sub> levels and their locations. In both models the tissues most affected by the highest SAR levels were found to be the cerebrospinal fluid CSF, skin and grey matter but in a different order depending on the model.

**Table 3.3. psSAR<sub>10g</sub> values, antenna worst case position around the head and tissue peak location as a function of the antenna distance in the two male models (Duke and Thelonious). Results are normalized to 1 W CW input power of the reader antenna.**

	10 cm	20 cm	50 cm
<b>Duke</b>			
psSAR <sub>10g</sub> [mW/kg]	754	301	77
Worst Case Position	R3	R3	R1
Peak Location	(skin)	(skin)	(skin)
<b>Thelonious</b>			
psSAR <sub>10g</sub> [mW/kg]	623	244	54
Worst Case Position	R3	R2	R2
Peak Location	(CSF)	(CSF)	(CSF)

The psSAR<sub>10g</sub> levels in the body tissues are, on average, higher in Thelonious than in Duke by 3.7 dB, with the largest increases in spleen, prostate, thymus gland, heart, kidney, lung, adrenal gland

and bronchi. However these variations could be due to the different distances among the above organs and the reader in the two models.

### 3.2 Variation of Dielectric Properties

The SAR levels estimated in Thelonious, when the reader was positioned in R3 (worst case position using adult dielectric properties) and using the set of dielectric properties as proposed by Peyman and Gabriel [2010], show a slight decrease in wbSAR (-0.1 dB) and a more noticeable increase of the maximum psSAR<sub>10g</sub> (+ 0.6 dB) with respect to the case in which the adult dielectric properties were used for all Thelonious tissues.

**Table 3.4. Difference in tissue conductivity and psSAR<sub>10g</sub> obtained in the worst case position for the child model (Thelonious) exposure R3, comparing the values using the child dielectric properties with the “adult approach” (see text for details).**

<i>Tissue</i>	<i>Conductivity increase [dB]</i>	<i>psSAR<sub>10g</sub> increase [dB]</i>	<i>Tissue</i>	<i>Conductivity increase [dB]</i>	<i>psSAR<sub>10g</sub> increase [dB]</i>
Bone	5.1	4.1	Mandible	5.0	2.6
Bone Marrow	12.8	8.0	Medulla obl.	0.6	-0.9
Brain grey matt.	0.2	-0.5	Midbrain	0.4	0.4
Brain white matt.	0.6	-0.3	Muscle	0.5	0.1
Cartilage	2.7	1.5	Pons	0.6	-0.1
Cornea	-1.0	-3.0	SAT	6.8	4.9
Diaphragm	0.5	-1.0	Skin	-0.3	-1.0
Ear cartilage	2.7	2.0	Skull	7.3	5.8
Ear skin	-0.3	-0.5	Spinal cord	0.2	-1.1
Fat	6.8	4.4	Teeth	5.0	1.9
Hippocampus	0.2	-1.0	Tongue	0.5	-1.4
Intervert. disc	2.7	2.5	Trachea	2.7	1.0
Larynx	2.7	3.3	Vertebrae	5.0	3.4

The most remarkable differences between the psSAR<sub>10g</sub> in the tissues (Table 3.4) obtained with the two approaches were observed in the bone marrow (+ 8 dB), where the conductivity increases by 12.6 dB.

### 3.3 Pregnant and Non-Pregnant Woman Exposure

The wbSAR values calculated in Ella, in the pregnant women, and in the fetuses, considering case-by-case the worst-case scenario for the positioning of the antenna, are shown in Table 3.5.

The SAR levels in the pregnant women were found slightly higher, with an increase of 0.07 dB and 0.4 dB at 10 cm for the 7 and 9 months pregnant women, respectively, than the values estimated in Ella. The 9 months fetus absorbs higher values of power than 7 months one, with an increase of about 0.7 dB at a distance of 10 cm, whereas the wbSAR increases 0.3 dB in the 9 months pregnant woman compared to the 7 months pregnant woman. Table 3.5 shows also the changes (in dB) in the SAR values with the distance of the model from the antenna. As expected, the fetuses were found more sensitive to the distance than the pregnant women (Table 3.5).

**Table 3.5. wbSAR computed by simulating the worst case position of the RFID antenna at 10 cm in front of the abdomen (indicated inside the brackets) and mean difference (across the three antenna positions) in the whole body SAR (with respect to the corresponding wbSAR at 10 cm) at 20 cm and 50 cm. Results are normalized to 1 W CW input power of the reader antenna.**

Distance	<i>wbSAR</i> [mW/kg]	<i>Mean difference of wbSAR</i> <i>across the antenna</i> <i>positions [dB]</i>	
		20 cm	50 cm
Ella	11.1 [R1]	-1.2	-3.1
7mo pregnant	11.3 [R1]	-1.4	-4.1
9mo pregnant	12.2 [R3]	-2.2	-3.6
7mo fetus	41.6 [R3]	-2.2	-7.7
9mo fetus	48.6 [R3]	-4.2	-9.0

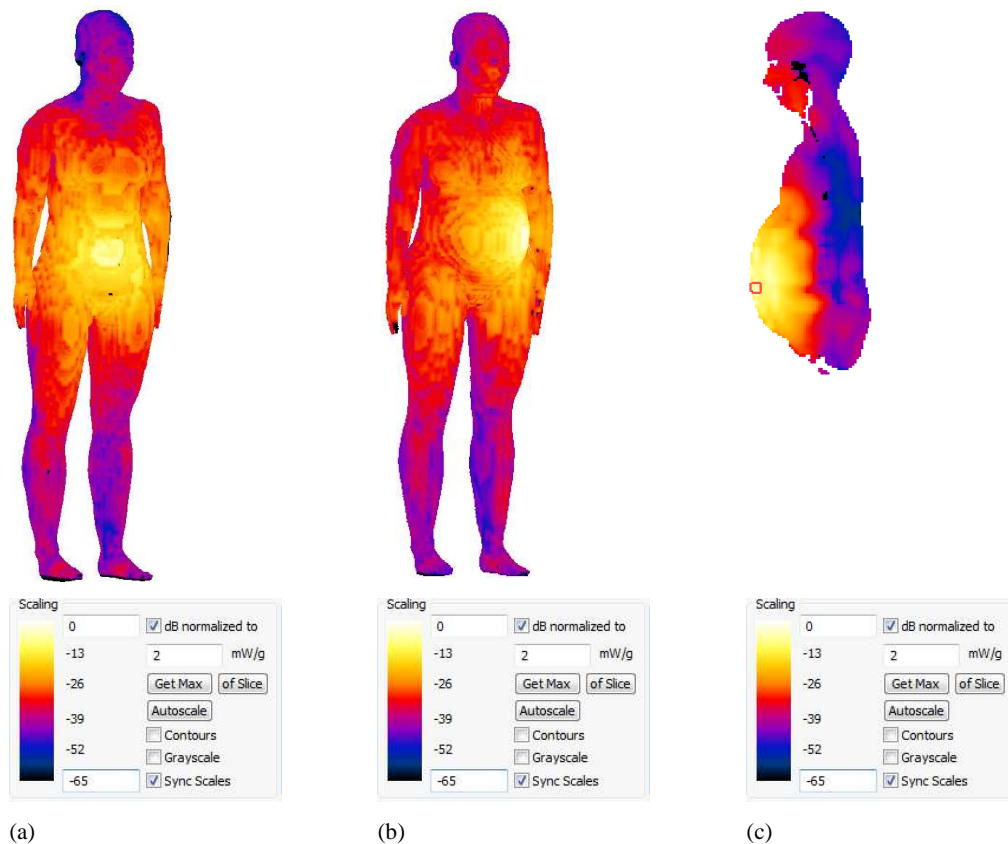


**Figure 3.5. Examples of 10g psSAR distribution. (a) SAR over Ella with the reader antenna in position R1. (b) SAR over the 9-month pregnant body with the reader in position R3. (c) SAR in a sagittal plane of the 7-month pregnant in position R1 (the little cube in this panel denotes the maximum location of 10g psSAR). R1 and R3 positions are described in Figure 3.4. Results are normalized to 1 W CW input power of the reader antenna.**

Figure 3.5 shows some examples of  $\text{psSAR}_{10\text{g}}$  distributions obtained from Ella (non-pregnant) and the two pregnant women, with the antenna positioned in different positions; as expected the maximum  $\text{psSAR}_{10\text{g}}$  levels were found in the regions close to the reader positions.

Table 3.6 shows the  $\text{psSAR}_{10\text{g}}$  computed in Ella, in the pregnant woman models and in the fetuses, considering the antenna in its worst-case position (R1 and R3 as a function of the model).  $\text{psSAR}_{10\text{g}}$  shows rather high values of about or even above 2 W/kg when the antenna is 10 cm away from the body. Even for all the other antenna positions the  $\text{psSAR}_{10\text{g}}$  were found around 2 W/kg (not shown in the Table). However, the levels decrease with the increase of the distance between the body and the antenna. The most exposed tissues for every exposure scenario are the ones close to the model surface (skin, muscle, uterus and amniotic fluid).

**Table 3.6. psSAR<sub>10g</sub> estimated in Ella, pregnant women and fetuses considering the worst case position for the antenna in front of the abdomen (indicated inside the brackets). The psSAR<sub>10g</sub> was found in the skin in all cases but one (in the amniotic fluid, 9-months pregnant woman). Results are normalized to 1 W CW input power of the reader antenna.**

	<i>psSAR<sub>10g</sub></i> [W/kg]		
	10 cm	20 cm	50 cm
Ella	1.98 [R1]	0.68 [R1]	0.15 [R1]
7mo pregnant woman	3.29 [R1]	1.20 [R1]	0.25 [R1]
9mo pregnant woman	3.22 [R3]	0.25 [R2]	0.08 [R2]
7mo fetus	0.53 [R3]	0.17 [R1]	0.04 [R1]
9mo fetus	1.97 [R3]	0.13 [R1]	0.04 [R1]

#### 3.4 Human and Source position Variability

wbSAR and psSAR<sub>10g</sub> as a function of age, computed in the children models (worst-case antenna scenario R3 at a distance of 10 cm) are shown in Table 3.7. It is clear from that figure, that wbSAR and psSAR<sub>10g</sub> decreases with age.

**Table 3.7. wbSAR and psSAR<sub>10g</sub> values as a function of age. The data are shown for the four child models. In all cases the antenna position was R3 around the head (that is the worst case exposure scenario), at a distance of 10 cm. The data for Thelonious has been previously calculated using the approach which consider dielectric properties dependency with age, and they are here reported for the sake of readability. psSAR<sub>10g</sub> values were found on CSF in all child models. Results are normalized to 1 W CW input power of the reader antenna.**

<i>Child Model</i>	<i>Age [years]</i>	<i>wbSAR [mW/kg]</i>	<i>psSAR<sub>10g</sub> [mW/kg]</i>
Thelonious	6	17.0	715
Roberta	5	18.2	684
Eartha	8	12.6	673
Louis	14	6.8	547

They show similar values for the youngest children (Thelonious, Roberta) and a decrease for Eartha and (mainly) for Louis. The dielectric properties in all models were set using the approach which considers their dependency with age described above (2.4 Dielectric Properties).

The effect of change in the source position around the abdomen is shown in Table 3.8, where is evident that the worst-case position of the antenna is R3.

**Table 3.8. wbSAR and psSAR<sub>10g</sub> values estimated in the 9-months pregnant woman and in the corresponding fetus with the antenna placed in different positions in front of the abdomen, at a distance of 10 cm. In the Table the data about the same models estimated in position R3 as shown in Table 3.5 and Table 3.6, are copied here for the sake of readability. Results are normalized to 1 W CW input power of the reader antenna.**

<i>Antenna position</i>	<i>Model</i>	<i>wbSAR [mW/kg]</i>	<i>psSAR [W/kg]</i>
R3	Pregnant woman	12.2	3.22
	Fetus	48.6	1.97
R3compl	Pregnant woman	8.63	1.19
	Fetus	0.23	$6.08 \cdot 10^{-3}$
R4	Pregnant woman	4.03	0.41
	Fetus	7.88	0.13
R5	Pregnant woman	5.32	0.59
	Fetus	21.70	0.30

#### 4. Discussion

Before entering into discussion and interpretation of the results of this study, one should take into consideration that, as stated above, the exposure assessment of UHF RFID operating in the European UHF RFID frequency range was explored. European standards [ETSI, 2010] define the technical characteristics for short range devices, including RFID; specifying a maximum radiated power of 500 mW for non-specific-use applications (in this study all the results were normalized to 1 W radiated power) and a duty cycle of 10%. Therefore, for the interpretation of the results presented in the current study (see, e.g., Table 3.3 and Table 3.6) with respect to the compliance of an RFID reader with the

International Commission on Non-Ionizing Radiation Protection (ICNIRP) exposure guidelines [ICNIRP, 1998], the data should be rescaled by multiplying them with a factor of 0.05.

The great variety of RFID applications and corresponding readers models, makes impossible to enlarge the results of this study to any RFID exposure situation. But since the modeling characteristics (dimensions, materials, resonance frequency) of the reader antenna used here are derived from a comprehensive market survey, the simulated antenna can be considered as a typical UHF RFID reader model.

The maximum levels of wbSAR (see, Table 3.2, Table 3.5, Table 3.7 and Table 3.8) are largely below the limits of the ICNIRP guidelines [1998]. This is not true for the adult exposure (more than -12 dB, -8.6 dB, -8.5 dB, -8.2 dB from the wbSAR limit of 0.08 W/kg for adult male, adult female, 7 and 9 months pregnant woman, respectively), but also for the child (-6.5 dB) and the fetuses (more than -2.8 dB and -2.2 dB for fetuses at gestational ages of 7 and 9 months, respectively) exposure. An increasing trend with age in wbSAR levels was found in every exposure scenario (see Table 3.7). This trend can be explained by considering the higher averaging mass for the same equivalent power sources in the adult model than in the child and fetus models. The position of the source affects especially the fetus exposure (Table 3.5 and Table 3.8).

The fetal wbSAR varies on average towards different exposure configurations by about 4.1 dB, while the wbSAR of the pregnant woman remains quite constant (mean variation of about 1 dB); similar results was obtained even when the local exposure is considered (i.e., psSAR<sub>10g</sub>), as shown in Table 3.6. This is mainly due to the different tissues distribution in front of the sources, due to the different geometrical development of the tissues with gestational age and to the different values of the conductivity of the tissues. As stated above, the wbSAR levels in the pregnant models were found slightly higher compared to the ones of the non-pregnant adult female model (Table 3.5). This is due to the addition to the non-pregnant woman model of high conductivity fetal tissues, including amniotic fluid without a realistic thickening of the low conductivity fat layer. As a matter of fact, as discussed by several authors (see, e.g., [Christ et al., 2006], [Conil et al., 2008]) the increase of fat/muscle ratio and the consequent rise in Body Mass Index (BMI), typical of pregnancy, produce a decrease in SAR. However, this assures that the results obtained on the pregnant models here can be considered as conservative predictors of SAR levels.

The psSAR<sub>10g</sub> levels (Table 3.3 and Table 3.7) are not critical with respect to the ICNIRP [1998] basic restriction, the maximum levels being lower than about 5 dB from the 2 W/kg provided for in the guidelines. The obtained values are in agreement with those reported by Hong and Yun [2010] in a similar exposure scenario for a UHF RFID reader. The maximum psSAR<sub>10g</sub> is slightly lower (from -

0.4 to -1.4 dB) in the child than in the adult models, but its location varies between them and with distance (Table 3.3 and Table 3.7). On the contrary, more concern could be raised with respect to trunk exposure (psSAR<sub>10g</sub> values in Table 3.6), where the maximum psSAR<sub>10g</sub> levels (Table 3.6) for the 7 and 9 months pregnant female resulted higher than the exposure guidelines [ICNIRP, 1998] (+2.2 dB and +2.1 dB, respectively). As a difference, the SAR values are close to the ICNIRP guidelines when non-pregnant woman and the fetus at a gestational age of 9 months are considered (-0.04 dB, and -0.06 dB, respectively).

As to the change of dielectric properties with age, the results obtained using for Thelonious tissues the dielectric properties proposed by Peyman and Gabriel [2010], show very slight differences compared to the ones obtained using adult properties, with a maximum change in wbSAR of -0.1 dB and in maximum psSAR<sub>10g</sub> of about 0.6 dB, the only major change being in voxel SAR estimated in isolated tissues.

These results are consistent with the results found by other authors [Mason et al. 2000; Gajšek et al. 2001; Keshvari et al., 2006; Dimbylow et al., 2009; Peyman et al., 2009; Christ et al., 2010b], who have shown that the change in dielectric properties does not necessarily lead to a significant change in the averaged psSAR<sub>10g</sub> values and that only for specific single tissue exposure, such as bone marrow, bone, and fat, the differences should not be neglected. The great differences of psSAR<sub>10g</sub> values found in those tissue, besides the large differences in conductivity experienced, can be also explained by the increased reflection coefficient at the boundaries between different tissue layers (skin/fat, muscle/fat) and to the consequent gain absorbed energy by organs with rather low conductivity and low primary SAR values from surrounding high conductivity organs with high primary SAR values.

As a final remark, one should note that, besides the uncertainty due to the choice of dielectric properties, there are several other factors, intrinsic to the computational simulation, that can influence the reliability of the estimated SAR values. Those heterogeneous sources of error are mainly related to the numerical limits of modeling of the source and anatomical body, discretization, resolution of the FDTD grid at a specific frequency, choice of the algorithm for SAR calculation [Huber et al., 2003; Laasko et al., 2010; Kuster et al., 2006; Bakker et al. 2010]. The worst-case total expanded uncertainty of the numerical modeling with 95% confidence interval ( $k=2$ ) can reach 58% for the psSAR<sub>10g</sub> according to Bakker et al. [2010].

---

## Estimate of the Human Fetus Temperature Increase due to UHF RFID Exposure

*(This chapter is based on “Fiocchi S, Parazzini M, Markakis I, Samaras T, Ravazzani P. “Temperature elevation in fetus exposed to UHF RFID readers” submitted to IEEE Trans Biomed Eng on April 2013 ”)*

### 1. Introduction

Children and adults have almost the same capability to dissipate whole-body heat loads, but children are more disposed to have a higher rate of heat absorption than adults and, moreover, dehydration may have a more damaging effect on children because of their greater dependence on elevated skin blood flow to dissipate heat. Hyperthermia during pregnancy can cause embryonic death, abortion, growth retardation, and developmental defects. In humans, epidemiologic studies suggest that an elevation of maternal body temperature by 2°C for at least 24 hours during fever can cause a range of developmental defects. In addition, young infants aged 2-3 months are even more vulnerable than neonates because of their higher metabolic rate, better tissue insulation, and slightly lower surface area/mass ratio [Kheifets et al. 2005].

Thermoregulation is an important aspect of fetal physiology and has attracted the attention of many researchers with respect to exercise during pregnancy (Bell and O’Neill [1994], Soultanakis-Aligianni, [2003]) perinatal management of the fetus [Asakura, 2004] and teratogenicity [Ziskin and Morrissey, 2011]. The fetus develops in the uterus under aerobic metabolism. Its metabolic rate is higher and its temperature remains 0.3 to 0.5 °C higher than that of an adult [Asakura, 2004]. Since fetal temperature is higher than maternal temperature, heat is transferred from the fetus to the mother. Gilbert et al. [1985] found that in sheep 85% of the heat produced by the fetal lamb is transferred to the mother via the umbilical circulation. The remaining 15% of the produced heat is conducted through the fetal skin, the amnion and, finally, the uterine wall to the maternal abdomen. If heat production and loss from the fetal body remain balanced, fetal temperature stays constant. However, if the heat transfer to the mother is disrupted for any reason, the fetal temperature may increase. Several biological, chemical

and physical agents, can change the temperature and/or the heat load of either the fetus or the mother and, thus, disturb normal fetal thermoregulation.

Being the main macroscopic effect induced by RF exposure the heating of tissues [ICNIRP, 1998], the increase in temperature due to RF exposure in pregnant women and hence fetus is of particular concern. This is for example at the basis of the question whether a pregnant woman can undergo an MRI examination without any risk for the fetus due to potential thermal effects from RF radiation has been the subject of several works (Hand et al. [2006]; Wu et al. [2006]; Gowland and De Wilde [2008]; Padiaditis et al. [2008]; Ruckhäberle et al. [2008]; Hand et al. [2010]; Kikuchi et al. [2010]; Murbach et al. [2011]). The assessment of the levels of exposure to RF is often limited to the estimation of the Specific Absorption Rate (SAR), a quantity directly related to thermal effects, This is in Hand et al. [2006]; Padiaditis et al. [2008]; Murbach et al. [2011]. Some other studies went one step further by assessing the increase in fetal temperature due to RF exposure using computational methods based on the application of a modified version of the bio-heat equation (BHE) introduced by Pennes [1948]. This is, for example in Wu et al. [2006]; Hand et al. [2010]; Kikuchi et al. [2010] O'Connor [1999]; Kainz et al. [2003]; Dimbylow [2007]; Nagaoka et al. [2007]; Lee et al. [2009b]; McIntosh et al. [2010]; Takahashi et al. [2010].

In the previous chapter (see Chapter 3 and [Fiocchi et al. 2012, submitted]), which was focused to assess the exposure to UHF RFID devices of pregnant women, high levels of SAR values in some fetal tissues were found In order to better investigate the possible effect induced by such a high exposure, in this chapter the temperature raise in the same exposure scenarios are estimated applying the classical approach based on the BHE resolution.

## **2. Material and Methods**

### *2.1 Anatomical models and exposure scenario*

The two pregnant women models are obtained from a partial deformations of the womb of the adult female model named “Ella” of the Virtual Family [Christ et al., 2010a]. In particular the 7th month pregnant woman model was obtained by integrating in “Ella” the segmented MR images of a pregnant woman abdomen, while the 9 months is based on that of the 7th month, but the fetus model was replaced by a model of a scaled newborn [Christ et al., 2012].

In addition to fetal tissues, placenta, amniotic fluid (and umbilical cord for the 7 months pregnant woman only) were also integrated in the anatomical models.

Temperature increase in fetal tissues was estimated considering the two worst cases exposure scenarios in terms of SAR levels obtained in the EM computation (see previous Chapter 3). These

coincide in particular with the RFID reader positioned at 10 cm from the 7 months pregnant woman skin in front of her fetus (in the previous chapter named R1), and at 10 cm from the 9 months pregnant woman, at -45 °C in the x-y plane, considering the reference system shown in Figure 3.4 of Chapter 3 (named “R3”) in which high peak SAR levels have been found even over the ICNIRP limits. For the sake of simplicity, in this chapter the two exposure scenarios will be indicate as “7 months fetus exposure” an “9 months fetus exposure”.

## 2.2 Thermal model

Temperature increase inside the tissue exposed to EMF generated by UHF RFID system, was calculated using the Pennes bioheat equation (BHE) [Pennes, 1948] as implemented by the thermal solver of the simulation platform SEMCAD X (Schmid & Partner Engineering AG, Zurich, Switzerland). This provides a finite different solution of the following differential equation:

$$\rho c \frac{\partial T}{\partial t} = \nabla \cdot (k \nabla T) + \rho Q + \rho S - \rho_b c_b \rho \omega (T - T_b) \quad (1)$$

Where  $T$  is the temperature of the tissue,  $t$  is the time,  $\rho$ ,  $c$  and  $k$  are the density, the specific heat and the thermal conductivity of the tissue/medium, respectively.  $Q$  is the metabolic heat generation rate,  $S$  is the specific absorption rate (SAR) due to EMF exposure,  $\omega$  is the volumetric blood perfusion rate and  $\rho_b$ ,  $c_b$  and  $T_b$  are the density, the specific heat and the temperature of the blood.

When the goal of the simulation is to obtain the temperature increase ( $T_{incr}$ ) due to SAR exposure and such increase is expected to be small ( $< 1$  °C), the tissue parameters ( $\rho$ ,  $c$ ,  $k$ ,  $\omega$ ,  $Q$ ,  $T_b$ ) and the parameters necessary to define boundary conditions (i.e. the heat transfer rate due to convection cooling through air contact  $h$ , the temperature outside the boundary, and the heat flux due to perspiration) can be considered time and temperature independent. Moreover, subtracting the equations (1) for the exposed and unexposed conditions cancels out the common terms (i.e. the one linked to the metabolic heat  $\rho Q$  and the one linked to the fixed blood temperature  $T_b$  ( $\rho_b c_b \omega T_b$ )) and it's possible to consider a simplified version of the previous equation (for further details on this approximation see [Bakker, 2012]):

$$\rho c \frac{\partial T_{incr}}{\partial t} = \nabla \cdot (k \nabla T_{incr}) + \rho S - \rho_b c_b \rho \omega T_{incr} \quad (2)$$

with mixed boundary conditions  $k \frac{\partial T_{incr}}{\partial n} + h T_{incr} = 0$  at the interface between maternal skin and air ( $h=8$  W/(m<sup>2</sup>·K) as in [Bakker et al. 2011]); Neumann boundary conditions  $k \frac{\partial T_{incr}}{\partial n} = 0$  at the interface between maternal air tissues (i.e. internal air, bronchi lumen, esophagus lumen, pharynx and trachea lumen) and the other tissues in contact with them; Dirichlet boundary conditions  $T_{incr} = 0$  at the interface between blood (i.e. artery and veins) and all the tissue perfused by blood (all the tissue

except air tissues, maternal and fetal CSF, maternal and fetal humor vitreous, amniotic fluid, teeth, stomach lumen and small intestine lumen.

In this work that second formulation (as implemented in the Thermal solver of SEMCAD) is used since the goal is the estimate of temperature increase due to the SAR distributions generated by the exposure to UHF RFID, which is expected to be less than 1 °C, even for long time exposure formulation (see for comparison the works of Wang and Fujiwara [1999], Bernardi et al [2000], Ibrahiem et al. [2005], who evaluated the temperature increase in the head due to the exposure to mobile phone antenna at 900 MHz and comparable output powers, finding lower temperature increases). In case the results should be higher than 1 °C the evaluation should be repeated using the complete BHE.

Temperature rise were calculated for each exposure scenario both at the steady state (by assuming a zero temporal gradient in Equation (2)) and as a function of time (considering a simulation time exposure of 3 hours as suggested in [Hirata et al. 2008]) to get information about transient effect in time.

### 2.3 Thermal parameters

Dielectric properties and density of the tissues of the pregnant women models are the same assigned in the electromagnetic simulation to determine SAR (Chapter 3) distributions  $S$ , which represent one of the entry data of the BHE.

In addition, thermal simulations require thermal parameters of the tissues (i.e  $k$ ,  $c$ ,  $c_b$ ,  $\omega$ ). Mothers tissues thermal parameters are taken from [Bakker et al. 2011] with exception of the values of the amniotic fluid and placenta that were taken from Hand et al. [2010] and umbilical cord whose properties are considered as for blood. Thermal properties of fetal tissues are considered here equivalent to the one used for the corresponding adult tissues.

## 3. Results

Figure 4.1 shows the temperature increase distribution at the steady-state on the surface of the fetus computed using the “7 months fetus exposure” and the “9 months fetus exposure”. As expected the location of the maximum values was the same of the maximum peak SAR value (see Figure 3.5, Chapter 3) and in correspondence with the position of the reader.

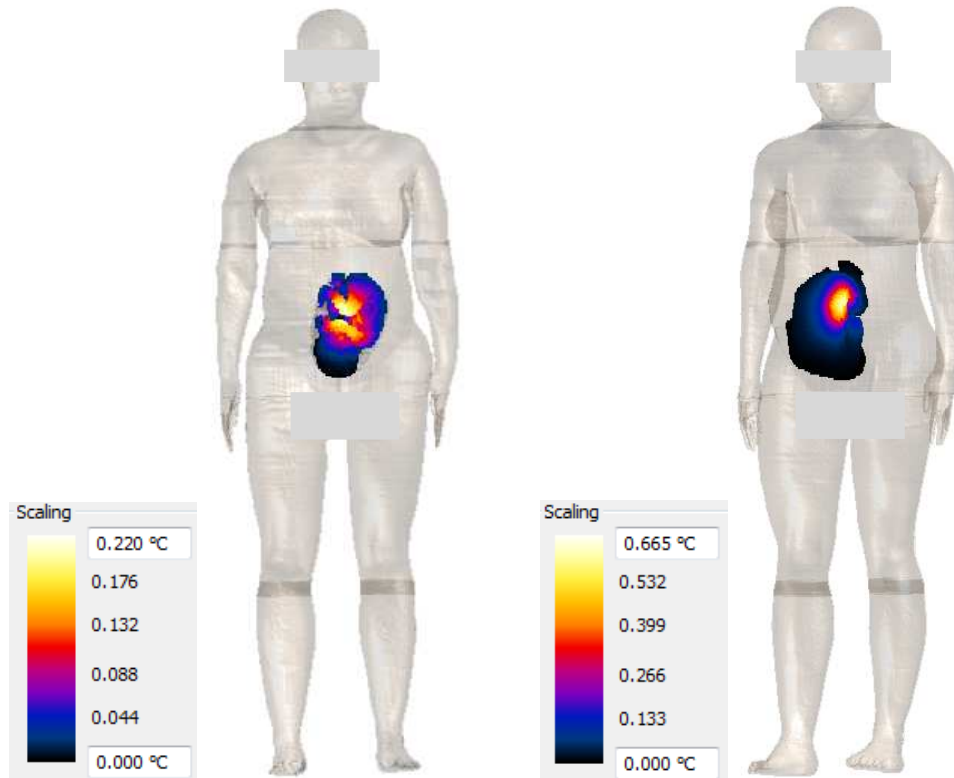


**Figure 4.1. Temperature increase distribution at the steady state on the surface of the fetus for the “7 months fetus exposure” (left) and the “9 months fetus exposure”. Color bars are clamped to the maximum value if temperature found in the fetal tissues. Results are obtained considering 1 W CW input power of the RFID reader antenna. In this figure and in all the figures of this thesis, faces and genitals of the models have been disguised in a non-recongnizable manner according to the agreement for the use of the Virtual Family.**

Maximum and median of the temperature increase distributions calculated at the steady-state in the “7 months fetus exposure” and in the “9 months fetus exposure” conditions are reported in Table 4.1 and Table 4.2, respectively.

Median value in place of mean value was chosen as a better descriptor of the distribution. The term “Fetus” in the table refers to all the tissues listed above the term itself, as a consequence the “Median  $T_{incr}$ ” is the median value of the distribution of  $T_{incr}$  over the whole fetus, and the “Maximum  $T_{incr}$ ” is the maximum value of the distribution of  $T_{incr}$  over the whole fetus (which coincides with maximum of the “Maximum  $T_{incr}$ ” of the same fetal tissues listed above the term itself.

**Table 1 Maximum and median values of  $T_{incr}$  distributions at the steady-state for fetal tissues, amniotic fluid, placenta and umbilical cord for the two exposure scenarios “7 months fetus exposure” and “9 months fetus exposure”. The term “Fetus” in the Table refers to all the tissues listed above the term itself. The corresponding values are associated to the total distribution of  $T_{incr}$  over the whole fetus. Results are obtained considering 1 W CW input power of the RFID reader antenna.**

Tissue	7 months fetus		9 months fetus	
	Median $T_{incr}$ [°C]	Maximum $T_{incr}$ [°C]	Median $T_{incr}$ [°C]	Maximum $T_{incr}$ [°C]
Adrenal gland			0.004	0.013
Bladder	0.006	0.016	0.020	0.059
Bone	0.006	0.143	0.002	0.166
Brain	0.000	0.019	0.000	0.002
CSF			0.001	0.003
Esophagus			0.003	0.006
Eye lens	0.022	0.051	0.001	0.001
Eye vitreous humor			0.001	0.003
Fat	0.012	0.196	0.008	0.528
Gallbladder	0.004	0.006	0.002	0.005
Heart_muscle	0.002	0.016	0.000	0.003
Kidney_cortex	0.000	0.014	0.002	0.021
Liver	0.002	0.035	0.001	0.006
Lung	0.002	0.064	0.001	0.013
Muscle	0.012	0.161	0.005	0.283
Ovary			0.020	0.037
Pancreas			0.004	0.009
SAT	0.022	0.220	0.006	0.590
Skin	0.015	0.217	0.005	0.662
Small_intestine	0.001	0.013	0.002	0.085
Spinal_cord	0.002	0.008	0.008	0.064
Spleen	0.000	0.001	0.011	0.053
Stomach	0.001	0.002	0.007	0.027
Thymus			0.000	0.001
Thyroid gland			0.000	0.000
Uterus			0.023	0.032
<i>Fetus</i>	<i>0.004</i>	<i>0.220</i>	<i>0.004</i>	<i>0.662</i>
Amniotic fluid	0.019	0.264	0.006	0.719
Placenta	0.000	0.007	0.000	0.010
Umbilical cord	0.061	0.141		

Figure 4.2 (“7 months fetus exposure”) and Figure 4.3 (“9 months fetus exposure”) show the normalized fractions of the volume of the six tissues in which the highest values of “Maximum  $T_{incr}$ ” were found, i.e., fat, muscle, SAT, skin, fetus and amniotic fluid, versus the experienced. They clearly show that the distribution of temperature increase in those tissues is strongly focused next to the maximum, but rapidly decrease moving away from them. That means that most of the volume is at very low  $T_{incr}$ .

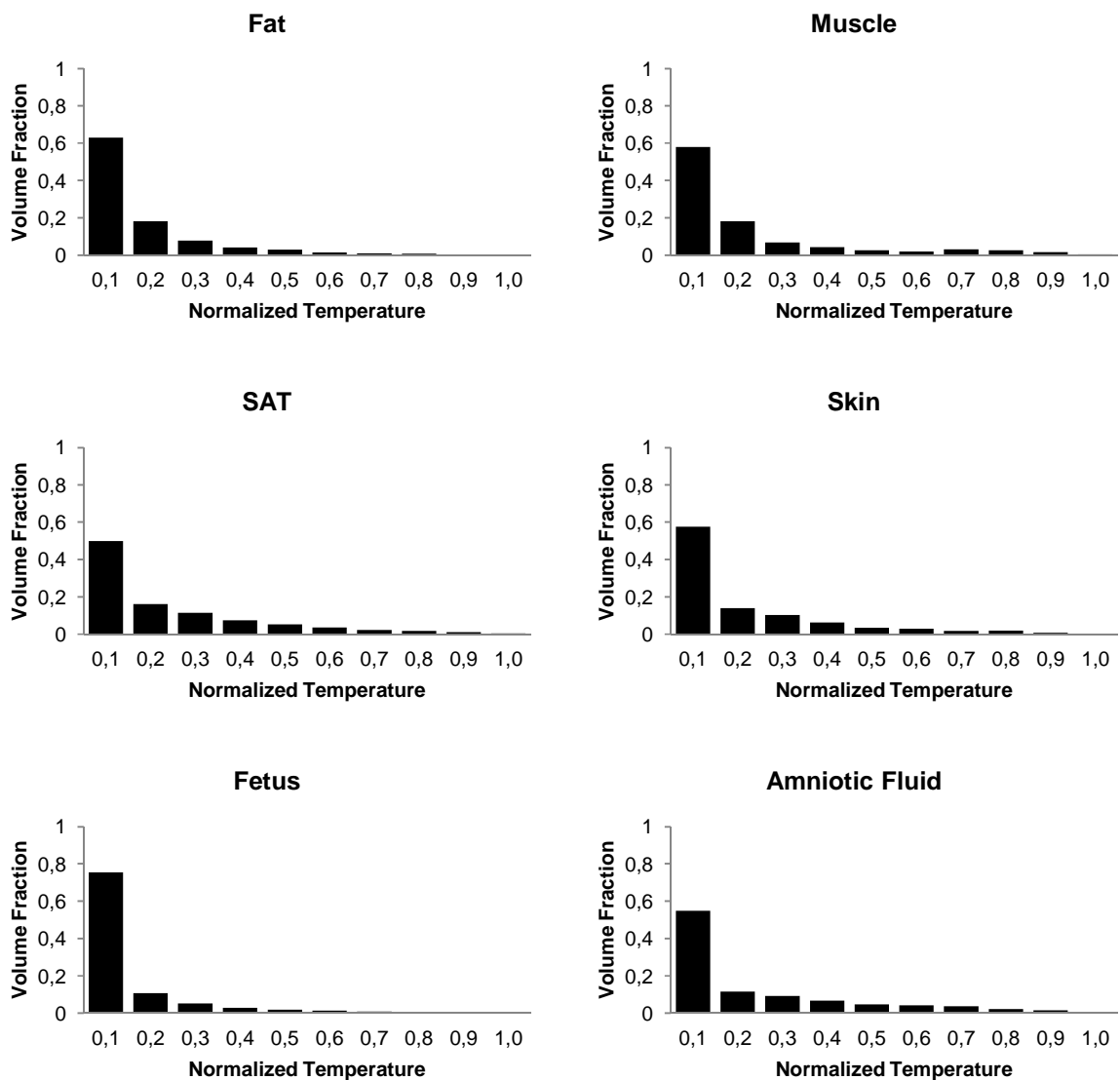
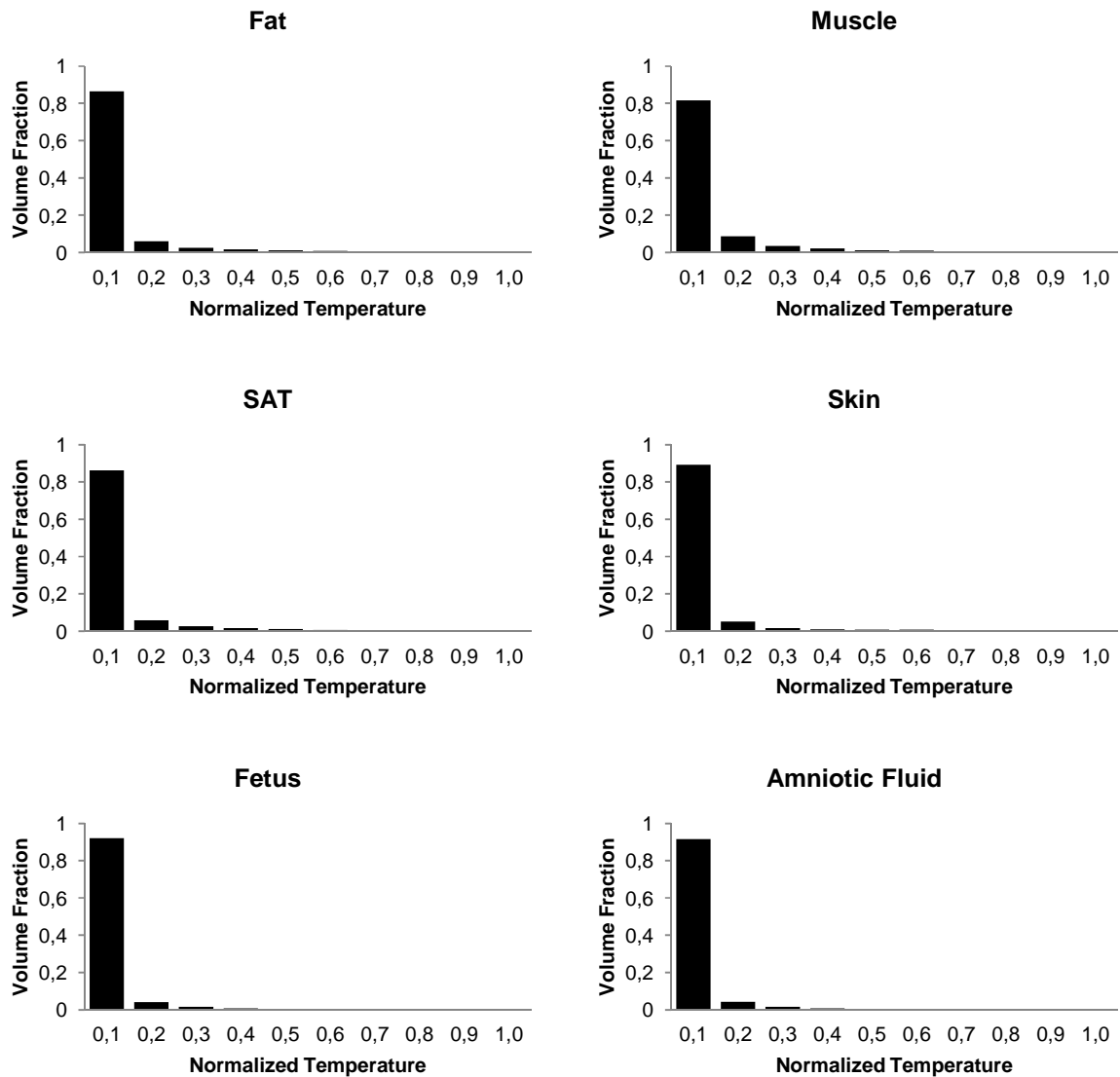
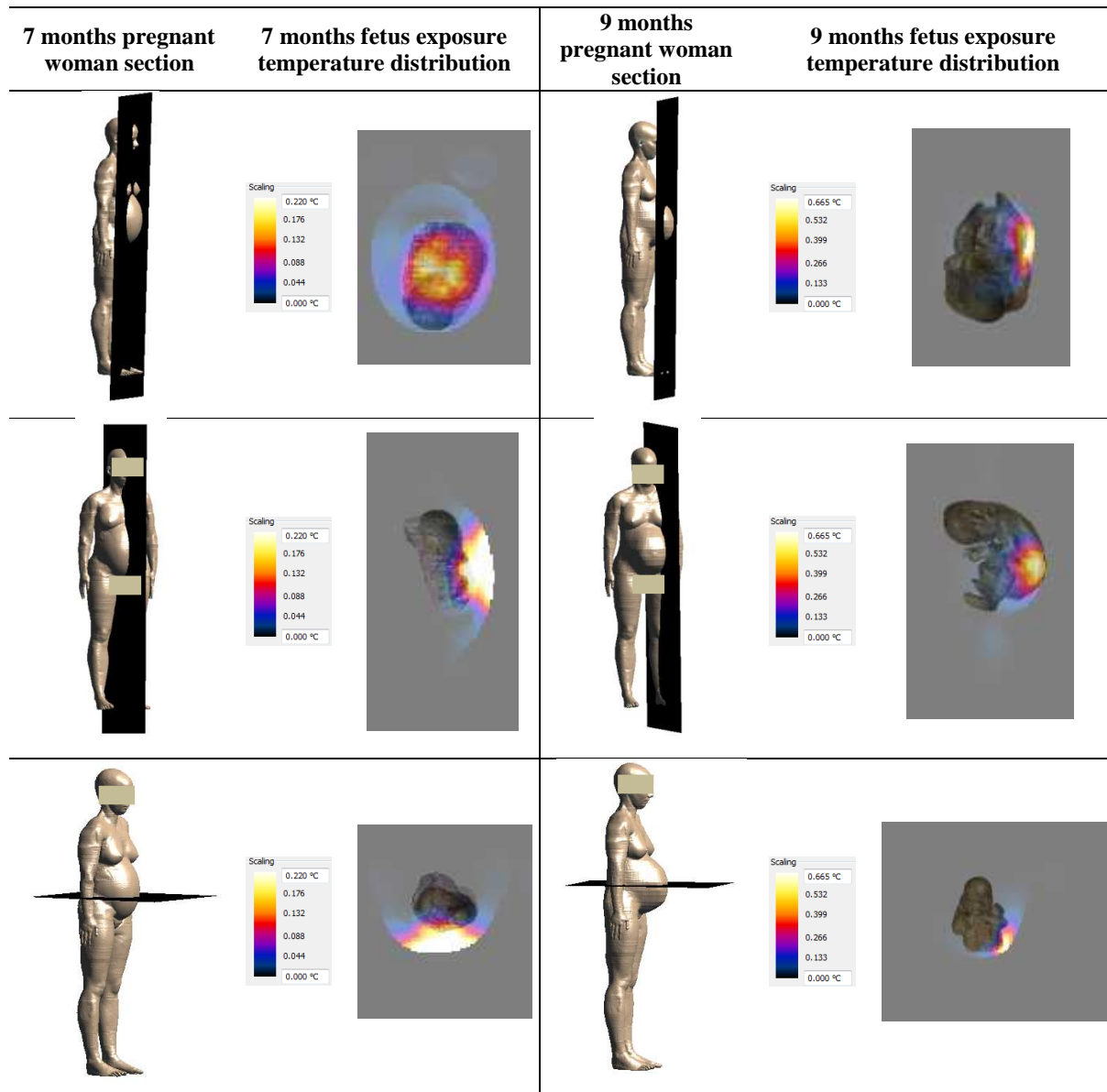


Figure 4.2 Histograms of the temperature increase distribution at the steady-state of six representative tissues for the “7 months fetus exposure”, normalized with respect to the “Maximum  $T_{incr}$ ” of each distribution.

This effect is particularly clear in the “9 months fetus exposure” (Figure 4.3) where in all the six tissues, more than 80% (versus the range 50 % - 75 % in the “7 month exposure” tissues of Figure 4.2) of the total volume of the tissue itself is at a  $T_{incr}$  within the 10% of the “Maximum  $T_{incr}$ ”.



**Figure 4.3** Histograms of the temperature increase distribution at the steady-state of six representative tissues for the “9 months fetus exposure”, normalized with respect to the “Maximum  $T_{incr}$ ” of each distribution.



**Figure 4.4** Temperature increase distributions at the steady state for “7 months fetus exposure” (left) and “9 months fetus exposure” (right) on coronal (1<sup>st</sup> row), sagittal (2<sup>nd</sup> row) and transversal (3<sup>rd</sup> row) plane where maximum value of temperature in fetus was found. Scaling bars are clamped to those maximum values. In each slice fetus model is superimposed to allow the reader understanding its position with respect to temperature distributions. Results are obtained considering 1 W CW input power of the RFID reader antenna.

Figure 4.4 shows temperature distributions for both “7 months fetus exposure” and “9 months fetus exposure” on coronal (1<sup>st</sup> row), sagittal (2<sup>nd</sup> row) and transversal (3<sup>rd</sup> row) planes. The sections were identified as those ones in which the maximum value of temperature in the fetus was found. Scaling

bars are clamped to those maximum values. In each slice fetus model is superimposed to allow the reader understanding its position with respect to the temperature raise distributions.

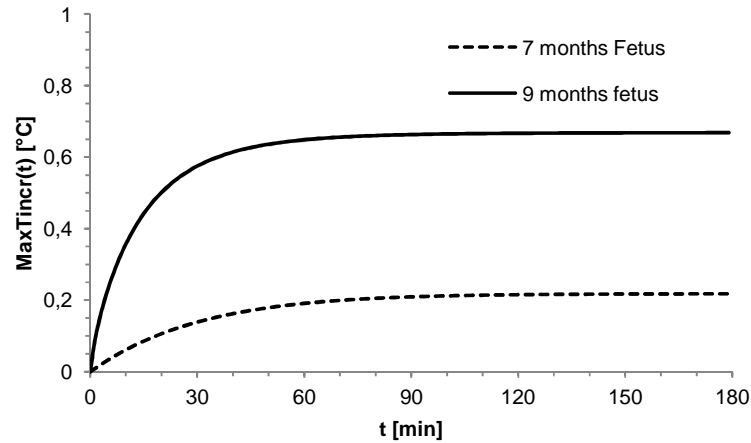


**Figure 4.5 Behavior with time of the “Maximum  $T_{incr}$ ” over fetus for both “7 months fetus exposure” and “9 months fetus exposure” scenarios in 7 months and 9 month fetal tissues). Results are obtained considering 1 W CW input power of the RFID reader antenna.**

Figure 4.5 shows the behaviour with time of the “Maximum  $T_{incr}$ ” over all fetal tissues estimated where the maximum of fetus  $T_{incr}$  distribution was found at the steady-state (i.e. as shown by the “Maximum  $T_{incr}$ ” listed in Table 4.1, in the SAT for the “7 months fetus exposure” and in the skin for the “9 months fetus exposure”). The figure shows the results for both “7 months fetus exposure” and “9 months fetus exposure” scenarios in 7 months and 9 month fetal tissues (named “Fetus” in Table 4.1, Figure 4.2 and Figure 4.3 ).

**Table 2 Percentage differences of the Maximum  $T_{incr}$  calculated in fetal tissues (Fetus) at some temporal instants (1<sup>st</sup> column) with respect to the Maximum  $T_{incr}$  at the steady state for the 7 months and the 9 months Fetus exposure.**

Time (min)	% of steady state	
	7 months Fetus	9 months Fetus
1	3.2	10.6
6	17.9	39.3
10	28.2	53.6
60	87.7	97.0
120	98.7	99.7
180	99.9	100.0

Moreover, Tables 2 displays the percentage of “the completion of the steady state”, which is calculated as the percentage difference between the “Maximum  $T_{incr}$ ” calculated, at a certain time, in

the position of the “ increase found at the steady-state, and the “Maximum  $T_{incr}$ ” at the steady state itself .

#### 4. Discussion

Temperature rise from RF radiation exposure has long been recognized as the major adverse effect in the RF frequency range [ICNIRP, 1998] which includes the operating frequencies of UHF RFID (i.e. 870-915 MHz). This effect could be more harmful for fetus since it has more limited capability to regulate its own temperature.

ICNIRP guidelines [ICNIRP, 1998] indicates that established biological and health effects in the frequency range from 10 MHz to a few GHz are consistent with responses to a body temperature rises of more than 1°C which has been correlated to a maximum whole-body-averaged specific absorption rate (wbSAR) of 4 W/kg for 30 minutes. From that threshold, reduction safety factor were applied to wbSAR limits to provide adequate protection for occupational exposure and public exposure. To prevent excessive localized tissue heating, additional restrictions on the localized maximum 10g-averaged peak spatial SAR ( $psSAR_{10g}$ ) are provided. These localized peak SAR, as shown in the previous chapter, can be exceeded in case of prolonged use of UHF RFID close to pregnant woman. However, since an absolute threshold temperature for such excessive heating is not given, it is not possible to determine if these restrictions are compliant. For that reason in that discussion the localized raise in temperature of 1 ° C will be considered as a threshold for comparison as suggested in [Bakker et al. 2011].

Maximum  $T_{incr}$  at the steady-state due to UHF RFID exposure were found around 0.2 °C in sat, skin, fat, muscle bone for the “7 months fetus exposure” and around 0.6 in the same tissues for the “9 months fetus exposure”. Differences between temperature increase values in the “9 month exposure” with respect to “7 month exposure” are probably due to the higher volume (of the high electric and thermal conductivity amniotic fluid and the higher  $psSAR_{10g}$  (see Table 6 of Chapter 3) values found in the first exposure scenario, even if, as found by [Bakker et al. 2011], position and value of  $psSAR$  don't correlate exactly with position and value of the maximum temperature increase.

Variation of thermal parameters (i.e  $k$ ,  $c$ ,  $cb$ ,  $\omega$ ) were not taken into account in this thesis, since distribution of the variance with age of those parameters has not been determined yet. However, considering that literature values can be described by a normal (Gaussian) probability distribution, as supposed in [Bakker et al. 2011], the maximum uncertainty in the peak temperature exposure should remain under the 25% for all thermal parameters after 2 hours of exposure, being the volumetric blood perfusion rate  $\omega$  the one that more affect that peak.

Moreover, the same authors found a maximum 4% of variation on the peak temperature increase after a variation of 30% in the heat transfer coefficient between skin and air ( $h_{\text{skin-air}}$ ).

Considering the most exposed tissues (Table 4.1), the peaks of the temperature increase are found in the most superficial tissues of the fetus and the ones close to the high conductivity amniotic fluid. On the other hand the same tissues are also the most extended ones and present distributions strongly shifted towards the low temperatures (Figure 4.3 and Figure 4.4). That is evident also looking at the skin (surface) temperature increase distributions (Figure 4.1.), which is very focused near the maximum values but decrease rapidly moving away from them.

Maximum asymmetry in the distribution of  $T_{\text{incr}}$  was found considering the “9 months fetus exposure”: 92 % of fetal volume is at a temperature lower than 0.065 °C (one tenth of the maximum). Smoother distributions were found in case of “7 months fetus exposure” where, as an example, the percentage of fetal volume lower than one tenth of the maximum (0.022) is 75%, thus indicating a decisive influence of the position of the source with respect to position of the fetus, besides a different absorption pattern over the two exposure scenarios.

Median values (Table 4.1) give further details about those statements. Tissues which experience the major maximum  $T_{\text{incr}}$ , have median  $T_{\text{incr}}$  values considerably low ( $< 0.03$  °C), thus assuring that most of tissue is weakly thermally stressed (i.e. considering the whole fetus, ratio between Maximum  $T_{\text{incr}}$  and Median  $T_{\text{incr}}$ , was found to be 50 and 175 for the “7 months fetus exposure” and “9 months fetus exposure”, respectively). Major median  $T_{\text{incr}}$  levels have been found over umbilical cord, SAT and eye for the “7 months fetus exposure”, over uterus, bladder and ovary for the “9 months fetus exposure”. That becomes clear considering the position of the fetus in the three view shown in Figure 4.4, that is 7 months fetus with the back on the right and 9 months fetus facing backwards with respect to the coronal plane view.

The different worst- case scenarios of RFID exposures, and the relatives different SAR distributions, should also explain the different time course (Table 4.5 and Table 4.2) and time constant, which is the time that the system takes to reach the value of  $1-1/e = 63.2\%$  of its final steady-state value, for fetal tissues maximum  $T_{\text{incr}}$  (i.e. about 29 minutes and 14 minutes for the “7 months fetus exposure” and “9 months fetus exposure”, respectively). Moreover, in general, RFID (and SAR exposures) will be shorter than 2 hours (Table 4.2), which is here estimated as the time of RF exposure for fetal temperature to reach the equilibrium, and the temperature rise will depend on exposure time. For reasonable and realistic time of ), UHF RFID exposure order of minutes, temperature increase is very far to be a potential harmful source for fetus.



---

## **Conclusions**

In view of the incredible diffusion of Radio Frequency Identification RFID among a huge number of general purpose applications, including the ones that can frequently expose children and pregnant women, an exposure assessment of the levels of electromagnetic fields EMF generated by these devices has been strongly encouraged by scientific community.

So far, although the interest aroused by this technology from its commercial inception and its possible adoption in a great number of areas of contexts, studies on the levels to which the general public and the workers are exposed, are completely lacking. Similar considerations held also for the specificity of children exposure, whose pattern of exposure could be even more harmful because of their possible biological susceptibility and because of their early exposure , but are completely unknown.

Considering these gaps in knowledge and open questions about children exposure to RFID systems, these dissertation aimed to give clear and scientific answers to such an essential topic. The results found, in terms of levels of EMF, EMF power absorption, and temperature raise in the organs and/or body tissues, represent a mandatory input in the process of health risk assessment related to any technology that makes use of EMF. This process is also particularly urgent to be addressed, as far as the general public exposure to RFID devices is irreversibly increasing.

RFID devices generally operate at low power levels, with very short duty cycle (generally about 10%), so they are supposed to be far from generated power and fields close to the exposure limits provided by the competent organizations [ICNIRP, 1998]. On the contrary, the exposure levels of EMF assessed in this work, show that for both the class of devices taken into consideration (i.e. HF RFID at 13.56 MHz and UHF RFID at 880 MHz) here, situations in which the compliance with the exposure limits is not achieved could exist.

The existence of critical situations for exposure to the HF RFID systems in general, and in particular for the ones used for newborn-mother identity reconfirmation is strictly related to the time of use of this devices close to the subject and the requested power to read. In other words, some of these systems, actually available on the market, have technical specifications, for instance the magnetic field threshold necessary to read the information stored in the tag, which can lead to an overexposure of the patients if used more than a limited time (20 seconds). The practical utility of the exposure assessment conducted here is also corroborate by some general indications about the use of these devices in healthcare: first, the results suggests the need to reduce as much as possible the exposure time and hence indicate the importance of specific training of the involved personnel, often

inclined to come closer to the subject to shorten the reading time, to the practical use of the RFID. Secondly, the choice of the optimal reader-tag system is particularly determinant for newborn exposure so as to make desirable to place the tag far from some sensitive organs (i.e. on the anklet in place of wrist) .

The second class of RFID systems reviewed (UHF RFID), presents different issues, since most of them, and in particular the ones fixed in a place like as at the cash desk and checkout, are designed to be continuously turned on and generates powers to allow communication at a distance of more than 1 m long. While negligible exposure levels have been found for children and adults, pregnant women, and their fetuses could be overexposed, being the maximum peaks SAR over the maximum allowable levels for public RF exposure [ICNIRP, 1998]. This in particular could justify some concerns in countries where technical standards don't provide strict duty cycle ( $> 10\%$ ) and high maximum emitted power ( $> 0.5$  W Effective Radiated Power ERP).

However, the results related to temperature assessment provided in the last part of this work showed that, despite the highly localized RFID exposure, the hypothetical short exposure duration of RFID exposure makes both maximum and average temperature increase largely far from a possible biological effect.

In conclusion, the great flexibility of RFID devices allowed their pervasive presence in a great number of general purpose applications and, as a consequence, it involves people diversified in gender and age. The result of the exposure assessment of EMF generated by those devices suggest that it's reasonable and advisable to choose devices taking into account the balance between power emission and the ease, speed and distance of reading to avoid any situation of overexposure. In addition, the two analysis addressed on HF and UHF RFIDs show how the exposure assessment should be considered one of the key factor in the identification of the optimal reader-tag system to be applied, because able to give clear scientific answers about overall people exposure levels .

Novel improvements in computational calculations have allowed to extend the assessment to a wide variety of exposure scenarios, including the ones still missing. To that purpose the broad spectrum of children taken into account in this work, allows to meet to the demands of the international organizations for health protection outlined in the introduction as well as to lay the foundation stone for their exposure to RFID devices. With regard to this latter a trend of higher EMF exposure patterns in the newborn models (both the more approximate scaled and the realistic models) compared to the mother model was found, thus suggesting that the exposure assessment of adult and children should be kept separated. Similar considerations hold also for children exposure, even though the differences with respect to adult are almost negligible and, in the specific case of UHF RFID exposure, don't

change the situation of compliance with exposure limits. Conversely, the main result, in terms of relevance and possible proximity to health effects, concerns pregnant women exposure, whose fetuses result to be higher affected by EMF source than other subjects. It was demonstrate that SAR alone may not provide an adequate description of the regional thermal environment, since peaks in temperatures are not directly related to the peak SAR location and value.

However, the temperature exposure assessment performed in those critic exposure scenarios, resulted in not only average temperature increase in the fetal body core (i.e. 0.004 °C at the steady-state) but also the peak temperature increase (i.e. 0.22 °C and 0.65 °C for the 7 months fetus and 9 months fetus, respectively) largely far from possible fetus developmental defects.

Other relevant results of these dissertation come from the contribution to the modeling dosimetric issues about children, newborns and fetuses exposure assessment. These comprehend the estimate of uncertainty due to the choice of accurate and realistic models with respect to the previous calculation on adult scaled model for neonates an children and the investigation of the sensitivity of the computation results to the variation of tissues dielectric parameters.

As to the first issue, the large discrepancy found in the exposure levels between scaled and realistic newborn model is such as to confirm that the great differences in the two models should not be disregarded, but the sign of the differences in the exposure matrix calculated in the two models is soothing, being the scaled model more conservative than the realistic one.

Secondly, the choice of the dielectric properties model was found not affecting the final conclusion about compliance in case of RFID exposure, but suggests a trend towards a slight underestimation of the exposure using adult properties and lead to a not negligible changes with regards to specific single tissue exposure, such as bone marrow. In turn, these results reinforces the need for further investigations based on accurate measurements of newborn dielectric properties, particularly in the lower frequency range (HF more than UHF), where they are supposed to be highly affected by the uncertainty implied in the measurements tools. Also to that purpose the model of dielectric properties assignment here used should be validated and join together to evaluate the total expanded uncertainty which affect the results.

The results of temperature raise assessment on two different exposure scenarios, involving pregnant women at two different gestational ages, suggest also that a better insight of the interactions between external exposure and fetal tissues , being the temperature distributions strongly asymmetric and

highly affected by the relative positions between fetus and source, can only be achieved through a tissue-specific dosimetry.

Furthermore, additional future research in the field of exposure assessment should include a more specific assessment on pregnant women, addressing also the assessment to subjects at different gestational ages, and to fetus in different positions. Other factors of uncertainty, including a better assessment of thermal parameters for fetus at different developmental stages, the enhancement of more appropriate thermoregulatory models, should be combined in a more comprehensive uncertainty budget which would allow a more complete answer to the issues aroused by the general public and the specialized community .

The integration of all these information in a such composite exposure scenario, as the one led by the exposure to devices, such as RFIDs, pervasively spreading , is a complex issue and it is not supposed to be depleted by this work of thesis. In the same way, a significant interpretation of results can be only accomplished by joining the results coming from the whole process of health risk assessment, in which the exposure assessment represents only one of the steps. On the other hand, the results discussed here give an important contribution in the process of filling gaps in knowledge related to the exposure to a great pervasive technology, such as RFID, allows to face up some important issues related to children exposure assessment.

---

## Bibliography

Akimoto S, Nagaoka T, Saito K, Watanabe S. 2010. Comparison of SAR in realistic fetus models of two fetal positions exposed to electromagnetic wave from business portable radio close to maternal abdomen. 32nd Annual International Conference of the IEEE EMBS, Buenos Aires, Argentina, August 31- September 4, 2010

Asakura H. 2004. Fetal and neonatal thermoregulation. *J Nihon Med Sch.* 71(6): 360–370.

Bakker JF, Paulides MM, Christ A, Kuster N, Van Rhoon GC. 2010. Assessment of induced SAR in children exposed to electromagnetic plane waves between 10 MHz and 5.6 GHz. *Phys Med Biol* 55(11): 3115-3130.

Bakker JF, Paulides MM, Neufeld E, Christ A, Kuster N, van Rhoon GC. 2011. Children and adults exposed to electromagnetic fields at the ICNIRP reference levels: theoretical assessment of the induced peak temperature increase. *Phys Med Biol.* 56(15):4967–89.

Bakker JF. 2012. Dosimetry of Exposure to Electromagnetic Fields in Daily Life and Medical Applications. PhD Thesis, Erasmus MC - Daniel den Hoed Cancer Center, Rotterdam, 2012. ISBN: 978-90-8891-457-7 (available at <http://repub.eur.nl/res/pub/37499/>, last accessed on November 28th, 2012)

Barry JS, Anthony RV. 2008. The pregnant sheep as a model for human pregnancy. *Theriogenology.* 69(1): 55–67.

Bernardi P, Cavagnaro M, Pisa S, Piuze E. 2000. Specific absorption rate and temperature increases in the head of a cellularphone user. *IEEE Trans. Microwave Theory & Tech.* 48:1118–1126.

Bell R, O'Neill M. 1994. Exercise during pregnancy. *Birth* 21(2): 85–95.

Brace RA. 1997. Physiology of Amniotic Fluid Volume Regulation. *Clinical Obstetrics & Gynecology.* 40(2): 280–289.

Brugger PC, Prayer D. 2012. Actual imaging time in fetal MRI. *Eur J Radiol.* 81(3): e194–196.

Cech R, Leitgeb N, Pedititis M. 2007. Fetal exposure to low frequency electric and magnetic fields. *Phys Med Biol.* 52(4):879–888.

Christ A, Samaras T, Klingeböck A, Kuster N. 2006. Characterization of the electromagnetic near-field absorption in layered biological tissue in the frequency range from 30 MHz to 6000 MHz. *Phys Med Biol.* 51: 4951–4965

Christ A, Kainz W, Eckhart Hahn G, Honegger K, Zefferer M, Neufeld E, Rascher W, Janka R, Bautz W, Chen J, Kiefer B, Schmitt P, Hollenbach HP, Shen J, Oberle M, Szczerba D, Kam A,

- Guag JW, Kuster N. 2010a. The Virtual Family—development of surface-based anatomical models of two adults and two children for dosimetric simulations. *Phys Med Biol* 55:N23-N38.
- Christ A, Gosselin MC, Christopoulou M, Kühn S, Kuster N. 2010b. Age Dependent Tissue-Specific Exposure of Cell Phone Users. *Phys Med Biol* 55(7):1767-1783.
- Christ A, Guldemann R, Bühlmann B, Zefferer M, Bakker JF, van Rhoon GC, Kuster N. 2012. Exposure of the Human Body to Professional and Domestic Induction Cooktops Compared to the Basic Restrictions. *Bioelectromagnetics*. 2012 Jun 1. doi: 10.1002/bem.21739. [Epub ahead of print]
- Christe B, Cooney E, Maggioli G, Doty D, Frye R, Short J. 2008. Testing potential interference with RFID usage in the patient care environment. *Biomed Instrum Technol* 42(6):479-484.
- Cole KS, Cole, RH. 1941. Dispersion and Absorption in Dielectrics - I Alternating Current Characteristics. *J Chem Phys* 9: 341–352.
- Conil E, Hadjem A, Lacroux F, Wong MF, Wiart J. 2008. Variability analysis of SAR from 20 MHz to 2.4 GHz for different adult and child models using finite-difference time-domain. *Phys Med Biol* 53:1511-1525.
- Dalton J, Kim IH, Lim BK. 2005. RFID Technologies in Neonatal Care. White Paper by Intel Corporation, LG CNS, ECO Inc and WonJu Christian Hospital. Available at: [http://cache-www.intel.com/cd/00/00/25/78/257831\\_257831.pdf](http://cache-www.intel.com/cd/00/00/25/78/257831_257831.pdf) , last accessed on September, 27, 2010.
- Dimbylow PJ. 1997. FDTD calculations of the whole-body averaged SAR in an anatomically realistic voxel model of the human body from 1 MHz to 1 GHz *Phys Med Biol*. 42(3): 479–490.
- Dimbylow PJ. 2002. Fine resolution calculations of SAR in the human body for frequencies up to 3 GHz. *Phys Med Biol*. 47(16):2835–2846.
- Dimbylow PJ. 2005. Development of the female voxel phantom NAOMI, and its application to calculations of induced current densities and electric fields from applied low frequency magnetic and electric fields. *Phys Med Biol*. 50(6), 1047–70.
- Dimbylow PJ. 2006. Development of pregnant female, hybrid voxel-mathematical models and their application to the dosimetry of applied magnetic and electric fields at 50 Hz. *Phys Med Biol*. 51(10):2383–2394
- Dimbylow PJ. 2007. SAR in the mother and foetus for RF plane wave irradiation. *Phys Med Biol* 52(13):3791–3802.
- Dimbylow PJ, Bolch W. 2007. Whole-body-averaged SAR from 50 MHz to 4 GHz in the University of Florida child voxel phantoms. *Phys Med Biol* 52(22):6639–6649.
- Dimbylow PJ, Nagaoka T, Xu XG. 2009. A comparison of foetal SAR in three sets of pregnant female models. *Phys Med Biol* 54: 2755–2767.
- Dimbylow PJ, Bolch W, Lee C. 2010. SAR calculations from 20 MHz to 6 GHz in the University of Florida newborn voxel phantom and their implications for dosimetry. *Phys Med Biol* 55(5):1519.

- ETSI The European Telecommunications Standards Institute EN 300 220-1 V2.3.1 (2010-02). 2010. Electromagnetic compatibility and Radio spectrum Matters (ERM); Short Range Devices (SRD); Radio equipment to be used in the 25 MHz to 1 000 MHz frequency range with power levels ranging up to 500 mW; Part 1: Technical characteristics and test methods. Available from: [http://www.rfdesignuk.com/Documents/en\\_30022002v020301p2010.pdf](http://www.rfdesignuk.com/Documents/en_30022002v020301p2010.pdf), last accessed on May 23, 2012
- Findlay RP, Dimbylow PJ. 2006. FDTD calculations of Specific energy Absorption Rate in a seated voxel model of the human body from 10 MHz to 3 GHz. *Phys Med Biol*. 51: 2339–2352
- Findlay RP, Lee AK, Dimbylow PJ. 2009. FDTD calculations of SAR for a child voxel models in different postures between 10 MHz and 3 GHz. *Radiation Protection Dosimetry*. 135: 226–231.
- Finkenzeller K. 1999. *RFID Handbook. Fundamentals and Applications in Contactless Smart Cards and Identification*. New York: Wiley.
- Fiocchi S, Parazzini M, Paglialonga A, Ravazzani P. 2011a. Computational exposure assessment of electromagnetic fields generated by an RFID system for mother-newborn identity reconfirmation. *Bioelectromagnetics*. 32(5): 408-16.
- Fiocchi S, Parazzini M, Ravazzani P. 2011b. RFID system for newborn identity reconfirmation in hospital: Exposure assessment of a realistic newborn model and effects of the change of the dielectric properties with age. *Progress in Biophysics and Molecular Biology* 107: 443–448.
- Fiocchi S, Markakis IA, Ravazzani P, Samaras T. 2013. SAR exposure from UHF RFID reader in adult, child, pregnant woman and fetus anatomical models. *Bioelectromagnetics*. In press.
- Fleming AH, Joyner KH. 1992. Estimates of absorption of radiofrequency radiation by the embryo and fetus during pregnancy. *Health Phys*.63(2): 149–159.
- Fung LC, Chan KH, Lam WK, Leung SW, Wong YF, Wu PWK, Tang CK. 2007. Electromagnetic assessment on human safety of RFID system at Hong Kong International Airport. *Microwave and Optical Technology Letters* 49(4): 924–928.
- Gabriel S, Lau RW, Gabriel C. 1996a. The dielectric properties of biological tissues: II. Measurements in the frequency range 10 Hz to 20 GHz. *Phys Med Biol* 41:2251-2269.
- Gabriel C. 1996b. Compilation of the dielectric properties of body tissues at RF and microwave frequencies. Report N.AL/OE-TR- -0037, Occupational and environmental health directorate. Radiofrequency Radiation Division, Brooks Air Force Base, Texas (USA).
- Gabriel C. 2005. Dielectric Properties of Biological Tissue: variation with age. *Bioelectromagnetics* 26 (7):S12-S18.
- Gajšek P, Hurt WD, Ziriak JM, Mason PA. 2001. Parametric dependence of SAR on permittivity values in a man model. *IEEE Trans. Biomed. Eng.* 48(10): 1169-1177

- Gandhi OP, Lazzi G, Furse CM. 1996. Electromagnetic absorption in the human head and neck for mobile telephones at 835 MHz and 1900 MHz. *IEEE Trans. Microw. Theory Techn.* 44: 1884–1897.
- Gandhi OP, Kang G. 2002. Some present problems and a proposed experimental phantom for SAR compliance testing of cellular telephones at 835 MHz and 1900 MHz. *Phys. Med. Biol.* 47: 1501–1518.
- Gilbert RD, Schröder H, Kawamura T, Dale PS, Power GG. 1985. Heat transfer pathways between fetal lamb and ewe. *J Appl Physiol.* 59(2): 634–638.
- Gowland PA, De Wilde J. 2008. Temperature increase in the fetus due to radio frequency exposure during magnetic resonance scanning. *Phys. Med. Biol.* 53(21): L15–L18.
- Grandjean P, Landrigan PJ. 2006. Developmental neurotoxicity of industrial chemicals. *Lancet.* 368(9553): 2167–78.
- Hand JW, Li Y, Thomas EL, Rutherford MA, Hajnal JV. 2006. Prediction of specific absorption rate in mother and fetus associated with MRI examinations during pregnancy. *Magn. Reson. Med.* 55(4): 883–893, Apr. 2006.
- Hand JW, Li Y, Hajnal JV. 2010. Numerical study of RF exposure and the resulting temperature rise in the foetus during a magnetic resonance procedure. *Phys. Med. Biol.* 55(4): 913–930.
- Harrington RF. 1964. Theory of loaded scatterers. *Proc Inst Elect Eng* 111(4):617–623.
- Heinonen S, Taipale P, Saarikoski S. 2001. Weights of placentae from small-for-gestational age infants revisited. *Placenta.* 22(5): 399–404.
- Hirata A, Kodera S, Wang J, Fujiwara O. 2007. Dominant factors influencing whole-body average SAR due to far-field exposure in whole-body resonance frequency and GHz regions. *Bioelectromagnetics* **28(6):484–487**.
- Hirata A, Asano T, Fujiwara O. 2008. FDTD analysis of body-core temperature elevation in children and adults for whole-body exposure. *Phys Med Biol*, 53:5223–5238
- Hong SE, Yun JH. 2010. SARs in Adult male models for 900 MHz RFID Reader Antenna. 32<sup>nd</sup> annual meeting of the Bioelectromagnetics society 2010, 13-18 June 2010, Seoul, Korea. Available from: [http://www.bioelectromagnetics.org/bems2010/supp\\_data/P-B-56.pdf](http://www.bioelectromagnetics.org/bems2010/supp_data/P-B-56.pdf), last accessed on May 23, 2012
- Huber R, Schuderer J, Graf T, Jütz K, Borbély AA, Kuster N, Achermann P. 2003. Radio frequency electromagnetic field exposure in humans: estimation of SAR distribution in the brain, effects on sleep and heart rate. *Bioelectromagnetics.* 24(4): 262–276.
- Ibrahiem A, Dale C, Tabbara W, Wiart J. 2005. Analysis of the temperature increase linked to the power induced by RF source. *Progress In Electromagnetics Research.* 52:23–46.

ICNIRP The International Commission on Non-Ionizing Radiation Protection. 1998. Guidelines for limiting exposure to time-varying electric, magnetic, and electromagnetic fields (up to 300 GHz). *Health Physics* 74(4):494–522.

ICNIRP International Commission on Non-Ionizing Radiation Protection. 2004. Medical magnetic resonance (MR) procedures: protection of patients. *Health Phys.* 87(2): 197–216.

ICRP International Commission on Radiological Protection. 2002. *Annals of the ICRP*. Publication 89. Basic anatomical and physiological data for use in radiological protection: reference values ICRP. 32 (3-4):5-265.

IFAC-CNR. (2011, June 10), “An Internet resource for the calculation of the dielectric properties of body tissues,” National Research Council, Institute for Applied Physics “Nello Carrara,” Florence, Italy [Online]. Available: <http://niremf.ifac.cnr.it/tissprop/>

Kaatze U.1989. Complex permittivity of water as a function of frequency and Temperature. *J Chem Eng Data.* 34: 371-374.

Kainz W, Chan DD, Casamento JP, Bassen HI. 2003. Calculation of induced current densities and specific absorption rates (SAR) for pregnant women exposed to hand-held metal detectors. *Phys. Med. Biol.* 48(15): 2551–2560.

Kainz W, Christ A, Kellom T, Seidman S, Nikoloski N, Beard B and Kuster N. 2005. Dosimetric comparison of the specific anthropomorphic mannequin (SAM) to 14 anatomical head models using a novel definition for the mobile phone positioning. *Phys Med Biol* 50(14): 3423–3445.

Keshvari J, Keshvari R, Lang S. 2006. The effect of increase in dielectric values on specific absorption rate (SAR) in eye and head tissues following 900, 1800 and 2450 MHz radio frequency (RF) exposure. *Phys Med Biol* 51: 1463–1477.

Kheifets L, Repacholi M, Saunders R, Kheifets L, Repacholi M, Saunders R, Van Deventer E. 2005. The sensitivity of children to electromagnetic fields. *Pediatrics.* 116(2):e303–313.

Kikuchi S, Saito K, Takahashi M, Ito K. 2010. Temperature elevation in the fetus from electromagnetic exposure during magnetic resonance imaging. *Phys. Med. Biol.* 55(8): 2411–2426.

Koelle A, Depp S, Freyman R. 1975. Short-range radio-telemetry for electronic identification using modulated backscatter. *Proc IEEE.* 63(8):1260–1261.

Kühn S, Jennings W, Christ A, Kuster N. 2009. Assessment of induced radio-frequency electromagnetic fields in various anatomical human body models. *Phys Med Biol* 54(4):875-90.

Kuster N, Torres VB, Nikoloski N, Frauscher M, Kainz W. 2006. Methodology of detailed dosimetry and treatment of uncertainty and variations for in vivo studies. *Bioelectromagnetics.* 27(5):378–391.

Laasko I, Uusitupa T, Ilvonen S. 2010. Comparison os SAR calculation algorithms for the finite-difference time-domain method. *Phys Med Biol* 55: 421–431

- Lee. AK, Byun JK, Seo Park J, Choi Hd, Yun J. 2009a. Development of 7-Year-Old Korean Child Model for Computational Dosimetry. *ETRI J* 31(2): 237–239.
- Lee HJ, Lee JS, Pack JK, Choi HD, Kim N, Kim SH, Lee YS. 2009b. Lack of teratogenicity after combined exposure of pregnant mice to CDMA and WCDMA radiofrequency electromagnetic fields. *Radiat. Res.* 172(5): 648–652.
- Lee AK, Choi HD. 2012. Determining the influence of Korean population variation on whole-body average SAR. *Phys Med Biol.* 57: 2709–2725.
- Lu Y, Cui H, Yu J, Mashimo S. 1996. Dielectric properties of human fetal organ tissues at radio frequencies. *Bioelectromagnetics.* 17(5): 425–426.
- Martínez-Búrdalo M, Martín A, Anguiano M, Villar R. 2010. Comparison of SAR and induced current densities in adults and children exposed to electromagnetic fields from electronic article surveillance devices. *Phys Med Biol* 55: 1041–1055.
- Mason PA, Hurt WD, Walters TJ, D’Andrea JA, Gajšek P, Ryan KL, Nelson PA, and Zirriax JA. 2000. Effects of frequency, permittivity, and voxel size on predicted specific absorption rate values in biological tissue during electromagnetic field exposure. *IEEE Microw. Theory & Techn*,48(11): 2050–2057.
- McIntosh RL, Deppeler L, Oliva M, Parente J, Tambuwala F, Turner S, Winship D, Wood AW. 2010. Comparison of radiofrequency exposure of a mouse dam and foetuses at 900 MHz. *Phys. Med. Biol.* 55(4): N111–N122.
- Murbach M, Cabot E, Neufeld E, Gosselin MC, Christ A, Pruessmann KP, Kuster N. Local SAR enhancements in anatomically correct children and adult models as a function of position within 1.5 T MR body coil. *Prog. Biophys. Mol. Biol.* 107(3): 428–433.
- Nagaoka T, Watanabe S, Sakurai K, Kunieda E, Watanabe S, Taki M, Yamanaka Y. 2004. Development of realistic high-resolution whole-body voxel models of Japanese adult males and females of average height and weight, and application of models to radio-frequency electromagnetic-field dosimetry. *Phys Med Biol.* 49(1):1–15.
- Nagaoka T, Togashi T, Saito K, Takahashi M, Ito K, Watanabe S. 2007. An anatomically realistic whole-body pregnant-woman model and specific absorption rates for pregnant-woman exposure to electromagnetic plane waves from 10 MHz to 2 GHz. *Phys Med Biol* 52(22): 6731–6745.
- Nagaoka T, Saito K, Takahashi M, Ito K, Watanabe S. 2008 Anatomically realistic reference models of pregnant women for gestation ages of 13, 18, and 26 weeks. In: *Conf Proc IEEE Eng Med Biol Soc.* 2008:2817–2820.
- Olawale KO, Petrell RJ, Michelson DG, Trites AW. 2005. The dielectric properties of the cranial skin of five young captive Steller sea lions (*Eumetopias jubatus*), and a similar number of young domestic pigs (*Sus scrofa*) and sheep (*Ovis aries*) between 0.1 and 10 GHz. *Physiological Measurement.* 26(5), 627–37.

- Ngai EWT, Poon JKL, Suk FFC, Ng CC. 2009. Design of an RFID-based Healthcare Management System using an Information System Design Theory. *Inf Syst Front* 11:405–417.
- O'Connor ME. 1999. Intrauterine effects in animals exposed to radiofrequency and microwave fields. *Teratology*. 59(4): 287–191.
- Pediaditis M, Leitgeb N, Cech R. 2008. RF-EMF exposure of fetus and mother during magnetic resonance imaging. *Phys. Med. Biol.* 53(24): 7187–7195.
- Pennes HH. 1998. Analysis of tissue and arterial blood temperature in the resting human forearm. 1948. *J. Appl. Physiol.* 85(1): 5–34.
- Peyman A, Rezazadeh AA, Gabriel C. 2001. Changes in the dielectric properties of rat tissues as a function of age at microwave frequencies. *Phys Med Biol* 46(6):1617-1629.
- Peyman A, Holden S, Gabriel C. 2005. Dielectric properties of tissues at microwave frequencies. RUM3 Final technical Report, MTHR (Mobile Telecommunications and health Research programme) available at [http://www.mthr.org.uk/research\\_projects/documents/Rum3FinalReport.pdf](http://www.mthr.org.uk/research_projects/documents/Rum3FinalReport.pdf)
- Peyman A., Holden SJ, Watts S, Perrott R, Gabriel C. 2007. Dielectric properties of porcine cerebrospinal tissues at microwave frequencies: in vivo, in vitro and systematic variation with age. *Phys Med Biol.* 52(8): 2229-2245.
- Peyman A, Gabriel C, Grant EH, Vermeeren G, Martens L. 2009. Variation of the dielectric properties of tissues with age: the effect on the values of SAR in children when exposed to walkie-talkie devices. *Phys Med Biol* 54(2):227-241.
- Peyman A, Gabriel C. 2010, Cole-Cole parameters for the dielectric properties of porcine tissues as a function of age at microwave frequencies. *Phys Med Biol* 55(15):N413-419
- Peyman A, Gabriel C, Benedickter HR, Fröhlich J. 2011. Dielectric properties of human placenta, umbilical cord and amniotic fluid. *Phys Med Biol* 56(7): 93–98.
- Peyman A. 2011. Dielectric properties of tissues; variation with age and their relevance in exposure of children to electromagnetic fields; state of knowledge. *Progress in Biophysics and Molecular Biology* 107: 434–438
- Rao KVS, Nikitin PV, Lam SF. 2005. Antenna design for UHF RFID tags: a review and a practical application. *IEEE Trans Antennas Propag* 53(12): 3870–3876.
- Rasanen J, Wood DC, Weiner S, Ludomirski A, Huhta JC. 1996. Role of the pulmonary circulation in the distribution of human fetal cardiac output during the second half of pregnancy. *Circulation.* 94(5): 1068–1073.
- Ruckhäberle E, Nekolla SG, Ganter C, Schneider KT, Peter A, Radit A, Kovacs L, Bockmeier SJ, Schwaiger M, Oberhoffer R, Papadopoulos NA. 2008. In vivo intrauterine sound pressure and

- temperature measurements during magnetic resonance imaging (1.5 T) in pregnant ewes. *Fetal Diagn. Ther.* 24(3): 203–210.
- Schmid G, Uberbacher R. 2005. Age dependence of dielectric properties of bovine brain and ocular tissues in the frequency range of 400 MHz to 18 GHz. *Phys Med Biol.* 50(19): 4711–4720.
- Schönborn F, Burkhardt M, Kuster N. 1998. Differences in energy absorption between heads of adults and children in the near field of sources. *Health Phys.* 74(2), 160–68.
- Schröder H, Gilbert RD, Power GG. 1988. Computer model of fetal-maternal heat exchange in sheep. *J. Appl. Physiol.* 65(1): 460–468.
- Sheiner E, Abramowicz JS. 2012. A symposium on obstetrical ultrasound: is all this safe for the fetus? *Clin. Obstet. Gynecol* 55(1): 188–198.
- Singh N, Gupta R. 1994. Anthropometric data in term newborns. *Indian Pediatrics* 31:466-467.
- Smith GCD, Cameron AD. Estimating human fetal blood volume on the basis of gestational age and fetal abdominal circumference. *BJOG.* 109(6): 721–722.
- Soultanakis-Aligianni HN. 2003. Thermoregulation during exercise in pregnancy. *Clin Obstet Gynecol.* 46 (2): 442–455.
- Stockman H. 1948. Communication by means of reflected power. *Proc. IRE.* 36(10): 1196–1204.
- Sutton MS, Theard MA, Bhatia SJ, Plappert T, Saltzman DH, Doubilet P. 1990. Changes in placental blood flow in the normal human fetus with gestational age. *Pediatr. Res.* 28(4): 383–387.
- Takahashi S, Imai N, Nabae K, Wake K, Kawai H, Wang J, Watanabe S, Kawabe M, Fujiwara O, Ogawa K, Tamano S, Shirai T. 2010. Lack of adverse effects of whole-body exposure to a mobile telecommunication electromagnetic field on the rat fetus. *Radiat. Res.* 173(3): 362–372.
- Thuemmler C, Buchanan W, Kumar V. 2007. Setting safety standards by designing a low-budget and compatible patient identification system based on passive RFID technology. *Int J Healthcare Technology and Management* 8(5):571-583.
- Thurai M, Goodridge, VD, Sheppard RJ, Grant EH. 1984. Variation with age of the dielectric properties of mouse brain cerebrum. *Phys Med Biol.* 29(9): 1133-1136.
- Thurai M, Steel MC, Sheppard RJ, Grant EH. 1985. Dielectric properties of developing rabbit brain at 37 degrees C. *Bioelectromagnetics.* 6(3): 235-242.
- Van der Togt R, Van Lieshout EJ, Hensbroek R, Beinat E, Binenkade JM, Bakker PJM. 2008. Electromagnetic interference from radio frequency identification inducing potentially hazardous incidents in critical care medical equipment. *Jama-Journal Of The American Medical Association* 299(24):2884–2890.

- Wang J, Fujiwara O. 1999. FDTD computation of temperature rise in the human head for portable telephones. *IEEE Trans. Microwave Theory & Tech.* 47: 1528–1534
- Wang J, Fujiwara O. 2003. Comparison and Evaluation of Electromagnetic Absorption Characteristics in Realistic Human Head Models of Adult and Children for 900-MHz Mobile Telephones. *IEEE Trans Microw Theory Tech.* 51(3): 966–971.
- Wang J, Fujiwara O, Watanabe S. 2006. Approximation of aging effect on dielectric tissue properties for SAR assessment of mobile telephones. *IEEE Trans Electromagn Compat* 48:408–413.
- Weiland T. 1977. A discretization method for the solution of the Maxwell's equations for six-component fields. *Electronics and Communication* 31:116–120.
- Wu D, Shamsi S, Chen J, Kainz W. 2006. Evaluations of specific absorption rate and temperature increase within pregnant female models in magnetic resonance imaging birdcage coils. *IEEE Trans. Microw. Theor. Tech.* 54(12): 4472–4478.
- Wiat J, Hadjem A, Gadi N, Bloch I, Wong MF, Pradier A, Lautru D, Hanna VF, Dale C. 2005. Modeling of RF head exposure in children. *Bioelectromagnetics. Suppl 7: S19-30.*
- Wiat J, Hadjem A, Varsier N, Conil E. 2011. Numerical dosimetry dedicated to children RF exposure. *Progress in Biophysic and Molecular Biology.* 107: 421–427.
- Xu XG, Taranenko V, Zhang J, Shi C. 2007. A boundary-representation method for designing whole-body radiation dosimetry models: pregnant females at the ends of three gestational periods--RPI-P3, -P6 and -P9. *Phys Med Biol.* 52(23):7023–7044
- Ziskin MC, Morrissey J. 2011. Thermal thresholds for teratogenicity, reproduction, and development. *Int J Hyperthermia.* 27(4): 374-387.

---

---

## List of Papers published during the PhD Course

The activity developed during the three years PhD resulted in the publication of the following papers (inherent to the thesis) published in international peer-reviewed Journals and as conference proceedings:

- **Fiocchi S**, Parazzini M, Markakis I, Samaras T, Ravazzani P. “Temperature elevation in fetus exposed to UHF RFID readers” submitted to IEEE Trans Biomed Eng on April 2013
- **Fiocchi S**, Markakis I, Ravazzani P, Samaras T. 2013 “SAR assessment in human anatomical body models exposed to handheld UHF RFID reader antenna” Bioelectromagnetics, in press.
- **Fiocchi S**, Parazzini M, and Ravazzani P. 2011. “RFID System For Newborn Identity Reconfirmation In Hospital: Exposure Assessment Of A Realistic Newborn Model And Effects Of The Change Of The Dielectric Properties With Age”. Progress in Biophysics and Molecular Biology, 107(3):443-48.
- **Fiocchi S**, Parazzini M, Paglialonga A, Ravazzani P. 2011. “Computational exposure assessment of electromagnetic fields generated by an RFID system for mother-newborn identity reconfirmation”. Bioelectromagnetics. 32(5), pp 408-16.
- **Fiocchi S**, Markakis I, Liorni I, Parazzini M, Samaras T, Ravazzani P. “Estimate of the fetal temperature increase due to UHF RFID exposure”. 35<sup>th</sup> Annual International Conference of the IEEE Engineering in Medicine and Biology Society (EMBC), Osaka, Japan, 3-7 July, 2013.
- **Fiocchi S**, Markakis I, Liorni I, Parazzini M, Samaras T, Ravazzani P. “Computational study of temperature elevation in fetal tissues due to UHF RFID exposure”. BioEM2013, Joint meeting of the Bioelectromagnetics Society (BEMS) and the European BioElectromagnetics Association (EBEA), Thessaloniki, Greece, 10-14 June, 2013.
- **Fiocchi S**, Markakis I, Liorni I, Parazzini M, Samaras T, Ravazzani P. “Estimate of the fetal temperature increase due to UHF RFID exposure”. BioEM2013, Joint meeting of the Bioelectromagnetics Society (BEMS) and the European BioElectromagnetics Association (EBEA), Thessaloniki, Greece, 10-14 June, 2013.
- **Fiocchi S**, Parazzini M, and Ravazzani P. “Effects of the dielectric properties changes in newborn: the case of the exposure to an RFID System for mother-newborn identity reconfirmation”. NIR & Children's Health Conference, Ljubljana, Slovenia, 18-20 May, 2011.

- 
- **Fiocchi S**, Parazzini M, and Ravazzani P. “EMF Dosimetry in Different Newborn Models for RFID System Exposure” EBEA 2011 10th International Conference of the European Bioelectromagnetics Association, Rome, 21-24 February, 2011.
  - **Fiocchi S**, Parazzini M and Ravazzani P. “Computational Exposure Assessment of an Identity Reconfirmation of Mother and Newborn by RFID system”, EMF Bordeaux Event, an EBEA, COST Action BM0704 and URSI Commission K Event, Bordeaux, May 26-29, 2010.